

## ABSTRACT

Title of Document: **Bio-Inspired Polymer Microparticles for Targeted Recognition and Response**

Chandamany Arya, Doctor of Philosophy, 2014

Directed By: Professor Srinivasa R. Raghavan  
Department of Chemical and Biomolecular Engineering

Microbeads and microcapsules are container structures that are frequently used in biomedical applications. In this dissertation, we have sought to impart new functionalities to these particles, inspired by phenomena observed with biological cells. We have engineered polymer microparticles that recognize and respond to specific species from the surroundings (e.g. cells, polymer chains, metal ions). Three classes of new microparticles are reported, which are each reminiscent of a different type of biological cell in terms of recognition capabilities and response.

In the first part of this dissertation, we create functionalized microbeads from the biopolymer, chitosan, and use these to selectively recognize and capture Circulating Tumor Cells (CTCs) from blood. The microbeads are functionalized with a protein (streptavidin) and packed into an array within a microfluidic device. Blood samples with biotin-labeled CTCs are flowed over the packed bed of chitosan beads. Similar to how macrophages adhere to foreign bacteria (i.e. antibody-antigen interactions), the streptavidin-labeled chitosan beads can selectively recognize and adhere to the biotin-labeled CTCs. We show that such a packed bed of chitosan beads could serve as an

inexpensive platform for customized capture of different rare cells (cancer cells, stem cells etc) from blood.

In the next study, we develop a class of microbeads that undergo clustering (aggregation) in the presence of specific polymers. The inspiration for this comes from the cells (e.g., platelets) and polymers involved during the formation of blood clots. Our system consists of chitosan microbeads coated with cyclodextrins (sugar molecules with a hydrophobic binding pocket), which are then exposed to a polymer that is decorated with hydrophobic units. The particles bind to the polymer chains via hydrophobic interactions and in turn, the particles are induced to form clusters. Subsequently, the polymer precipitates and forms a matrix around the particle clusters, leading to a structure that is reminiscent of a blood clot (platelets enveloped by a mesh of fibrin chains).

Lastly, we develop a class of microparticles that have the ability to selectively destroy other microparticles. The inspiration here is from the body's immune system, where cells like the killer T cells selectively destroy cancer and virus infected cells without harming healthy cells. Towards this end, we synthesize two types of microparticles: chitosan capsules that contain the enzyme glucose oxidase (GOx), and beads of a different biopolymer, alginate that are crosslinked with copper ( $\text{Cu}^{2+}$ ) ions. The chitosan capsules enzymatically convert glucose from the surroundings into gluconate ions. When these capsules approach the alginate/ $\text{Cu}^{2+}$  beads, the gluconate ions chelate the  $\text{Cu}^{2+}$  ions, leading to the disintegration of the alginate beads. Other beads that do not contain  $\text{Cu}^{2+}$  are not affected in this process.

**Bio-Inspired Polymer Microparticles for Targeted  
Recognition and Response**

By

Chandamany Arya

Dissertation submitted to the Faculty of the Graduate School of the  
University of Maryland, College Park, in partial fulfillment of  
the requirements for the degree of  
Doctor of Philosophy  
2014

**Advisory Committee:**

Prof. Srinivasa R. Raghavan, Dept. of Chemical and Biomolecular Engineering, Chair

Prof. Don L. DeVoe, Dept. of Mechanical Engineering

Prof. Panagiotis Dimitrakopoulos, Dept. of Chemical and Biomolecular Engineering

Prof. Sheryl H. Ehrman, Dept. of Chemical and Biomolecular Engineering

Prof. Ian M. White, Fischell Dept. of Bioengineering

© Copyright by  
Chandamany Arya  
2014

## **DEDICATION**

This dissertation is dedicated to my life mentor: Theodore “Ted” Patlovich. I will always do my best to use his sagely wisdom as a moral compass for my life.

## ACKNOWLEDGEMENTS

First of all, I would like to thank my advisor, Professor Srinivasa Raghavan for his support and mentoring throughout my graduate school career. I have learned so much over the past few years and feel very lucky to have had such an enriching experience as a member of his research group. He was great mentor and heavily influenced how I tackle scientific and technical challenges. Overall, under his tutelage, I became a much better engineer, writer, presenter, and thinker. For that I am truly grateful.

I would also like to thank Dr. Samuel P. Forry, my mentor at the National Institute of Standards and Technology (NIST) during my early years in graduate school. His mentoring gave me a strong foundation in analytical thinking skills that helped me overcome various technical challenges. In addition, it was a pleasure working with and learning from Dr. Jason Kralj at NIST. To my fellow lab members in the *Complex Fluids and Nanomaterials Group*, thank you for all the help and support over the years. It really was a wonderful and productive work environment. Thank you all for working towards making the lab such a great place full of excitement, professionalism, and creativity.

And finally, to my friends and family, thank you for your unending love and support. I am particularly grateful to my parents, who prepared me well for the world through a consistent emphasis on hard work and integrity. I have been truly blessed to have such great role-models and people in my life.

*Vires acquirit eundo*

# TABLE OF CONTENTS

<b>Dedication</b> .....	ii
<b>Acknowledgements</b> .....	iii
<b>Table of Contents</b> .....	iv
<b>List of Tables</b> .....	vi
<b>List of Figures</b> .....	vii
<b>Chapter 1. Introduction and Overview</b> .....	1
1.1. Problem Description and Motivation .....	1
1.2. Proposed Approach.....	2
1.2.1. Particles Capable of Capturing Specific Biological Cells.....	4
1.2.2. Particles that Cluster in the Presence of a Specific Polymer.....	5
1.2.3. Particles Engineered to Destroy Other Particles.....	6
1.3. Significance of this Work.....	7
<b>Chapter 2. Background</b> .....	9
2.1. Biopolymers.....	9
2.1.1. Chitosan.....	9
2.1.2. Hydrophobically-Modified Chitosan.....	11
2.1.3. Alginate.....	12
2.2. Interactions of Biopolymers.....	14
2.2.1. Chitosan and Chemical Cross-linkers.....	14
2.2.2. Hydrophobically Modified Chitosan and Cyclodextrins.....	15
2.2.3. Alginate Hydrogel Dissolution via Chelators.....	17
2.3. Optical Microscopy.....	18
2.3.1. Brightfield and Phase Contrast Microscopy.....	18
2.3.2. Fluorescence Microscopy.....	20
<b>Chapter 3. Microparticles for Capture of Rare Cells from Blood</b> .....	22
3.1. Introduction .....	22
3.2. Experimental Section.....	25
3.3. Results and Discussion.....	29
3.3.1. Generation of Chitosan Microbeads.....	29
3.3.2. Functionalization of Chitosan Microbeads.....	31
3.3.3. Rare Cell Capture with Chitosan Microbeads.....	36
3.4. Conclusions.....	38
<b>Chapter 4. Inducing Microparticle Clustering with an Associating Polymer</b> .....	40
4.1. Introduction.....	40
4.2. Experimental Section.....	43

4.3. Results and Discussion.....	45
4.4. Conclusions.....	53
<b>Chapter 5. Development of “Killer” Microparticles.....</b>	<b>54</b>
5.1. Introduction.....	54
5.2. Experimental Section.....	56
5.3. Results and Discussion.....	60
5.4. Conclusions.....	70
<b>Chapter 6. Conclusions and Recommendations.....</b>	<b>72</b>
6.1. Project Summary and Principal Contributions.....	72
6.2. Recommendations for Future Work.....	74
6.2.1. Future Work with Microparticles Presented in this Dissertation.....	74
6.2.2. Red Blood Cell Shaped Microparticles.....	75
<b>Appendix: Detailed Procedures Microbead Synthesis.....</b>	<b>78</b>
<b>References.....</b>	<b>83</b>



## LIST OF TABLES

<b>Table 2.1.</b> Stability constants of common divalent metal ion chelators.....	17
---	----

## LIST OF FIGURES

<b>Figure 1.1.</b> Cell-selective microbeads of the biopolymer, chitosan are used for capturing rare cells from blood. The microbead surface is modified with streptavidin. Cells coated with biotin selectively adhere to these beads.....	3
<b>Figure 1.2.</b> Microbeads that cluster in the presence of an associating polymer (i.e., a polymer with a hydrophilic backbone and hydrophobic pendant groups). Once the cluster forms, the polymer forms a precipitate around the cluster. The overall structure resembles a blood clot formed by blood platelets and the protein fibrin.....	4
<b>Figure 1.3.</b> Killer capsules that can selectively target neighboring microbeads for destruction. Over time, the killer capsule releases molecules that remove the metal ion cross-links from the target microbead, thereby leading to its destruction .....	6
<b>Figure 2.1.</b> Structures of the monomer sugars in (a) chitin and (b) chitosan. The N-acetyl-D-glucosamine sugar in chitin is deacetylated to generate the D-glucosamine sugar in chitosan.....	10
<b>Figure 2.2.</b> Chemical Structure of hydrophobically-modified chitosan with C <sub>12</sub> hydrophobic tails.....	11
<b>Figure 2.3.</b> Chemical Structure of sodium alginate .....	12
<b>Figure 2.4.</b> Schematic demonstrating gelation of alginate upon addition of calcium ions through “egg-box” junctions .....	13
<b>Figure 2.5.</b> Schematic demonstrating crosslinking of chitosan with glutaraldehyde ...	14
<b>Figure 2.6.</b> Truncated cone-shaped structure of $\beta$ -cyclodextrin .....	15
<b>Figure 2.7.</b> Effect of adding $\alpha$ -CD to a gel formed by combining blood with hm-chitosan. Gelation is due to the bridging of adjacent cells into a network via polymer chains. The addition of $\alpha$ -CD reverses the gelation.....	16
<b>Figure 2.8.</b> Phase relations between S, D and P waves in brightfield microscopy. The D wave is slowed by $\frac{1}{4}$ of a wavelength relative to the S wave, upon diffracting at the object, causing minimal destructive interference with the S wave to generate the resultant P wave .....	19
<b>Figure 2.9.</b> Phase relations between S, D and P waves in phase contrast microscopy. The S and D wave have maximized destructive interference to generate a resultant P wave that allows for greater contrast in the image .....	20

**Figure 2.10.** Schematic that shows light path in fluorescent microscopy ..... 21

**Figure 3.1.** Photographs and schematic of the tubing device used to generate chitosan microbeads. The device (a) is formed by inserting capillary microtubing into slightly larger PTFE tubing. A close-up of the device is shown in (b) and a schematic at the junction between the two phases is shown in (c). An aqueous chitosan solution is pumped through the inner tubing. Oil pumped through the outer tubing exerts shear on the aqueous phase at the annular junction, causing uniform microdroplets containing chitosan to break away and flow down the tubing. These microdroplets are collected and cross-linked into uniform microbeads..... 29

**Figure 3.2.** Particle Sizing. Optical micrographs of chitosan microbeads (a) showed that the microbeads were uniform and nearly monodisperse. The mean particle diameter (b) was  $\approx 164 \mu\text{m}$  with a relative standard deviation of 4.3% ( $n = 91$ ). The solid line in (b) is a Gaussian fit to the data..... 31

**Figure 3.3.** Chitosan encapsulation of carbon black nanoparticles. Bare chitosan microbeads cross-linked by glutaraldehyde (a, b) were transparent and exhibited an intrinsic autofluorescence. By encapsulating 1 % by weight carbon black (c, d), the microbeads were rendered opaque, and autofluorescence was reduced 50-fold. (Image contrast is identical for (b) and (d).).....32

**Figure 3.4.** Fluorescent image of DiI-stained cells and chitosan microbeads (diameter  $\approx 164 \mu\text{m}$ ). The chitosan microbeads were loaded with 1% by weight carbon black to attenuate their intrinsic autofluorescence. The one bright microbead contained no carbon black and emitted a strong autofluorescence that was much brighter than the microbeads encapsulating carbon black or fluorescently stained cells. This image was taken using an inverted fluorescent microscope and a TRITC filter set (Ex: 520-570; Em: 535-675) at 10 $\times$  magnification..... 32

**Figure 3.5.** Fluorescent biotin increased the fluorescent intensity of streptavidin-functionalized chitosan microbeads. The chitosan microbeads, which encapsulated 1% by weight carbon black, were covalently functionalized with streptavidin. Following exposure to fluorescent biotin in solution followed by washing, a significant increase in fluorescent intensity was observed. These images were taken using an inverted fluorescent microscope and a TRITC filter set (Ex: 520-570; Em: 535-675) at 10 $\times$  magnification..... 33

**Figure 3.6.** Attachment of small biotinylated polystyrene spheres (6-8  $\mu\text{m}$ ) to streptavidin-functionalized chitosan microbeads. When chitosan microbeads were mixed with the commercially available biotinylated polystyrene spheres, significant surface attachment of the spheres to the chitosan microbead demonstrated that covalently bound streptavidin was present at the microbead surface..... 34

**Figure 3.7.** Specificity of cell-binding to chitosan microbeads. Chitosan microbeads functionalized with BSA (a) exhibit no specific interaction with biotin covered MCF-7 cells (the MCF-7 cells were treated with biotinylated anti-EpCAM against highly expressed surface proteins). However, streptavidin-functionalized chitosan microbeads (b) are able to capture the same cells due to non-covalent biotin-streptavidin interactions..... 35

**Figure 3.8.** Image of the packed bed microfluidic capture device. Top and side view of the chip shows that the beads are packed against a shallow weir (a,b)..... 36

**Figure 3.9.** Capture of cancer cells from whole blood. The streptavidin functionalized chitosan microbeads were loaded into a microfluidic channel. The uniform size of the microparticles led to the generation of a uniform packed bed (a). After pumping through model CTC blood samples (200  $\mu$ L), captured cancer cells were imaged by fluorescence microscopy (b; expanded view of the rectangle in (a)). The total number of cancer cells captured and enumerated in the packed bed exhibited a linear response across the physiologically relevant range (c). A linear regression and Working-Hotelling 95% confidence bands are shown; capture efficiency was  $\approx$ 31%..... 37

**Figure 4.1.** Schematic illustrating proposed interactions of cyclodextrins on the surface of the bead with hm-chitosan. Commercially available sulphated  $\alpha$ -cyclodextrins (negatively charged) are mixed with positively charged beads to allow for surface coating of the microbeads with  $\alpha$ -cyclodextrins (a). hm-chitosan polymer interacts with the surface of the microbeads due to hydrophobic interactions (b).....42

**Figure 4.2.** Comparison of relative fluorescent intensity of chitosan microbeads after exposure to anionic fluorescent nanoparticles. Typical images are shown of: (a) Bare chitosan bead (control); (b) Bead after incubation with nanoparticles, followed by extensive washing. The higher fluorescence shows the strong binding of the nanoparticles to the bead surface; (c) Bead after incubation with nanoparticles in the presence of salt (NaCl; 2M), followed by washing. The lack fluorescence in this case indicates negligible binding of the nanoparticles..... 46

**Figure 4.3.** Optical microscopy images showing clustering of cyclodextrin coated microbeads ( $\approx$  165  $\mu$ m) upon mixing with hm-chitosan. Microbeads, which are covered with cyclodextrins, are mixed on a slide glass with hm-chitosan solution and microbead clustering is observed within a minute after exposure.....47

**Figure 4.4.** Optical microscopy images showing growth over time of a visible hm-chitosan precipitation around the microbead clusters after initial cluster formation..... 48

**Figure 4.5.** Optical microscopy images showing polymer precipitation around individual and small groups of microbeads. An individual cyclodextrin coated microbead is observed with precipitation around the bead surface upon hm-chitosan stimulation (a). Pair of cyclodextrin coated microbeads are held together in hm-chitosan precipitated web (b). Fluorescent labelled hm-chitosan is used to confirm that the precipitated web on the surface of the beads is hm-chitosan (c). For Image (c), brightfield and fluorescent microscopy image were taken and overlaid. Note: carbon black was encapsulated for visualization and to reduce autofluorescence (b, c)..... 49

**Figure 4.6.** Visual and optical microscopy observations of hm-chitosan precipitation out of solution. Initially, hm-chitosan is dissolved in an aqueous solution; however, upon addition of sulfated  $\alpha$ -cyclodextrins, the hm-chitosan precipitates out of solution (a). When unmodified chitosan beads (not pre-exposed to sulfated cyclodextrins), were mixed simultaneously with dissolved hm-chitosan and sulfated  $\alpha$ -cyclodextrins, the precipitation was observed to nucleate within the solution and not directly around the chitosan microbeads (b)..... 50

**Figure 4.7.** Two sets of beads are mixed together and exposed to hm-chitosan. One of set of beads (transparent beads) are covered in cyclodextrins and the second set of beads (encapsulated with carbon black) do not have cyclodextrins on the surface (a). Upon exposure to hm-chitosan, the transparent beads generate a surrounding precipitated polymer web (b), while the inert carbon black beads do not generate their own polymer matrix; they either remain as independent beads (c), or they are trapped within the polymer web of the transparent beads (d)..... 51

**Figure 4.8.** Images showing the entire bead-polymer matrix being moved with a magnet. The carbon black beads are completely inert (i.e. nonmagnetic and not covered in cyclodextrins) and they are trapped in the polymer matrix of the transparent beads (magnetic beads that are covered in cyclodextrins). The magnetic beads move the entire matrix, including the inert carbon black beads, from left to right. (Scale bar = 1 mm)....52

**Figure 5.1.** Schematic illustrating destruction of an infected cell in the body by a killer T cell. This is a simplified illustration of how a killer T cell attacks infected cells. Once the killer T cell is near the infected cell, it binds and delivers a “lethal burst” of cytotoxic proteins at the infected cell, resulting in apoptosis (programmed cell death) of the infected cell..... 55

**Figure 5.2.** Schematic of proposed bead degradation method. The enzyme glucose oxidase (GOx) can catalyze the production of gluconate from ambient glucose (a). As a chemical chelator, the gluconate ions have strong interactions with the copper cross-links of an alginate bead, and thereby remove the copper ion cross-links from the target alginate bead, resulting in destruction of the alginate bead (b).....60

**Figure 5.3.** Optical microscopy images over time of an alginate microbead (cross-linked with copper ions) in the presence of GOx enzyme. In the presence of glucose, at  $t = 0$ , the glucose oxidase enzyme is added to the sample and the alginate bead degrades over the course of 6 hours (a). When the same experiment is conducted without glucose, the alginate bead remains intact, as the enzyme has no source to generate gluconate chelator ions (b)..... 61

**Figure 5.4.** Preparation of killer chitosan capsules. The enzyme (GOx) is dispersed in a cationic polymer solution (chitosan) and a syringe pump generates droplets, which are collected in a cross-linking solution containing the anion, tripolyphosphate (TPP). The chitosan droplets are cross-linked into a solid hydrogel capsule by the TPP molecules, which results in immobilized enzymes within the chitosan capsule.....62

**Figure 5.5.** Schematic of chitosan capsule with encapsulated glucose oxidase (GOx) enzyme that targets neighboring alginate-copper cross-linked beads. Ambient glucose diffuses into the killer capsule, wherein, immobilized GOx converts glucose to gluconate ions, which diffuses out and targets neighboring alginate-copper cross-linked beads, resulting in destruction of the neighboring alginate bead..... 70

**Figure 5.6.** Visual observations depicting the degradation of a target copper-alginate bead in the presence of a GOx loaded killer chitosan capsule. At  $t=0$ , the killer capsule and target bead are placed together in a buffered glucose solution; Over the course of 18 hours, the target bead is completely destroyed..... 64

**Figure 5.7.** Fluorescent microscopy images demonstrating release of fluorescent nanoparticles from a degrading copper-alginate bead. At  $t=0$  the killer chitosan capsule was placed next to the target copper-alginate bead. The top row of optical microscopy images depicts destruction of the target bead by the killer capsule and the corresponding fluorescent images in the bottom row depict the release of fluorescent particles as the target bead is degraded..... 65

**Figure 5.8.** Quantifying release of fluorescent nanoparticles from a target alginate-copper bead. Relative fluorescent intensities were measured hourly in a plate reader from aliquots of the surrounding solution. Target copper-alginate beads exposed directly to pure chelator (sodium gluconate) quickly dissolved (within 1 hr) and released the fluorescent particles into the surrounding solution. Samples containing the killer chitosan capsules slowly degraded and the fluorescent intensity of the surrounding solution steadily increased. Negligible relative fluorescent intensity values were detected for the negative control (fluorescent target beads alone in buffer solution) indicating that the fluorescent nanoparticles cannot leak out of intact copper-alginate beads. Error bars for each point represent one standard deviation among 5 runs..... 66

**Figure 5.9.** Preparation of killer chitosan microcapsules using a pulsed gas flow device. Smaller microdroplets, which results in smaller microbeads, were generated by flowing the chitosan solution through a microcapillary (diameter  $\approx 100 \mu\text{m}$ ) and coaxial pulses of gas (regulated by a digital gas flow controller) sheared the chitosan solution into micron-sized droplets that were collected in a TPP cross-linking solution, resulting in cross-linked microcapsules. GOx enzyme was dispersed in the chitosan solution to generate killer chitosan capsules, similar to Figure 5.4. ....67

**Figure 5.10.** Optical microscopy images depicting degradation of a target copper-alginate microbead by a neighboring killer chitosan microcapsule.....68

**Figure 5.11.** Optical microscopy images depicting selective degradation amongst 3 population sets of microparticles. One set of particles comprised of killer chitosan capsules, another population contained the target cu-alginate beads, and the third population was composed of black inert chitosan-glutaraldehyde beads used in previous chapters. Due to selective degradation, only two sets of particles (inert black beads and killer chitosan beads) remained at the end of the experiment.....70

**Figure 6.1.** Images of red blood cell shaped alginate beads from: (a) optical microscopy; and (c) SEM. In (b) the size distribution of microbeads in (a) is plotted. The average diameter is  $111.5 \mu\text{m}$  with a relative standard deviation of 4.8% ( $n = 100$ ). The solid line in (b) is a Gaussian fit to the data.....76

**Figure A1.** Microfluidic tubing device setup for the generation of chitosan microbeads. The 5 mL syringe (top) is loaded with the chitosan solution and the 20 mL syringe (bottom) is loaded with the oil solution. The collection vial, placed at the center of the stir plate, contains the cross-linking solution, which turns turbid when the glutaraldehyde is dispersed in the oil. The tip of the PTFE tubing is submerged in the GA solution, but should be held close to the surface of the liquid (i.e. it should not be in contact with the bottom or the walls of the vial)..... 80

**Figure A2.** Chitosan microbeads in the cross-linking solution (2 wt% Span 80, 2 % by volume glutaraldehyde in hexadecane) after a five-day storage period. The beads are allowed to settle to the bottom before removing most of the cross-linking solution..... 81

**Figure A3.** Picture a) shows the vial of beads after removing the cross-linking solution and before adding the pure 1-decanol. After approximately half of the vial containing the beads is filled with 1-decanol, the transfer pipette is placed in the vial (b). Then, the vial is taped to the supporting platform and the nitrogen gas valve is opened (1-2 psi). Adding nitrogen gas to the solution will create convection and air bubbles (b). The configuration of the needles (covered with plastic transfer pipettes) that deliver the nitrogen gas is illustrated in both pictures.....81

## Chapter 1

# INTRODUCTION AND OVERVIEW

---

### 1.1. PROBLEM DESCRIPTION AND MOTIVATION

Through advances in scientific understanding and clever engineering, humankind has been able to mold and shape many facets of the world around them. Currently, there is a great deal of interest in engineering systems on smaller scales, i.e., in micro and nanotechnology.<sup>1,2</sup> Although there has been tremendous progress in this area, man-made micro and nanomaterials are still nowhere as intricate and functional as the systems designed by nature. The biological cell is still the most complex and sophisticated micro-nano machine ever created. An open question for researchers is whether it is possible to take inspiration from biology to bridge this gap between man-made and natural systems and thereby propel the next generation of micro/nanotechnology.

At the interface of biology, materials science, and chemistry many research groups have focused on developing cellular mimetic structures, and “artificial cells” (frequently referred to as protocells) with varying degrees of complexity.<sup>3-6</sup> In synthetic biology, this type of research employs a top-down approach using genetic engineering techniques and existing cell infrastructure in combination with synthetic components to manipulate complex functions associated with “life” (i.e. self replication).<sup>7</sup> Others have taken a bottom-up approach using simpler building blocks to design more primitive protocells with more basic functions, employing both biotic (i.e. DNA, proteins) and nonbiotic components.<sup>8,9</sup> Polymer microparticles represent a simple template for



protocells in the most basic form as a container at the microscale. The vast majority of research involving polymer microparticles has focused on end-user applications in areas such as cosmetics, chromatography, and drug delivery.<sup>10</sup> However, a few research groups have used bio-inspired design in the development of novel functionalities and applications for microparticles.<sup>11,12</sup>

Recently, the integration of microfluidic technology as a platform in microparticle synthesis has led to significant advancements in control over the size, shape, and functional properties of these particles.<sup>13,14</sup> This additional level of control opens further possibilities towards advancing new kinds of microparticles.<sup>15</sup> For example, cell-like compartments and hierarchal structures can now be mimicked through design of controlled double and triple emulsions.<sup>16</sup> Microfluidic platforms are now ubiquitous and inexpensive: they can be implemented even with simple capillary tubing and do not require expertise in lithography or microfabrication.

## **1.2. PROPOSED APPROACH**

What lessons can we learn from biology in the context of microparticle engineering? Two important observations to consider are the following:

- 1) Biological cells are specialized in design and function (e.g. red blood cells can transport oxygen but cannot produce insulin; conversely cells in the pancreas can secrete insulin but are not designed to transport oxygen).

- 2) Cells are biochemically designed to have capabilities for specific (targeted) interactions with their own unique environments (e.g. immune cells can recognize and target specific pathogens in blood).

In this dissertation we draw inspiration from biology to engineer microparticles that can selectively respond to their surroundings. Specifically, we design microparticles that can recognize and respond to particular species from their surroundings (e.g. cells, polymer chains, metal ions). These responses are designed to mimic functions associated with biological cells. Three examples of microbeads with bio-inspired recognition capabilities and functionalities are discussed in this work:

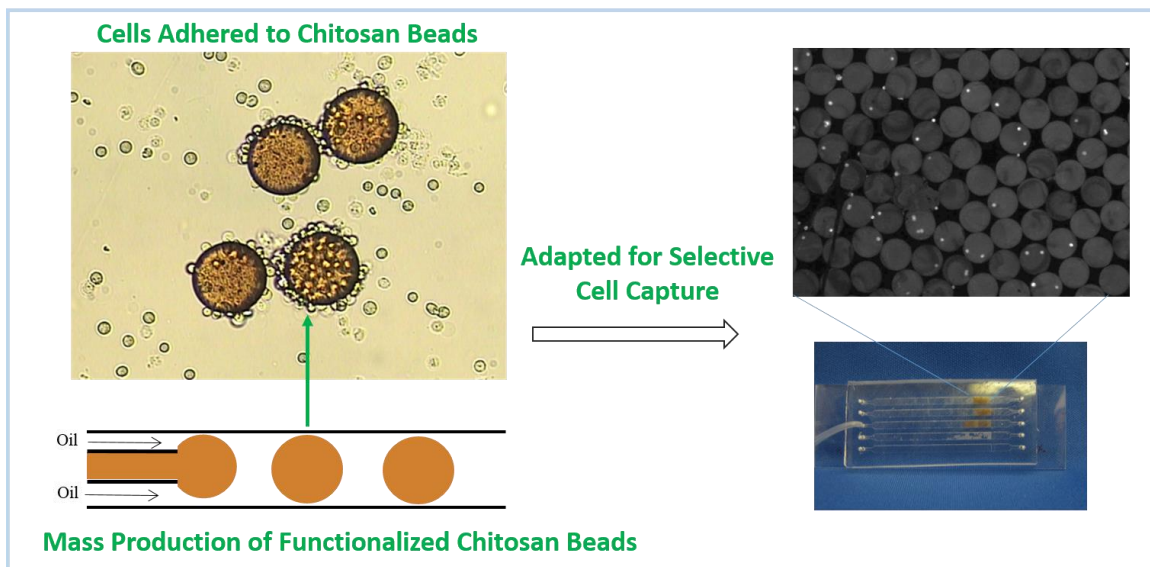


**Figure 1.1.** Cell-selective microbeads of the biopolymer, chitosan are used for capturing rare cells from blood. The microbead surface is modified with streptavidin. Cells coated with biotin selectively adhere to these beads.

### 1.2.1. Particles Capable of Capturing Specific Biological Cells

The surfaces of many biological cells are designed to selectively adhere to specific objects within their environment. For example, leukocytes within the immune system can adhere to various micron-sized objects such as foreign cells (pathogens) or even to other leukocytes and endothelial cells.<sup>17</sup> In Chapter 3, we develop polymer microparticles that can selectively adhere to a type of rare cells found in the blood of patients with metastatic cancer, called Circulating Tumor Cells (CTCs). The polymer microparticles are coated with the protein, streptavidin, which has the ability to recognize and adhere to objects coated with the small molecule, biotin. We first tag the CTCs with a biotinylated antibody and then flow it through a packed bed of the polymer microparticles within a microfluidic channel. The bound CTCs can then be detected by fluorescence microscopy (Figure 1.1). The concept of using a packed bed of custom-synthesized particles can be further adapted for detecting other kinds of rare cells such as stem cells in blood.

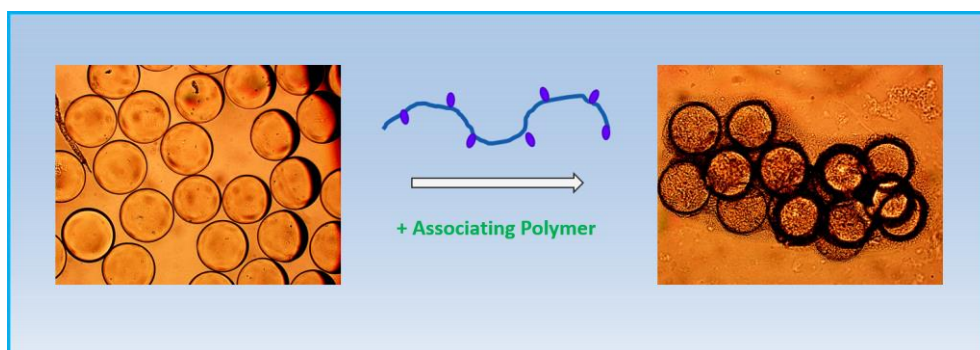


**Figure 1.2.** Microbeads that cluster in the presence of an associating polymer (i.e., a polymer with a hydrophilic backbone and hydrophobic pendant groups). Once the cluster forms, the polymer forms a precipitate around the cluster. The overall structure resembles a blood clot formed by blood platelets and the protein fibrin.

### **1.2.2. Particles that Cluster in the Presence of a Specific Polymer**

Next, in Chapter 4, we develop microparticles that mimic the cluster formation seen with platelets during blood clotting. Platelets are a specific class of cells present in blood. When a wound occurs, surface receptors on the platelets are reconfigured so that they become sticky to a water-soluble protein also present in blood, called fibrinogen. As a result, fibrinogen bridges platelets together to generate “platelet plugs” (weak clusters). At the same time, fibrinogen is polymerized into water-insoluble fibrin through activation of the enzyme thrombin. The precipitated fibrin forms a web that traps aggregates of platelets and surrounding red blood cells to form the blood clot.<sup>18</sup> In our work, we coat polymer microbeads with a hydrophobic supramolecule called cyclodextrin. These beads bind specifically to a soluble polymer that contains hydrophobic pendant groups. The binding results in clusters of the microbeads, which resemble “platelet plugs”. Subsequently, we find that the polymer precipitates out of solution in real-time, forming a web around the clusters (Figure 1.2), and this web can also trap surrounding inert objects. Thus, the overall structure is reminiscent of a blood clot.

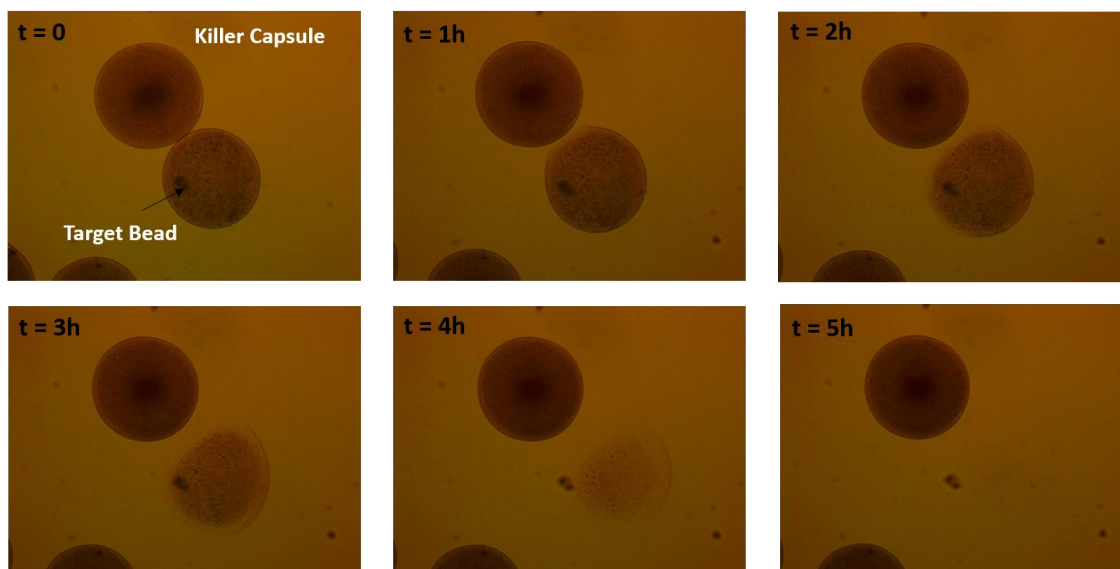


**Figure 1.3.** Killer capsules that can selectively target neighboring microbeads for destruction. Over time, the killer capsule releases molecules that remove the metal ion cross-links from the target microbead, thereby leading to its destruction.

### 1.2.3. Particles Engineered to Destroy Other Particles

Finally, in Chapter 5, we develop microparticles that can destroy a specific type of surrounding particle. The inspiration in this case is from the immune system, where cytotoxic T lymphocytes (also referred to as “killer T cells”) are able to selectively kill cells that are infected with pathogens and not harm the surrounding healthy cells in our body. In our work, we synthesize polymer capsules that contain an enzyme. In the presence of the substrate, glucose, the killer capsule releases a product that recognizes and chelates with metal ions. Correspondingly, we develop a second class of polymer bead that is crosslinked by the same metal ions. When the two particles are brought into close proximity, the product from the killer capsule ends up chelating the ions that crosslink the target bead, thereby resulting in the disintegration of the target bead (Figure

1.3). Other particles that are not dependent on metal ions for their crosslinking are not affected in this process.

### **1.3. SIGNIFICANCE OF THIS WORK**

The newly synthesized microparticles described in this dissertation are significant from two different standpoints: (1) the particles could have some direct applications in various technologies and (2) the studies lay a foundation for the design of biomimetic and bioinspired materials and processes.

Direct applications for our particles include biological detection (assays), microrobotics, drug delivery and controlled release, and embolization in the context of treating internal hemorrhage. For instance, the functionalized microbeads in Chapter 3 could provide an adaptable system for capturing and detecting rare cells in blood such as circulating tumor cells (CTCs) or stem cells. The microbead clustering system in Chapter 4 could be used as embolic agents to treat internal hemorrhage. Finally, the concepts in Chapter 5 involving destruction of specific target particles could be adapted for the localized and targeted release of drugs or other solutes in the context of drug delivery.

The larger significance of this thesis is in laying a foundation for the bioinspired design of complex microparticles. As emphasized earlier, the most “intelligent” and complex microsystems that currently exist have been designed by nature. Thus, endowing synthetic particles with “cell-like” functionalities could be a fruitful approach to guide new micro and nano technologies. We have specifically created structures and responses

that are reminiscent of those occurring during the blood clotting cascade or during the function of immune cells. In the coming years, as additional “cell-like” functionalities for microparticles are reported, such capabilities will hopefully be integrated to produce exceptionally “intelligent” and useful microparticles from what began as initially very simple building blocks. Finally, it is worth emphasizing that the starting materials used to synthesize our microparticles are all inexpensive and widely available, while the methods used for synthesis are also straightforward and easy to replicate. We therefore believe that our approaches can be easily adapted and used by others with minimal training.

## Chapter 2

# BACKGROUND

---

This dissertation focuses on the development of polymer-based microparticles with new bio-inspired functionalities. In this Chapter, we begin with a brief introduction to the polymers, notably the biopolymers chitosan and alginate, which are used throughout our studies. We then discuss the interactions of these polymers with various small molecules (e.g. metal ions, cyclodextrins); this will be relevant for the development of microbeads with specialized functions. Finally, we discuss the basics of optical and fluorescence microscopy.

## 2.1. BIOPOLYMERS

### 2.1.1. Chitosan

Chitosan is derived from the deacylation of chitin, a linear polysaccharide found in the hard exterior of insects and crustaceans.<sup>19</sup> In terms of abundance, after cellulose, chitin is the world's second most common biopolymer. However, chitin is insoluble in water, which limits use in potential applications. Through deacetylation of chitin, the water soluble derivative (chitosan) is formed. The free amine groups along the chitosan backbone, which were made available through deacetylation, are ionized under acidic conditions, allowing for solubility of chitosan in water.<sup>20</sup> The protonation of the amine groups under acidic conditions also causes the chitosan backbone to have a net positive charge.<sup>21</sup> Chitosan is a copolymer of majority  $\beta$ -(1,4) linked D-glucosamine (deacetylated



unit) sugars and the remaining N-acetyl-D-glucosamine sugars from the parent polymer, chitin. The chemical structures of these sugars are shown in Figure 2.1.

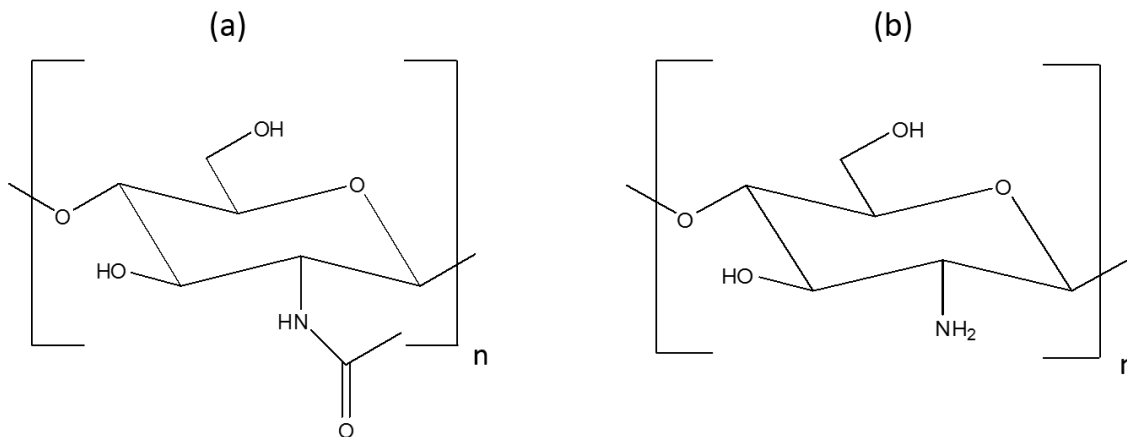


**Figure 2.1.** Structures of the monomer sugars in (a) chitin and (b) chitosan. The N-acetyl-D-glucosamine sugar in chitin is deacetylated to generate the D-glucosamine sugar in chitosan.

Chitosan is used in a variety of applications, ranging from tissue engineering to wound dressings to environmental remediation to drug delivery, due to its beneficial properties.<sup>19,20</sup> It is not only a biodegradable and biocompatible polymer, but is also one of the few cationic biopolymers. This confers antibacterial properties to chitosan, which can be useful in tissue engineering and for wound dressings. Moreover, chitosan is inexpensive and readily available; the parent polymer, chitin, is often obtained from food processing waste (e.g. crab and shrimp shells).<sup>2</sup> Additionally, many researchers have explored various chemical modifications in attempts to augment chitosan's already existing functional properties.<sup>22,23</sup> One type of modification is to graft hydrophobic groups to the free amines on the chitosan sugars, which is discussed below.

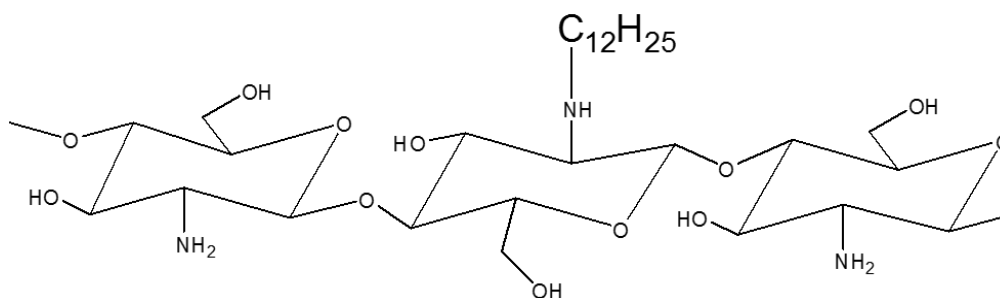


**Figure 2.2.** Chemical Structure of hydrophobically-modified chitosan with  $C_{12}$  hydrophobic tails.

### 2.1.2. Hydrophobically-Modified Chitosan

Chitosan can be easily modified due to the free amines that are available on each glucosamine sugar. This allows the synthesis of hydrophobically-modified chitosan (hm-chitosan) to be fairly straightforward; the free amines can be targeted by reaction with n-alkyl-aldehydes via reductive amination.<sup>24</sup> In this reaction, the primary amine groups are converted into NH-R groups, where R is the n-alkyl moiety. In this study,  $C_{12}$  hydrophobic tails were grafted to the chitosan chains as the n-alkyl moiety. The structure of hm-chitosan containing  $C_{12}$  hydrophobic tails is shown in Figure 2.2. A general procedure for synthesizing hm-chitosan with  $C_{12}$  tails involves the following steps. First, chitosan is dissolved in an acidic water-ethanol mixture and then exposed to n-dodecyl aldehyde. Then sodium cyanoborohydride is added to complete the reductive amination reaction, which yields hm-chitosan. The hm-chitosan is then precipitated by increasing the pH with the addition of sodium hydroxide. Next, the precipitate is washed multiple times in ethanol and subsequently in deionized water to remove any residual unreacted sodium cyanoborohydride, which is highly toxic. The purified hm-chitosan precipitate is then vacuum dried, re-dissolved in acetic acid solution; this solution tends to be more viscous than unmodified chitosan due to associations between hydrophobes,

which serves as a useful qualitative indication that the modification of chitosan has been successful. The degree of hydrophobic substitution in the final product corresponds to the initial molar ratio of aldehyde to chitosan monomer(s). This stoichiometrically expected degree of hydrophobic substitution in the final product can be confirmed using NMR.

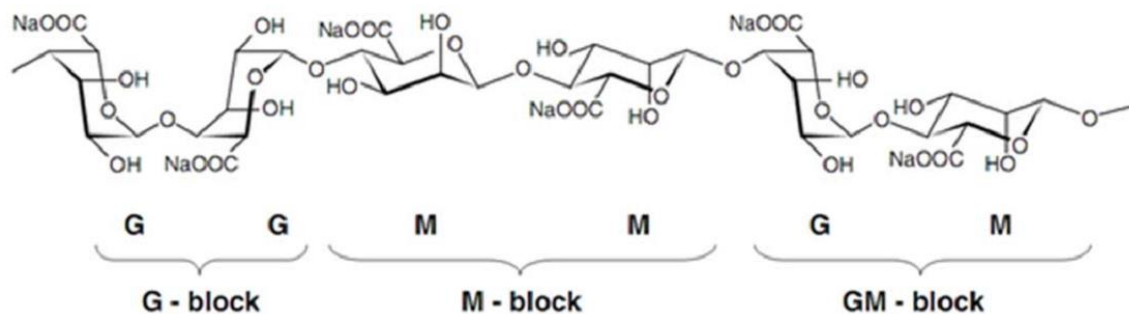


**Figure 2.3.** Chemical Structure of sodium alginate (adapted from Javvaji<sup>25</sup>)

### 2.1.3. Alginate

Sodium alginate, which is derived from brown algae, is another common polysaccharide. Due to its ease of crosslinking, biocompatibility, abundance, and low cost, alginate has been extensively studied as a biomaterial. Applications include wound healing, drug delivery, and cell transplantation for tissue engineering.<sup>26</sup> Sodium alginate is a linear unbranched polymer made up of blocks of 1,4-linked β-D mannuronic (M) and α-L guluronic (G) residues.<sup>27</sup> Figure 2.3 demonstrates a general chemical structure of sodium alginate. Unlike chitosan, alginate is an anionic biopolymer that can interact with positively charged ions. Specifically, G-blocks of adjacent linear polymer chains can be cross-linked through formation of “egg-box” junctions with multivalent cations (e.g. Ca<sup>2+</sup>, Sr<sup>2+</sup>, or Cu<sup>2+</sup>). This concept is illustrated in Figure 2.4 with calcium ions; the formation of

these egg-box junctions results in the conversion of liquid alginate solution into a cross-linked alginate hydrogel. The strength and stiffness of these hydrogels are dependent on the concentrations of alginate and the multivalent cation, as well as on the type (source) of the alginate (because different sources of alginate have varying molecular weights and varying ratios of M/G content).<sup>28</sup>

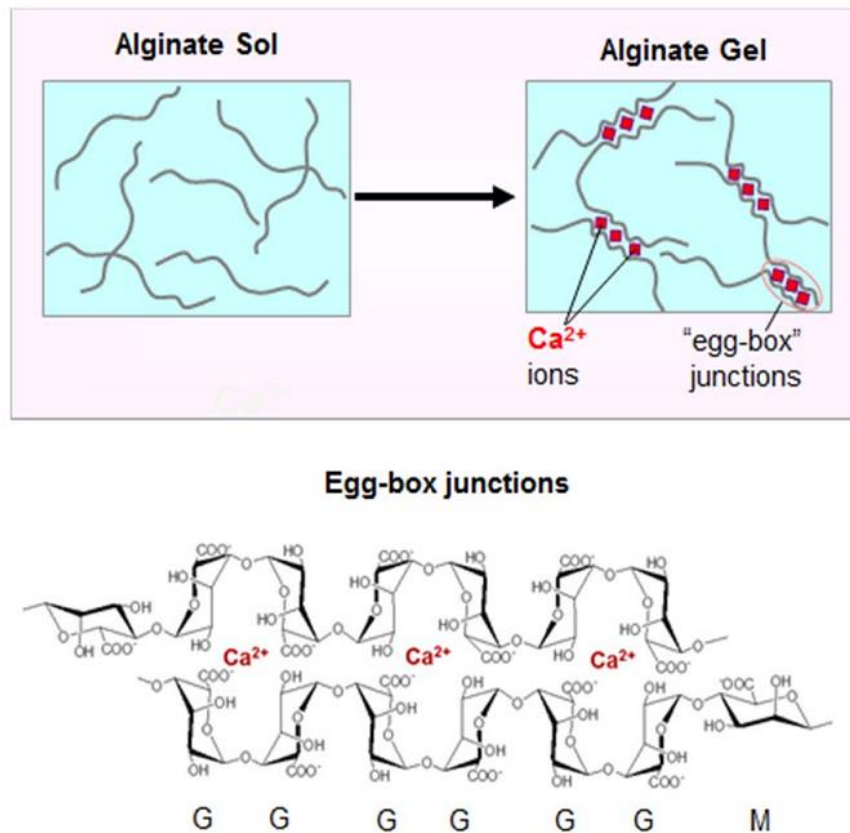


**Figure 2.4.** Schematic demonstrating gelation of alginate upon addition of calcium ions through “egg-box” junctions (adapted from Javvaji<sup>25</sup>).

## 2.2. INTERACTIONS OF BIOPOLYMERS

### 2.2.1. Chitosan and Chemical Cross-linkers

As mentioned earlier, native chitosan can be dissolved in acidic water. This polymer solution can be easily converted into a gel through chemical crosslinkers such as dialdehydes.<sup>29</sup> In particular, glutaraldehyde is a crosslinker for chitosan that is both soluble in water and in oily liquids. Since our droplet generators (Chapters 3 and 4) involve use of a continuous oil phase to shear and stabilize the aqueous droplets, glutaraldehyde can be introduced in the oil phase and it can diffuse into the aqueous chitosan droplets and thereby crosslink them into crosslinked structures.<sup>30</sup>

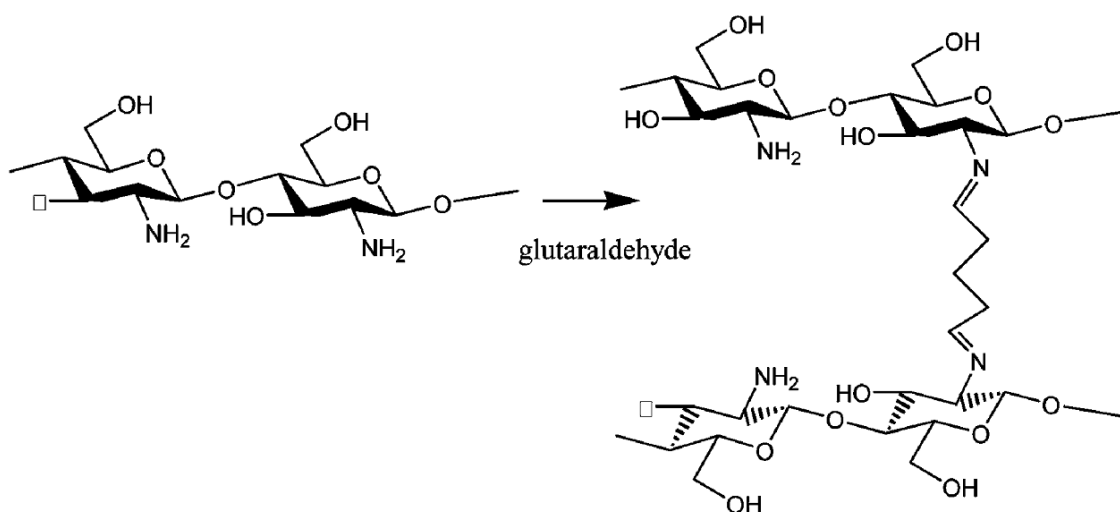


**Figure 2.5.** Schematic demonstrating the crosslinking of chitosan with glutaraldehyde (adapted from Macquarrie<sup>29</sup>).

Chitosan solutions can also be gelled non-covalently using multivalent anions like sodium tripolyphosphate (TPP). In solution, the positively charged amino group ( $\text{NH}_3^+$ ) of chitosan and  $\text{P}_3\text{O}_{10}^{5-}$  anions of TPP electrostatically bind to induce a rapid gelation of the solution.<sup>31</sup>

## 2.2.2. Hydrophobically Modified Chitosan and Cyclodextrins

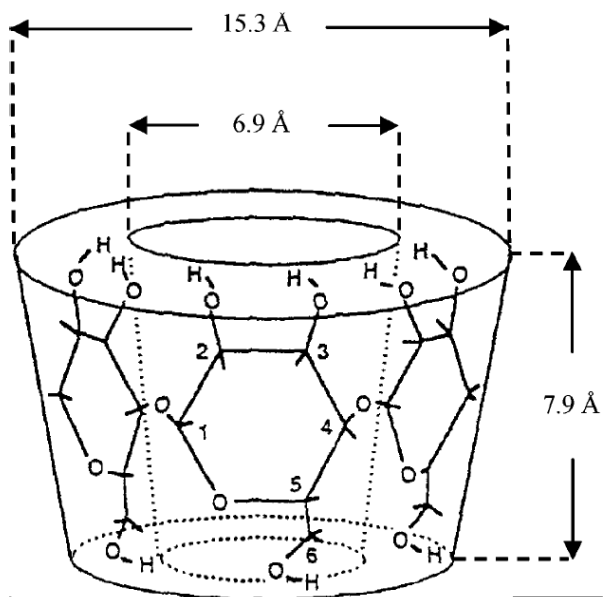


**Figure 2.6.** Truncated cone-shaped structure of  $\beta$ -cyclodextrin (adapted from Galant<sup>32</sup>).

Cyclodextrins (CDs) are cyclic oligosaccharides, typically composed of 6-8  $\alpha$ -D-glucopyranose units, that form a rigid truncated cone-shaped structure with an internal cavity size of 5-8 Å, depending on the number of glucopyranose units.<sup>32</sup> Interestingly, all the hydroxyl groups are located on the outside of the molecular cavity, thereby creating a hydrophilic outer surface with a relatively hydrophobic inner cavity. These hydrophobic pockets, can form host-guest inclusion complexes with various hydrophobic guest molecules.<sup>33</sup> It should be noted that binding between the cyclodextrin host and the guest hydrophobic molecule is through non-covalent interactions, allowing the binding to be reversible.

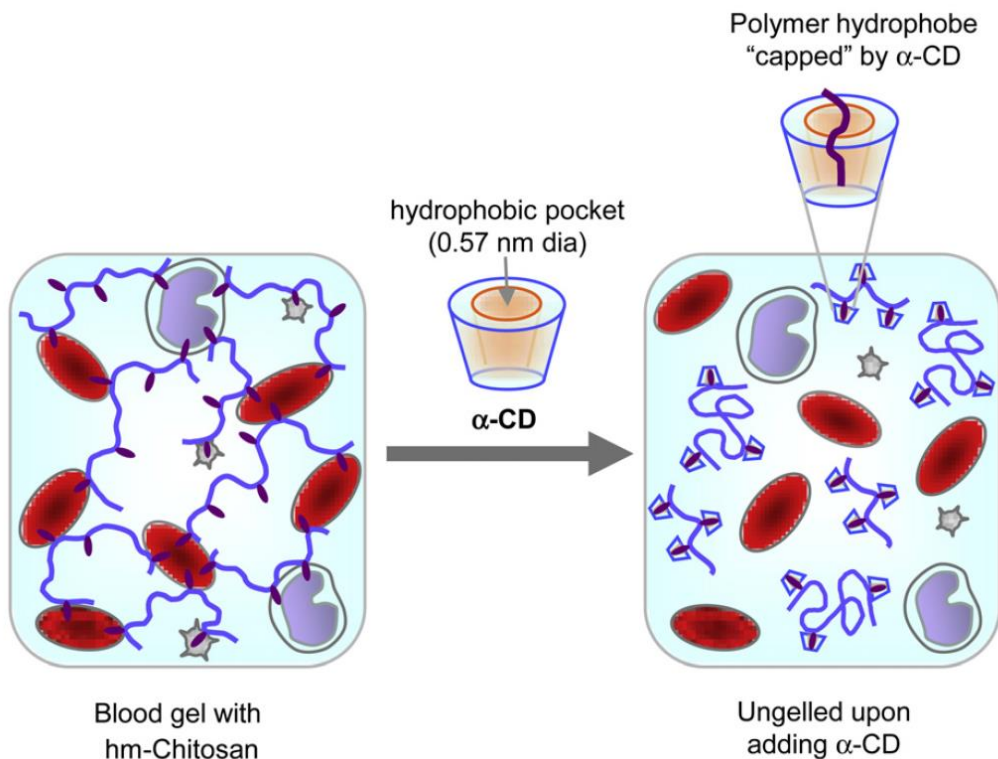
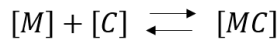


**Figure 2.7.** Effect of adding  $\alpha$ -CD to a gel formed by combining blood with hm-chitosan. Gelation is due to the bridging of adjacent cells into a network via polymer chains. The addition of  $\alpha$ -CD reverses the gelation, as shown on the right (adapted from Dowling<sup>34</sup>).

Our group has previously studied how hydrophobically modified chitosan (hm-chitosan) interacts with vesicles and biological cells, both of which are covered by lipid bilayers.<sup>34-36</sup> This interaction results in the formation of a gel, as shown in Figure 2.7. The driving force is the hydrophobic interaction between the hydrophobes on the polymer and the bilayers of cells/vesicles. Due to such interactions, polymers bind to cells, and this results in the cells being bridged by polymer chains into a 3-D network. Furthermore, this gelation was found to be reversible through addition of  $\alpha$ -CD. The hypothesis is that  $\alpha$ -CD molecules form inclusion complexes with the hydrophobes on hm-chitosan, thereby freeing the blood cells from the network (Figure 2.7).

#### 2.1.4. Alginate Hydrogel Dissolution via Chelators

As mentioned previously, alginate can be easily cross-linked into a gel using multivalent cations (e.g.  $\text{Ca}^{2+}$ ,  $\text{Sr}^{2+}$ ,  $\text{Cu}^{2+}$ ) that form “eggbox” junctions between adjacent alginate chains. Conversely, the removal of these cations from the the junctions leads to degradation or dissolution of the alginate hydrogel. Many chemical chelators (e.g. EDTA) can strongly bind to cations and thus can induce gel dissolution.<sup>37</sup> The binding is commonly represented through a stability constant,<sup>38</sup> which is defined as below:



$$K = \frac{[MC]}{[M][C]}$$

$$\text{Stability Constant} = \text{Log} (K)$$

where [M] is the concentration of the (metal) cation, [C] is the concentration of chelator, and [MC] is the concentration of the metal-chelator complex. Stability constants are equilibrium constants (expressed as a logarithm) of the above chelator-metal binding. Higher stability constants indicate strong chelation. Stability constants for commonly used chelators for divalent cations are summarized in Table 2.1. Note that gluconate ions have a high stability constant with copper ( $\text{Cu}^{2+}$ ) ions. We will explore the use of gluconate ions to remove  $\text{Cu}^{2+}$  crosslinks from an alginate bead in Chapter 5.

	Calcium ( $\text{Ca}^{2+}$ )	Strontium ( $\text{Sr}^{2+}$ )	Copper ( $\text{Cu}^{2+}$ )
EDTA	10.6	8.68	18.7
Gluconic Acid	1.21	1.01	18.3
Citric Acid	3.50	3.05	5.90

**Table 2.1.** Stability constants for common divalent cations and chelators.<sup>39</sup>



## 2.3. OPTICAL MICROSCOPY

### 2.3.1. Brightfield and Phase Contrast Microscopy

For the microparticles described in this dissertation, visual observations through brightfield microscopy offer a simple means to characterize them. In brightfield microscopy, objects are visualized through intensity differences between the specimen and the surroundings. For instance, when observing a polymer microparticle that is opaque or translucent, much of the light that is directly hitting the particle is absorbed, resulting in reduced intensity, whereas the light that does not hit the particle remains at the original intensity.<sup>40</sup> This contrast allows real-time visualization of changes in microparticle morphologies (e.g. clustering, degradation). Overall, brightfield microscopy can be used to image objects that are larger than the wave length of visible light (400-700 nm).

When imaging a transparent microparticle, the contrast, i.e., the intensity difference between the absorbed and surrounding light is reduced. However, through the use of phase-rings, one can modify conventional absorption-based brightfield techniques to provide greater contrast.<sup>40</sup> Phase contrast takes advantage of the relationship between diffracted light from the specimen and the undiffracted background light. Diffraction of light by the specimen causes a phase shift—the light passing through the specimen slows down ( $\approx \frac{1}{4}$  of a wavelength) due to the difference in refractive index between the specimen and surrounding air (Figure 2.8). Alternatively, the surrounding light that passes through with no diffraction remains in phase (S wave) and meets the diffracted light waves (D wave) at the objective lens where they destructively interfere to generate a

resultant particle wave (P wave), which determines the contrast with which we see the specimen.<sup>40</sup> Maximizing this destructive interference generates the most contrast between the sample and the surroundings. Thus, the ratio of the amplitudes of the S and D waves are the most important variables for enhancing contrast. Since only a small fraction of incident waves are diffracted by typical objects, in traditional brightfield microscopy, the destructive interference from diffraction is hardly noticeable with the human eye. Thus, phase rings are used to absorb more surrounding S waves (reducing the overall amplitude of the S waves) and advance the S waves out of phase to the point of maximum destructive interference with the D waves (Figure 2.9).

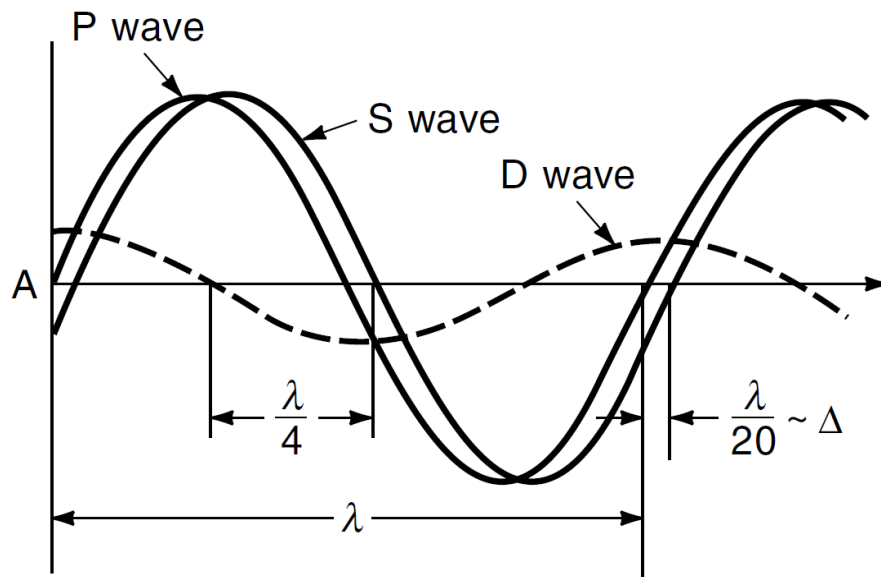


**Figure 2.8.** Phase relations between S, D and P waves in brightfield microscopy. The D wave is slowed by  $\frac{1}{4}$  of a wavelength relative to the S wave, upon diffracting at the object, causing minimal destructive interference with the S wave to generate the resultant P wave (adapted from Murphy<sup>40</sup>).

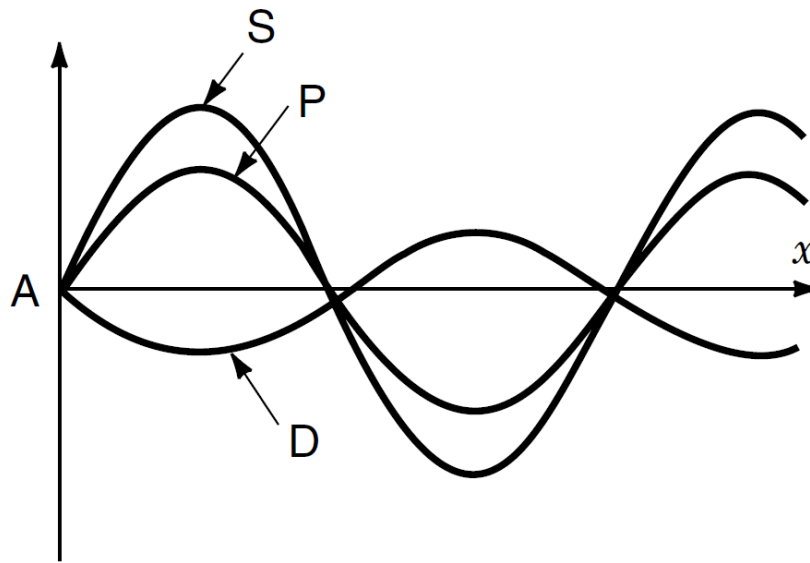


**Figure 2.9.** Phase relations between S, D and P waves in phase contrast microscopy. The S and D wave have maximized destructive interference to generate a resultant P wave that allows for greater contrast in the image (adapted from Murphy<sup>40</sup>).

### 2.3.2. Fluorescence Microscopy

Fluorescence microscopy allows for easy visualization of fluorescently labeled objects, which stand out in high contrast compared to the untagged surrounding environment. Throughout this dissertation, various elements of our microsystems are tagged with fluorescent markers to enable their tracking via fluorescence microscopy. Unlike brightfield microscopy, which relies on transmitted light, fluorescence microscopy relies on reflected light.<sup>40</sup> Sharp contrast between the specimen and environment is achieved through the use of excitation and emission filters to allow for specific detection of only the fluorescently labeled specimen. As shown in Figure 2.10, the basic components of a fluorescence microscope comprise a light source, excitation and emission filters, dichroic mirror, and a detector. The source light is first passed through an excitation filter and then is reflected off the dichroic mirror towards the sample. The

fluorescently labeled sample, upon excitation, then emits fluorescence at a lower frequency (i.e. higher wavelength) that passes through the dichroic mirror and emission filter to be collected by the detector.<sup>40</sup>

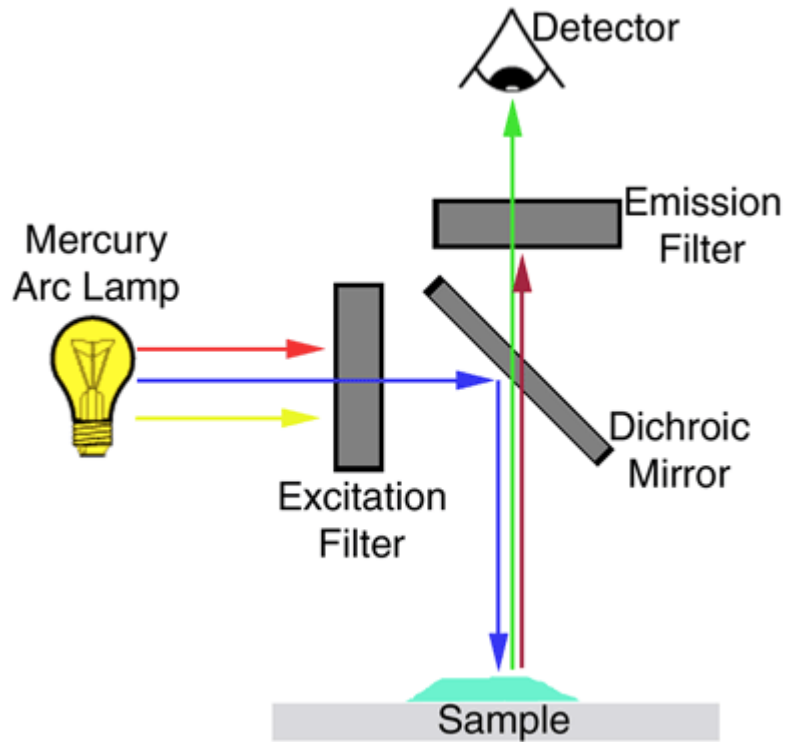


**Figure 2.10.** Schematic showing the light path in fluorescence microscopy (adapted from [www.jic.ac.uk](http://www.jic.ac.uk)).

## Chapter 3

# MICROPARTICLES FOR CAPTURE OF RARE CELLS FROM BLOOD\*

---

\*The results presented in this Chapter have been published in the following journal article: Chandamany Arya, Jason G. Kralj, Kunqiang Jiang, Matthew S. Munson, Thomas P. Forbes, Don L. DeVoe, Srinivasa R. Raghavan, and Samuel P. Forry, “*Capturing Rare Cells from Blood Using a Packed Bed of Custom Synthesized Chitosan Microparticles.*” *Journal of Materials Chemistry B*, 1, 4313-4319 (2013).

### 3.1. INTRODUCTION

The surfaces of many biological cells are designed to selectively adhere to specific objects within their environment. For example, leukocytes within the immune system can adhere to various micron-sized objects such as foreign cells (pathogens) or even to other leukocytes and endothelial cells.<sup>17,41,42</sup> Cellular adhesion relies on an array of specific biochemical interactions between the surface of one object and another. This ability of surfaces to recognize and bind to specific counterparts is also at the core of many diagnostic devices and assays. In this study, we apply the same surface-recognition concepts for the synthesis of functionalized microbeads, and we then adapt these microbeads for a diagnostic application.

Over the past decade, there has been much interest in the isolation of rare cells such as circulating tumor cells (CTCs) or stem cells from whole human blood. Rare cell isolation remains a technical challenge because these cells are present in low numbers relative to red and white blood cells.<sup>3,43,44</sup> For example, hematopoietic stem cells are estimated to occur at a frequency of 1 per  $10^5$  blood cells and for patients with metastatic

cancer, just 1 per  $10^9$  blood cells are estimated to be CTCs. Isolation of these rare cells is thereby especially challenging as large quantities of other cells must be sorted and removed to provide sufficient purity of CTCs. Due to low throughput, conventional techniques for cell purification using fluorescence-activated cell sorting (FACS) are limited in CTC isolation.<sup>45</sup> A wide variety of other approaches to capture CTCs from whole blood have been used. Some groups have used size-based techniques for isolation of CTCs,<sup>46</sup> which are usually larger than leukocytes; however, CTCs originating from different tissues (i.e. different types of cancer) have varying size distributions.<sup>47</sup> Other groups have used buoyancy and density based methods for CTC isolation.<sup>48,49</sup> However, these methods are typically insufficient in isolation purity.<sup>45</sup> Other methods for isolation involve targeting distinguished CTC surface markers using antibodies. Most commonly, these antibodies target the surface marker EpCAM (epithelial cell adhesion molecule), which is highly expressed on many epithelial cancer cells and thereby CTCs.<sup>50</sup> It should be noted that although EpCAM is the most commonly used marker to capture CTCs, expression levels of EpCAM can vary based on the type of cancer. For instance, high expression of EpCAM is found in 95% of colon cancers, and only in 40% of breast cancers.<sup>50</sup> The only current FDA-approved CTC detection technique (CellSearch™) involves targeting EpCAM; the technique relies on bulk mixing of whole blood with paramagnetic anti-EpCAM coated nanoparticles.<sup>43</sup>

Compared to this bulk-mixing technique, microfluidic methods promise to substantially increase the capture efficiency due to their higher surface-to-volume ratios.<sup>47,51</sup> One popular microfluidic device for CTC capture relies on an array of

antibody-coated posts to further enhance the contacts between cells and antibodies.<sup>3</sup> However, such devices are expensive and difficult to construct, especially for researchers who do not have specialized training in microfabrication techniques.

Recently, a new design was introduced in collaboration with Dr. Forry's group at NIST wherein near-monodisperse polystyrene beads (diameter  $\approx 150 \mu\text{m}$ ) were packed into a bed within a microchannel containing a weir.<sup>52</sup> The beads were commercially available with a surface functionality comprising the linker protein avidin. Pre-stained EpCAM expressing breast cancer cells were spiked into whole blood as a model CTC sample. After the addition of anti-EpCAM antibodies that were conjugated with biotin, this blood was pumped through the packed bed of avidin coated polystyrene microbeads. Cells labeled with the biotinylated anti-EpCAM became bound to the beads through biotin-avidin interactions and were enumerated through fluorescence microscopy.

In this Chapter, we describe a similar device where, instead of commercial polystyrene beads, we develop custom-manufactured microbeads of the biopolymer, chitosan. Chitosan is derived from the deacetylation of chitin, a polysaccharide found in the exoskeleton of crustaceans and insects.<sup>53</sup> It is inexpensive and abundant (chitin is the world's second most common biopolymer),<sup>54</sup> commercially available, water soluble below pH 6, and easily functionalized through its primary amine groups that allow covalent attachment of enzymes, antibodies, and DNA.<sup>54</sup> The chitosan microparticles are created in-house using a microfluidic tubing device, with two-phase flow being used to generate uniform droplets that template monodisperse microbeads.<sup>55-61</sup> The tubing

device allows uniform particles to be prepared continuously in a single step at a throughput of about 5000 particles/h. No training in microfabrication techniques is necessary for preparing the particles. The microbeads are then functionalized by reaction with the primary amines along the chitosan backbone, allowing covalent attachment of the protein streptavidin. The core of the microbeads can also be put to use by encapsulating moieties of interest in it such as magnetic nanoparticles, fluorescent markers or other optical stains. Here, we encapsulate carbon black within the microbeads as a means to attenuate their auto-fluorescence. The final functionalized chitosan microbeads are packed into a bed and used to capture cancer cells spiked into whole blood at physiologically relevant densities. Captured cells are enumerated using fluorescence microscopy. Overall, the microbeads used here are low-cost and versatile, and their use within a microfluidic packed bed could prove to be a viable approach for capturing CTCs or other rare cells.

### 3.2 EXPERIMENTAL SECTION

**Materials and Chemicals.** Chitosan (medium molecular weight; degree of deacetylation  $\approx 80\%$ ), the nonionic detergent SPAN80, nonpolar solvent hexadecane, the reducing agent sodium cyano-borohydride, the cross linking reagent glutaraldehyde (grade 1, 70%), 1-decanol, phosphate buffer saline (PBS, P4417), Albumin from bovine serum (BSA), and streptavidin (from *Streptomyces Avidinii*) were obtained from Sigma-Aldrich. Ethyl Alcohol was obtained from Pharmco-AAPER (180 Proof). Carbon black (N110) was obtained from Sid Richardson Carbon Company, fluorescent biotin (Atto 590-Biotin) was obtained from Santa Cruz Biotechnology, small biotinylated polystyrene spheres



were purchased from Spherotech ((6-8)  $\mu\text{m}$ ), biotinylated anti-EpCAM was purchased from AbCAM (ab79079), and DiI, the fluorescent cell stain, was purchased from Life Technologies (V-22885).

**Tubing Device Design.** Two-phase flow was generated in a microtubing device. Oil and aqueous chitosan solutions were loaded in plastic syringes (BD part # 301030) and pumped through an annular junction as shown in Figure 3.1. The aqueous solution was pumped (1.5  $\mu\text{L}/\text{min}$ ) through silica capillary tubing (i.d. 150  $\mu\text{m}$ , o.d. 260  $\mu\text{m}$ ; SGE Analytical Science), inserted inside PTFE microtubing (i.d. 300  $\mu\text{m}$ ; Cole Parmer), which carried the immiscible oil phase (30  $\mu\text{L}/\text{min}$ ). Fluidic connections to the silica capillary and PTFE microtubing were made using five-minute epoxy (Devcon) and Luer-lock fittings (1/16" hose barb; Cole Parmer). The rate of aqueous shearing and droplet formation depended on the oil and aqueous phase flow rates and was controlled using two independent syringe pumps (New Era Pump Systems Inc.; part # NE-300).

**Chitosan Microbead Synthesis.** Two-phase flow was generated by a continuous oil phase (2 % by weight SPAN80 in hexadecane) and a dispersed aqueous phase (2 % by weight chitosan in DI water); flow rates used for the aqueous phase and continuous phase were 1.5  $\mu\text{L}/\text{min}$  and 30  $\mu\text{L}/\text{min}$ , respectively. For generation of carbon black encapsulated chitosan microbeads, the chitosan solution was mixed with 1 % by weight carbon black, prior to injection into the syringe. The droplets generated from the tubing device were collected in a cross-linking solution (2 % by weight glutaraldehyde, 2 % by weight SPAN80 in hexadecane) with gentle stirring. Chitosan droplets were collected

over 20 h to generate over  $10^5$  chitosan microparticles. The microparticles were left to incubate in the cross-linking solution overnight. They were then washed, by allowing the beads to settle to the bottom of the solution and replacing the existing solution, in a series of solvent exchange steps: pure hexadecane (5 times), 1-decanol (5 times), ethanol (5 times) and PBS (5 times). After washing, the chitosan microparticles did not aggregate and they also retained their original monodispersity; however, their size shrank by  $\approx$  40 % through cross-linking and solvent exchange. The final diameters of the chitosan microbeads were measured using brightfield transmission microscopy images. The images were analyzed in MATLAB, using a Hough Transformation to measure their projected diameter.<sup>62</sup> This approach is susceptible to error in determining the absolute particle size (due primarily to accurate edge determination), but provides a good assessment of size heterogeneity between particles. The measured sizes from individual microparticles (n=91) were then arranged as a histogram (bin size = 6.5  $\mu$ m) in Figure 3.2 along with a Gaussian fit to the data.

**Functionalization of Chitosan Microbeads.** Chitosan microbeads in PBS were exposed to glutaraldehyde (8 % by weight, 2 h) and washed in PBS (3 times). The microparticles were then exposed to either BSA or streptavidin (100  $\mu$ g/mL in PBS) overnight at 4 °C, and sodium cyano-borohydride (1 % by weight, 30 minutes) was added to fix the binding between the chitosan microparticles and streptavidin.<sup>63</sup> Finally the chitosan microbeads were washed in PBS (7 times). Fluorescent intensity was measured on an inverted fluorescent microscope (Axio Observer, DI, Zeiss; 60 $\times$  magnification, using a TRITC filter set (excitation at (520-570) nm; emission at (535-675) nm) and compared between

samples containing 0 % by weight and 1 % by weight carbon black as outlined in Figure 3.3. Functionalization of the streptavidin was tested using fluorescently labeled biotin. The streptavidin functionalized beads were incubated in a working concentration of 4  $\mu\text{g}/\text{mL}$  Atto-590 biotin, overnight at 4 °C. The beads were washed in PBS (7 $\times$ ) and then the fluorescent intensity was measured using the TRITC filter set. Functionalization at the bead surface was verified by mixing the streptavidin functionalized chitosan microbeads with biotinylated polystyrene microspheres (500 000 beads/mL) on a rotary shaker (90 RPM, 30 min). Similarly, human breast cancer cells (MCF-7, cultured as described previously<sup>52</sup>) were functionalized by incubation with biotinylated anti-EpCAM (0.2  $\mu\text{g}/\text{mL}$ ) for 30 minutes, and the cells were washed in PBS (3 $\times$ ). Binding of biotinylated cells to streptavidin-functionalized chitosan microbeads was tested (Figure 3.7) by mixing the MCF-7 cells (100 000 cells in 1 mL PBS) with the chitosan microbeads on a rotary shaker (90 RPM, 30 minutes).

**Rare Cell Capture Device and Experiments.** Streptavidin functionalized chitosan microbeads that encapsulated carbon black were used for the rare cell capture in a microfluidic device. The experiments testing for rare cell capture in a PDMS microfluidic device were similar to previous work<sup>52</sup>, except chitosan microbeads were used instead of polystyrene particles. MCF-7 cells were stained with a membrane dye (DiI, Life Technologies), following the manufactures recommendations, and spiked into whole human blood at known densities to mimic clinical CTC samples. Biotinylated anti-EpCAM (0.2  $\mu\text{g}/\text{mL}$ ) was then added to the blood sample, directly labeling the EpCAM expressing cancer cells for capture on the streptavidin-functionalized microfluidic packed

bed. The whole blood samples were then pumped through the microfluidic packed bed. Immobilized MCF-7 cells within the microfluidic packed bed were washed with 200  $\mu$ L PBS and then identified by fluorescent intensity in ImageJ.<sup>64</sup>

### 3.3. RESULTS AND DISCUSSION

#### 3.3.1. Generation of Chitosan Microbeads

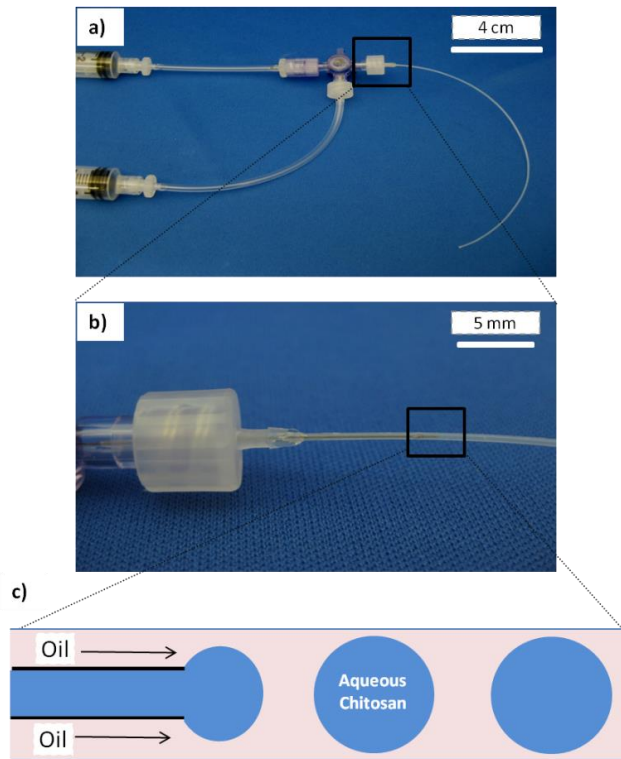


**Figure 3.1.** Photographs and schematic of the tubing device used to generate chitosan microbeads. The device (a) is formed by inserting capillary microtubing into slightly larger PTFE tubing. A close-up of the device is shown in (b) and a schematic at the junction between the two phases is shown in (c). An aqueous chitosan solution is pumped through the inner tubing. Oil pumped through the outer tubing exerts shear on the aqueous phase at the annular junction, causing uniform microdroplets containing chitosan to break away and flow down the tubing. These microdroplets are collected and cross-linked into uniform microbeads.

We used a co-flow tubing device made with commercially available tubing (Figure 3.1a) to synthesize the chitosan microbeads. Others have reported using similar devices to generate droplets.<sup>65,66</sup> This device allowed a stream of oil (hexadecane) in the annulus region to contact an aqueous stream containing dissolved chitosan in the inner tube. The oil flow sheared the aqueous chitosan solution into uniform spherical droplets (Figure 3.1b). The droplet size correlated with the inner diameter of the outer tubing and therefore the size could be varied by appropriate selection of the tubing. Using the tubing device, regular chitosan droplets were formed continuously at a rate of  $\approx 5000$  per hour.

Chitosan droplets were converted to microbeads using glutaraldehyde as the cross-linker similarly to previous microfluidic studies, where chitosan microbeads were manufactured using microfluidic T-junctions.<sup>30</sup> Using the co-flow tubing device, the aqueous chitosan droplets were collected in a solution of glutaraldehyde in hexadecane and were left to cross-link for  $\geq 20$  h. We typically synthesized batches of about  $10^5$  discrete beads. The beads were transferred from the hexadecane phase to an aqueous buffer (phosphate-buffered saline, PBS) by a series of solvent exchange washing steps. In PBS, the beads remained stably dispersed (i.e. no aggregation) for over 2 years. Figure 3.2a shows a bright-field optical micrograph of the beads. The size distribution determined from these micrographs (Figure 3.2b) shows that the microbeads have a narrow size distribution (4.3% RSD). Thus, our method yields near-monodisperse chitosan microbeads at a reasonably high throughput.

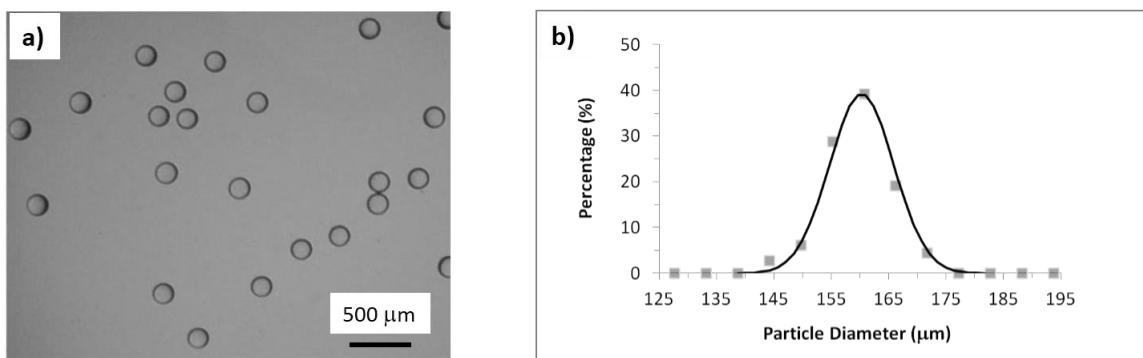


**Figure 3.2.** Particle Sizing. Optical micrographs of chitosan microbeads (a) showed that the microbeads were uniform and nearly monodisperse. The mean particle diameter (b) was  $\approx 164 \mu\text{m}$  with a relative standard deviation of 4.3% ( $n = 91$ ). The solid line in (b) is a Gaussian fit to the data.

### 3.3.2. Functionalization of Chitosan Microbeads

Chitosan microbeads cross-linked with glutaraldehyde exhibit an intrinsic autofluorescence across multiple wavelengths (Figure 3.3a,b), as has been noted before.<sup>67-68</sup> Here, the autofluorescence is not a desirable feature since it could interfere with the enumeration of cells by fluorescence microscopy.<sup>69</sup> Others have shown carbon black, a nanoparticle pigment, as a fluorescence quencher.<sup>70</sup> To attenuate the autofluorescence in the chitosan microbeads, we encapsulated nanoparticles of carbon black (nominal size 12 nm). For this, 1 % by weight of carbon black was dispersed in the aqueous chitosan solution used in the tubing device. Chitosan droplets bearing carbon black were cross-linked by glutaraldehyde as before. The resulting microparticles containing carbon black (Figure 3.3c,d) were almost completely opaque and showed a 50-fold reduction in detectable autofluorescence across multiple wavelengths. This enabled fluorescent cell detection without interference from the native chitosan autofluorescence (Figure 3.4).

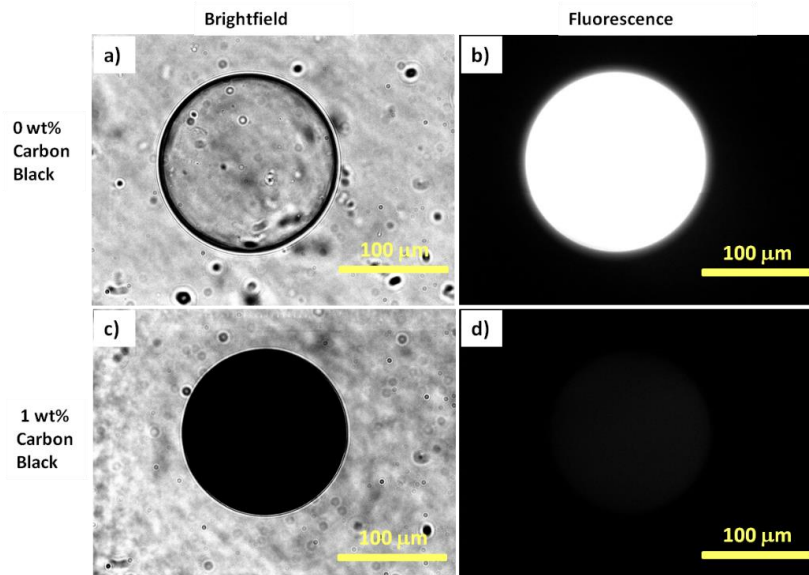


**Figure 3.3.** Chitosan encapsulation of carbon black nanoparticles. Bare chitosan microbeads cross-linked by glutaraldehyde (a, b) were transparent and exhibited an intrinsic autofluorescence. By encapsulating 1 % by weight carbon black (c, d), the microbeads were rendered opaque, and autofluorescence was reduced 50-fold. (Image contrast is identical for (b) and (d).)

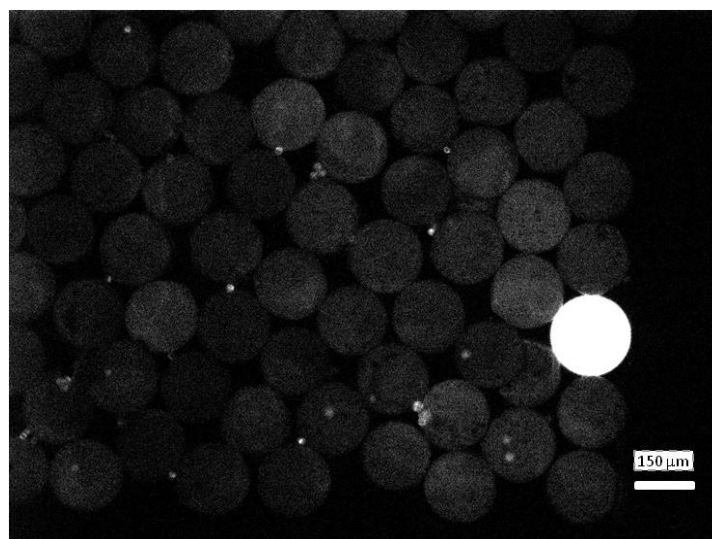


**Figure 3.4.** Fluorescent image of DiI-stained cells and chitosan microbeads (diameter  $\approx 164 \mu\text{m}$ ). The chitosan microbeads were loaded with 1% by weight carbon black to attenuate their intrinsic autofluorescence. The one bright microbead contained no carbon black and emitted a strong autofluorescence that was much brighter than the microbeads encapsulating carbon black or fluorescently stained cells. This image was taken using an inverted fluorescent microscope and a TRITC filter set (Ex: 520-570; Em: 535-675) at 10 $\times$  magnification.

Next, we functionalized the chitosan microbeads with the protein streptavidin. Others have reported covalently anchoring proteins to thin films of chitosan<sup>71</sup>, using glutaraldehyde to attach the chitosan amines to primary amines on proteins. Since glutaraldehyde was already used here to cross-link the chitosan microbeads, additional glutaraldehyde was added (to completely saturate free amine groups with aldehydes linkages). Subsequent addition of a streptavidin solution yielded streptavidin covalently anchored to the chitosan backbone. This was verified by incubating the particles with fluorescently tagged biotin, followed by washing to remove unbound moieties. A significant increase in fluorescence intensity was observed (Figure 3.5), indicating the binding of biotin to covalently attached streptavidin throughout the microbead volume.

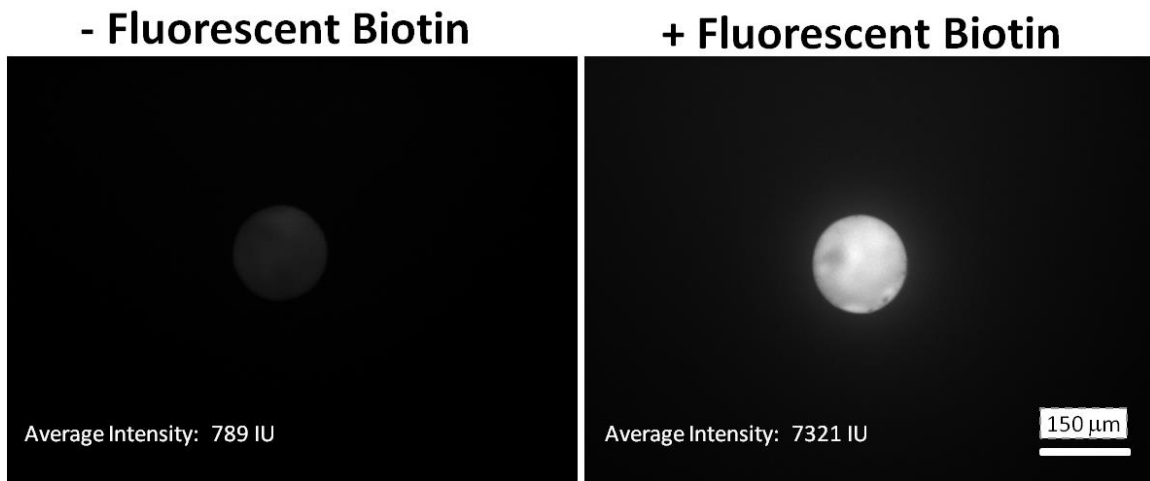


**Figure 3.5.** Fluorescent biotin increased the fluorescent intensity of streptavidin-functionalized chitosan microbeads. The chitosan microbeads, which encapsulated 1% by weight carbon black, were covalently functionalized with streptavidin. Following exposure to fluorescent biotin in solution followed by washing, a significant increase in fluorescent intensity was observed. These images were taken using an inverted fluorescent microscope and a TRITC filter set (Ex: 520-570; Em: 535-675) at 10× magnification.



For the application of rare cell capture, we were particularly interested in streptavidin functionalization at the microbead surface. This was tested using micron sized biotinylated spheres; the polystyrene based biotinylated microspheres were too large ((6-8)  $\mu\text{m}$  diameter) to diffuse into the chitosan microbead, but exhibited significant interaction with streptavidin conjugated to the chitosan microbead surface (Figure 3.6).

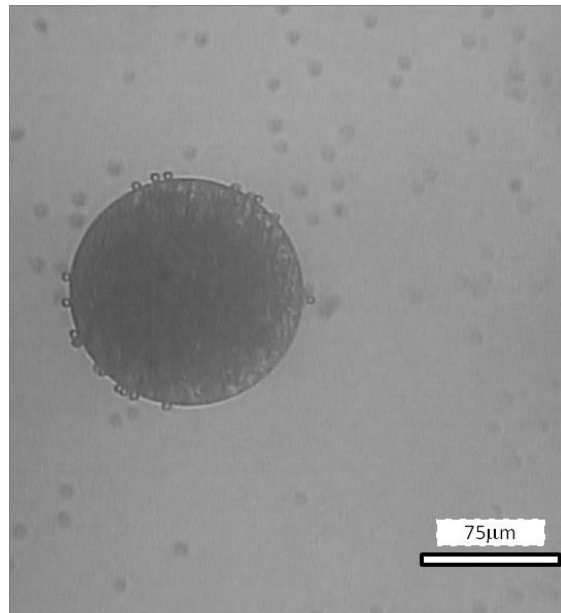


**Figure 3.6.** Attachment of small biotinylated polystyrene spheres (6-8  $\mu\text{m}$ ) to streptavidin-functionalized chitosan microbeads. When chitosan microbeads were mixed with the commercially available biotinylated polystyrene spheres, significant surface attachment of the spheres to the chitosan microbead demonstrated that covalently bound streptavidin was present at the microbead surface.

Finally, as a prelude to our rare cell capture experiments, we studied the binding of MCF-7 breast cancer cells to chitosan microbeads in free solution (Figure 3.7). The cells were first combined with a biotinylated antibody to EpCAM, which is a ligand that is highly expressed by MCF-7 cells. Cell binding was studied with BSA-functionalized microbeads (control experiment) as well as streptavidin-functionalized microbeads (Figure 3.7). (Note that, for these studies, microbeads without carbon black were chosen so as to facilitate visualization in bright-field images.) In the case of the BSA-functionalized microbeads, little or no binding of biotinylated MCF-7 cells was seen (Figure 3.7a). Conversely, the MCF-7 cells substantially cover the surfaces of the streptavidin-functionalized microbeads (Figure 3.7b). These studies show that functionalized chitosan microbeads can specifically target biotinylated cells.

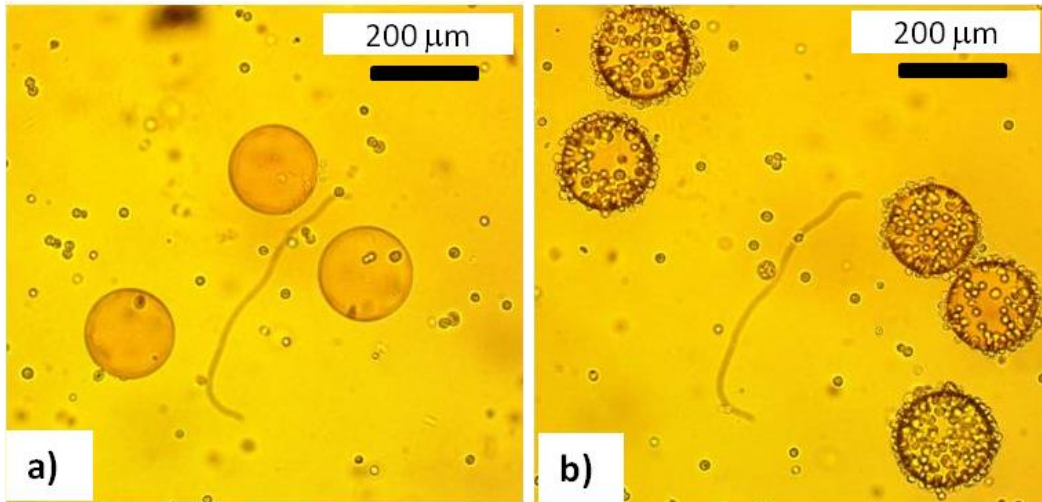


**Figure 3.7.** Specificity of cell-binding to chitosan microbeads. Chitosan microbeads functionalized with BSA (a) exhibit no specific interaction with biotin covered MCF-7 cells (the MCF-7 cells were treated with biotinylated anti-EpCAM against highly expressed surface proteins). However, streptavidin-functionalized chitosan microbeads (b) are able to capture the same cells due to non-covalent biotin-streptavidin interactions.

### 3.3.3. Rare Cell Capture with Chitosan Microbeads

The microfluidic chip design for rare cell capture was identical to the studies done in collaboration with Dr. Forry.<sup>52</sup> The Polydimethylsiloxane (PDMS) glass slide microfluidic chip consisted of a simplistic design containing 5 parallel capture channels (170  $\mu\text{m}$  tall, 2 mm wide, 45 mm long) with a shallow weir that was 120  $\mu\text{m}$  tall, 2 mm wide and 1 mm long as shown in Figure 3.8. Streptavidin-functionalized chitosan microbeads were loaded into a microfluidic channel in such a way that the microparticles formed a packed bed against the weir (which restricted channel height to 50  $\mu\text{m}$ ).

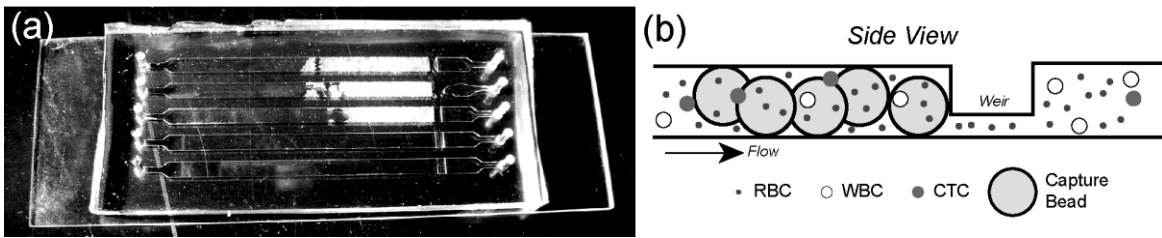


**Figure 3.8.** Image of the packed bed microfluidic capture device.<sup>52</sup> Top and side view of the chip shows that the beads are packed against a shallow weir (a,b).

A model sample to mimic CTCs in blood was prepared using MCF-7 breast cancer cells labeled with a fluorescent membrane stain. These cells were spiked into whole blood at clinically relevant densities ((0-1000) cells per mL of blood). This sample was then exposed to a biotinylated anti-EpCAM antibody to specifically tag the MCF-7 cells with biotins. Thereafter, the whole blood sample was pumped through the microfluidic packed bed at a flow rate of 0.2 mL/h. Figure 3.9b shows a closer fluorescence microscopy image of discrete MCF-7 cells captured in the packed bed. As

noted earlier, the autofluorescence of the chitosan microbeads has been sufficiently attenuated so that the captured fluorescently labeled cells show up as bright spots in the image, which allowed the cells to be counted easily in ImageJ.<sup>64</sup> When the total number of captured cells observed throughout the packed bed was plotted against the number of cells spiked into blood samples, a linear correlation was observed (Figure 3.9c). The ratio of these quantities represents the overall capture efficiency  $\approx 31\%$ .

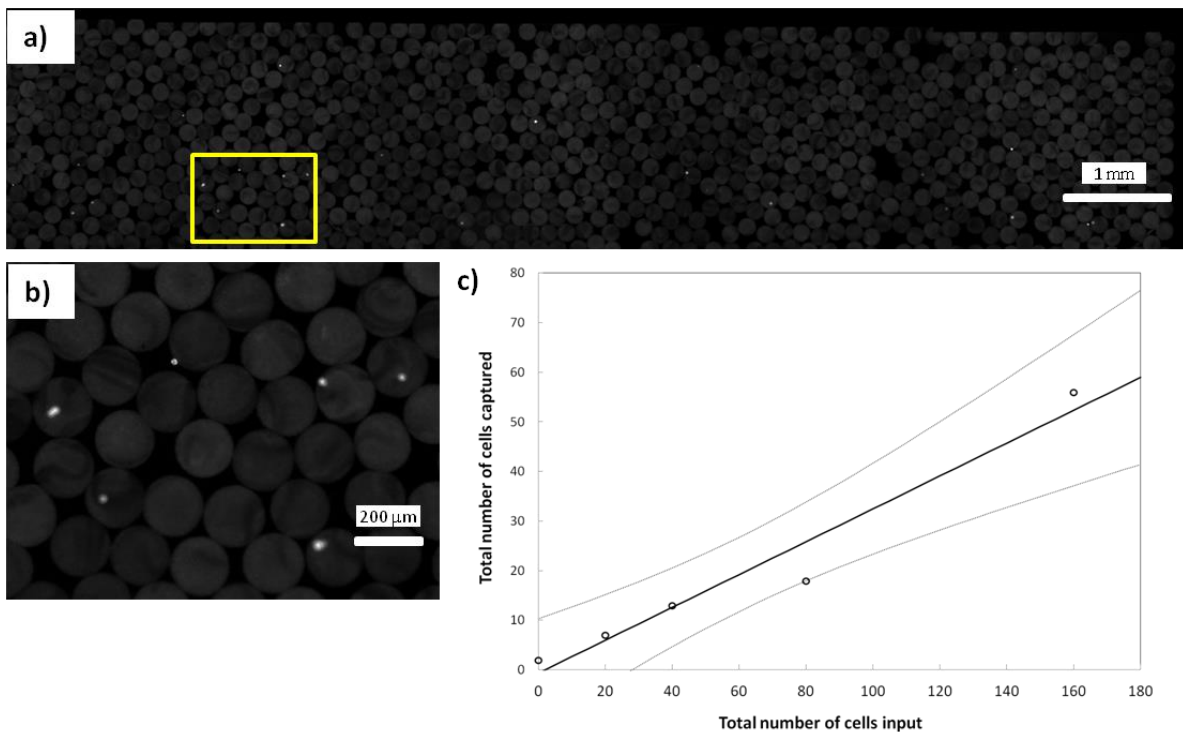


**Figure 3.9.** Capture of cancer cells from whole blood. The streptavidin functionalized chitosan microbeads were loaded into a microfluidic channel. The uniform size of the microparticles led to the generation of a uniform packed bed (a). After pumping through model CTC blood samples (200  $\mu$ L), captured cancer cells were imaged by fluorescence microscopy (b; expanded view of the rectangle in (a)). The total number of cancer cells captured and enumerated in the packed bed exhibited a linear response across the physiologically relevant range (c). A linear regression and Working-Hotelling 95% confidence bands are shown; capture efficiency was  $\approx 31\%$ .

For comparison, the earlier packed bed based on polystyrene beads gave similar variability between different blood donors and a capture efficiency of about 40 %.<sup>52</sup> We speculate that some of the cells captured by the chitosan-based packed bed could not be counted because of the opacity of the carbon black in the microbeads – i.e., if the cells were captured on the far side of the microbeads. Overall, these results are promising and demonstrate the utility of functionalized chitosan microbeads for rare cell capture. Our calculations show that a single batch of  $10^5$  chitosan microbeads prepared using our tubing device is sufficient to fill over 50 packed beds like the one shown in Figure 3.9. This process was not fully optimized, but based on the costs of the materials (not including labor), this translates to a cost of  $\approx$  \$1.50 per packed bed of chitosan microbeads; for comparison, a similar packed bed of commercially available streptavidin-coated polystyrene beads costs  $\approx$  \$25. In addition to lower cost, the chitosan microbeads offer key advantages in versatility since both their inner contents as well as their outer surfaces can be tailored very easily.

### **3.4. CONCLUSIONS**

We have shown development of monodisperse chitosan microbeads that can selectively recognize and adhere to specific types of biological cells. To do so, we have utilized a simple device based on inexpensive and commercially available microtubing for bulk generation of uniform chitosan microbeads. Microbead properties were modulated through both physical encapsulation and covalent chemistry: inclusion of carbon black provided a means to attenuate the intrinsic autofluorescence of the microbeads; covalent chemistry was used for the attachment of streptavidin to the cross-

linked microbeads, thereby allowing the particles to bind to any biotinylated antibody. For applications in potential diagnostics, we have adapted use of the custom-functionalized chitosan microbeads into a microfluidic platform. The uniform chitosan microbeads were loaded into a microfluidic packed bed for proof-of-concept studies in rare cell capture. Using this packed bed, model cancer cells (MCF-7) were captured from whole blood at physiologically relevant levels. In comparison to the commercial polystyrene microparticles used previously, chitosan microbeads were an order of magnitude cheaper and could offer unique advantages as a tunable biopolymer-based material. The versatility of custom synthesized chitosan microbeads allows for generation of more advanced capture devices. For example, alternate capture antibodies could allow isolation of other types of rare cells such as hematopoietic stem cells (HSCs)<sup>72</sup>, and the incorporation of magnetic nanoparticles could allow magnetic manipulation of the chitosan microbeads. Our overall approach should be attractive to researchers interested in customized in-house cell isolation and DNA capture studies through the simplest, inexpensive, and most accessible methods possible.

## Chapter 4

# INDUCING MICROPARTICLE CLUSTERING WITH AN ASSOCIATING POLYMER

---

### 4.1. INTRODUCTION

Microparticles have found relevance in a variety of fields ranging from drug delivery<sup>73</sup> to environmental science<sup>74</sup> to biosensing.<sup>75</sup> Microfluidic methods have become popular as a means to generate microparticles of controlled size,<sup>61</sup> morphology,<sup>76</sup> and functional properties.<sup>77</sup> Moreover, methods have been developed to assemble individual microparticles into larger structures<sup>78</sup> including chains,<sup>30,79</sup> rings,<sup>80</sup> and various cubic and hexagonal three-dimensional lattices.<sup>81</sup> Also, clustering or agglutination of microparticles into larger aggregates serves as the basis for several assays, including for the detection of pathogens.<sup>82</sup>

Much of the interest in studying aggregation of microparticles in response to stimuli stems from the existence of similar processes in nature. For example, in the cytoskeleton of cells, individual subunits of globular actin (G-actin) self-assemble into long semi-flexible filaments (F-actin).<sup>83</sup> Another example is the clotting cascade that is initiated in response to bleeding. Here, the particles involved are the blood platelets, and the net result of particle aggregation is the formation of a blood clot. Although blood clotting is a complex multi-step biochemical process, two physical processes can be distinguished: (1) in response to an injury or bleeding, surface receptors on platelets are

reconfigured to allow binding with the water-soluble fibrinogen protein<sup>84</sup> and (2) fibrinogen is polymerized into water-insoluble fibrin chains through activation of the enzyme thrombin. As these steps proceed, fibrin/fibrinogen chains stick to multiple platelets and thereby bridge the platelets into clusters that are called “platelet plugs”. Subsequently, the precipitated fibrin forms a mesh or web around the platelet plugs, and in the process this web also traps the surrounding red and white blood cells (RBCs and WBCs). The overall result is a blood clot.<sup>85</sup>

In this Chapter, we will present a new way to generate clusters of microbeads through hydrophobic interactions accompanied by precipitation of a polymer on the surface of the beads. We use an associating biopolymer (i.e. a water soluble polymer bearing hydrophobic groups along the backbone) that can interact with our functionalized bead surface through hydrophobic interactions. The biopolymer is the polysaccharide, chitosan<sup>53</sup> (which is positively charged at acidic pH); we attach n-dodecyl tails to the chitosan backbone to obtain hydrophobically-modified chitosan (hm-chitosan). Over the past few years, our group has studied hm-chitosan in conjunction with vesicles<sup>35,36</sup> and biological cells.<sup>34</sup> We have shown that hm-chitosan converts vesicle/cell suspensions into a gel via hydrophobic interactions. Moreover, this gelation can be reversed by adding  $\alpha$ -cyclodextrin ( $\alpha$ -CD), a sugar-based supramolecule with a hydrophobic binding pocket.<sup>85,86</sup> The reversal occurs because the hydrophobes on hm-chitosan get sequestered within the binding pockets of  $\alpha$ -CD molecules.<sup>34</sup> Here, we exploit the same affinity between hm-chitosan and  $\alpha$ -CD, but in the context of microparticles. That is, we functionalize polymer microbeads with  $\alpha$ -CDs, as shown in Figure 4.1a. The beads are



then combined with hm-chitosan chains, thus facilitating specific binding interactions between the chains and the bead surfaces (Figure 4.1b). To our knowledge, the use of hydrophobic interactions to induce polymer-particle binding is new and distinct from previous antibody-antigen<sup>86,87</sup> based approaches.

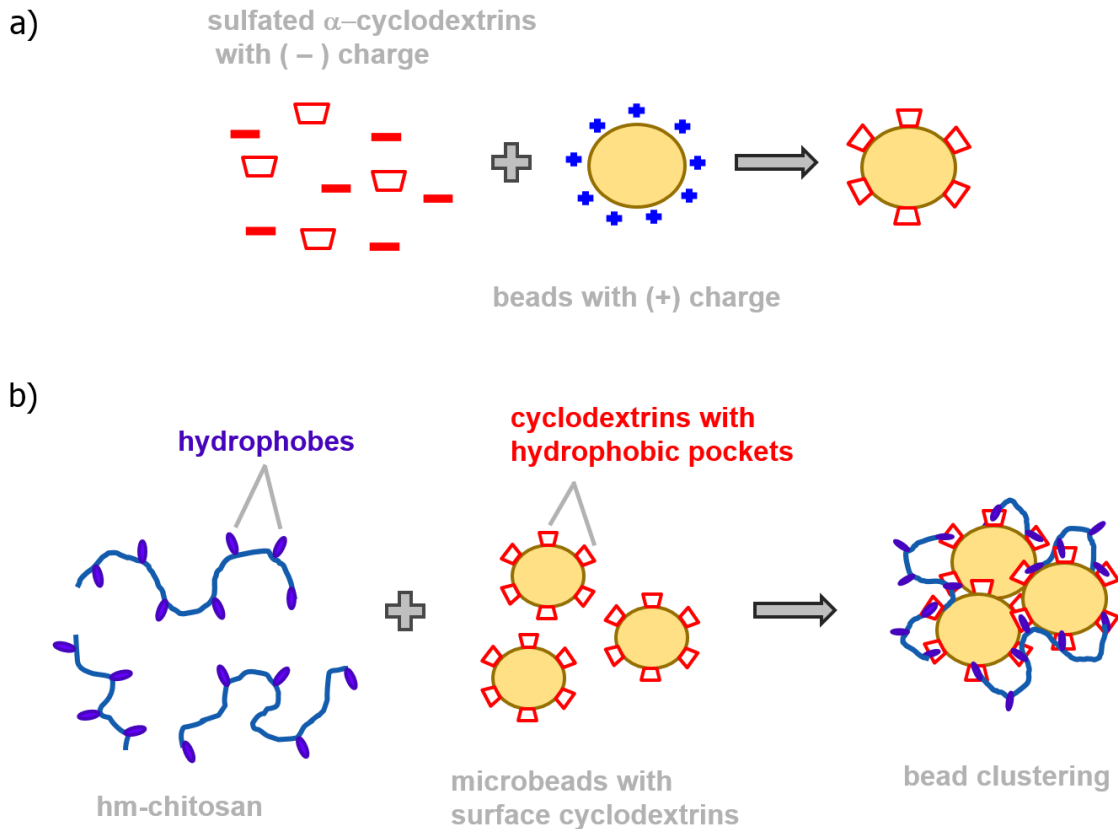


**Figure 4.1.** Schematic illustrating proposed interactions of cyclodextrins on the surface of the bead with hm-chitosan. Commercially available sulphated  $\alpha$ -cyclodextrins (negatively charged) are mixed with positively charged beads to allow for surface coating of the microbeads with  $\alpha$ -cyclodextrins (a). hm-chitosan polymer interacts with the surface of the microbeads through hydrophobic interactions (b).

A further distinctive feature of our study is that we are able to visualize clustering of our microbeads in real time using brightfield microscopy. Our observations reveal a

two-step process that is reminiscent of blood clot formation: that is, first, loose clusters of microbeads are formed, akin to “platelet plugs”. Subsequently, the polymer (hm-chitosan) precipitates around these clusters and thereby fortifies these clusters. These hybrid clusters have sufficient density and integrity so that inert particles can get trapped within them, much like RBCs within a blood clot. This kind of particle clustering could have further applications in embolization,<sup>88</sup> where biopolymer-based beads are used to clot and occlude blood flow to either prevent internal hemorrhaging or to prevent the growth of tumors.<sup>89</sup>

## 4.2 EXPERIMENTAL SECTION

**Materials and Chemicals.** Chitosan (medium molecular weight; degree of deacetylation  $\approx 80\%$ ), the nonionic detergent SPAN80, nonpolar solvent hexadecane, the cross-linking reagent glutaraldehyde (grade 1, 70%), 1-decanol,  $\alpha$ -cyclodextrin sulfated sodium salt hydrate, sodium chloride (NaCl), and NHS-fluorescein (Fluorescein-5-EX N-hydroxysuccinimide ester) were obtained from Sigma-Aldrich. Ethanol was obtained from Pharmco-AAPER (190 Proof). Red-fluorescent carboxylate-modified nanospheres (100 nm) were obtained from Life Technologies (F-8801). Carbon black (N110) was obtained from Sid Richardson Carbon Company. Magnetic iron (III) oxide, gamma-phase ( $\gamma$ -Fe<sub>2</sub>O<sub>3</sub>) nanoparticles (surface area  $\approx 42\text{ m}^2\text{ g}^{-1}$ ) were purchased from Alfa Aesar.

**Chitosan Microbead Synthesis and Analysis.** A two-phase co-flow microfluidic device, as shown by Arya et al.<sup>90</sup>, was used to generate chitosan droplets (2 wt%), which were cross-linked into microspheres using glutaraldehyde (2% weight by volume). Similarly,

chitosan solution was mixed with 1 wt% carbon black to generate carbon black encapsulated chitosan microparticles. Likewise, magnetic chitosan microspheres were generated by dispersing  $\gamma$ -Fe<sub>2</sub>O<sub>3</sub> nanoparticles (0.5 wt%) into the chitosan solution, prior to cross-linking, as described in a previous study.<sup>30</sup> Residual positive charge of crosslinked chitosan microbeads in acidic aqueous solutions was tested using red-fluorescent carboxylate modified nanoparticles (100 nm). Chitosan microbeads (encapsulated with carbon black to attenuate auto-fluorescence) were mixed with fluorescent nanoparticles (1:200 dilution of stock in acetic acid water, pH 4.5) for 30 min, washed in pH 4.5 water (3 times), and observed under an inverted fluorescent microscope (Zeiss Axiovert 135, 20× magnification) using Zeiss Filter set 15 (excitation BP 530-560 nm; emission LP 590 nm). Relative fluorescent intensity was then measured and compared to chitosan beads that were not exposed to the fluorescent nanoparticles and also to chitosan beads that were exposed to fluorescent nanoparticles in presence of salt (NaCl; 2 M) to demonstrate that electrostatic interactions were indeed responsible for nanoparticle interaction with the microbeads.

#### **Cyclodextrin Coating and Clustering Experiments with Chitosan Microbeads.**

Chitosan microbeads in DI water containing acetic acid (pH=4.5) were exposed to sulfated  $\alpha$ -cyclodextrin (5 wt%) for an hour under gentle mixing, then washed five times with acidic water (pH=4.5). The beads were maintained in acidic water solution prior to use in the clustering experiments. The hm-chitosan used in this study was synthesized as described in previous work.<sup>16</sup> Fluorescently labeled hm-chitosan was prepared following similar procedures as described by Wu *et al.*<sup>91</sup> for generating fluorescently labeled

unmodified chitosan. For microbead clustering studies, hm-chitosan was dissolved (0.1 wt%) in aqueous salt solution (0.9 wt% NaCl). Chitosan beads ( $\approx 200$ ) functionalized with  $\alpha$ -CD were placed on a slide glass in 25  $\mu$ L of solution (acidic water) and 25  $\mu$ L of hm-chitosan solution was added. A micropipette tip was used to gently mix the sample. The results were observed under brightfield microscopy (Zeiss Axiovert 135; 10x magnification).

### 4.3. RESULTS AND DISCUSSION

We used a simple process for functionalizing chitosan microbeads with cyclodextrins.<sup>92</sup> The starting materials are the chitosan microbeads produced by our microfluidic method. These beads are nearly monodisperse with a diameter of 164  $\mu$ m (same as those used in Chapter 3). Note that the beads are formed by crosslinking chitosan using glutaraldehyde. Since chitosan is a cationic polymer, the beads retain significant residual positive charge on their surface. As a result, anionic molecules or particles can be bound to the bead surface by electrostatic interactions.

To show this, we first exposed the chitosan microbeads to anionic (carboxylate-functionalized) nanoparticles (100 nm diameter) that are labeled with a red fluorescent dye. After exposure for 30 min, the beads were washed extensively and then observed under a fluorescence microscope (Figure 4.2). We find substantially higher fluorescence for these beads (Figure 4.2b) relative to the bare beads (Figure 4.2a) (the fluorescence is about 3 times higher for the former). This indicates the binding of anionic nanoparticles to the cationic bead surface via electrostatic interactions. Note that this binding is strong

enough such that the nanoparticles are not removed from the bead surface even after extensive washing of the beads. Also, the nanoparticle-bead binding is much less if the two were incubated in the presence of salt (2 M NaCl), as shown by Figure 4.2c. Salt is known to screen and thereby diminish the attractive electrostatic interactions between charged species. Thus, the results from Figure 4.2 confirm that electrostatic interactions are sufficient to ensure the stable binding of nanoparticles to bead surfaces.

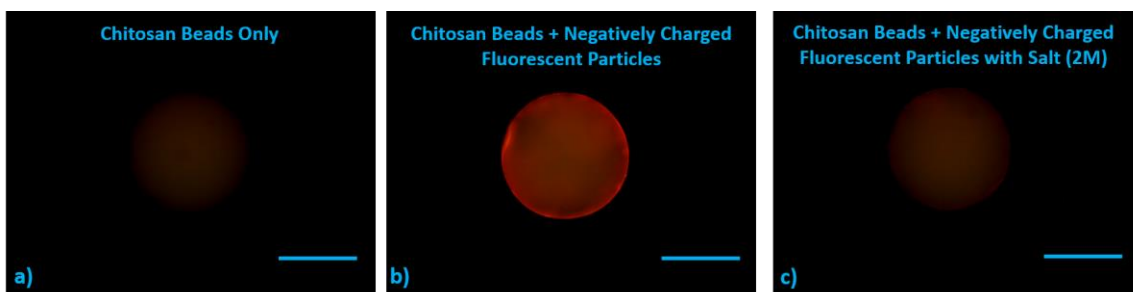


**Figure 4.2.** Comparison of relative fluorescent intensity of chitosan microbeads after exposure to anionic fluorescent nanoparticles. Typical images are shown of: (a) Bare chitosan bead (control); (b) Bead after incubation with nanoparticles, followed by extensive washing. The higher fluorescence shows the strong binding of the nanoparticles to the bead surface; (c) Bead after incubation with nanoparticles in the presence of salt (NaCl; 2M), followed by washing. The lack of fluorescence in this case indicates negligible binding of the nanoparticles. Scale bars: 100  $\mu$ m.

Based on the above results, we proceeded to functionalize chitosan microbeads with cyclodextrins. For this, an anionic form of  $\alpha$ -CD, i.e., sulfated  $\alpha$ -CD was used (Figure 4.1a). The sulfated  $\alpha$ -CD (5 wt%) was combined with the chitosan microbeads (1000 beads/mL) for a period of 1 h. Note that the concentration of sulfated  $\alpha$ -CD is in large excess of that needed for saturating the surface of the beads. Following this step, the beads were washed 3 times and then stored in aqueous solution, where they remain stable without aggregation. Our studies below also indicate that the surface coating of CD is

stable with time, at least over a period of a week. That is, both freshly prepared beads as well as beads stored for a week give identical results.

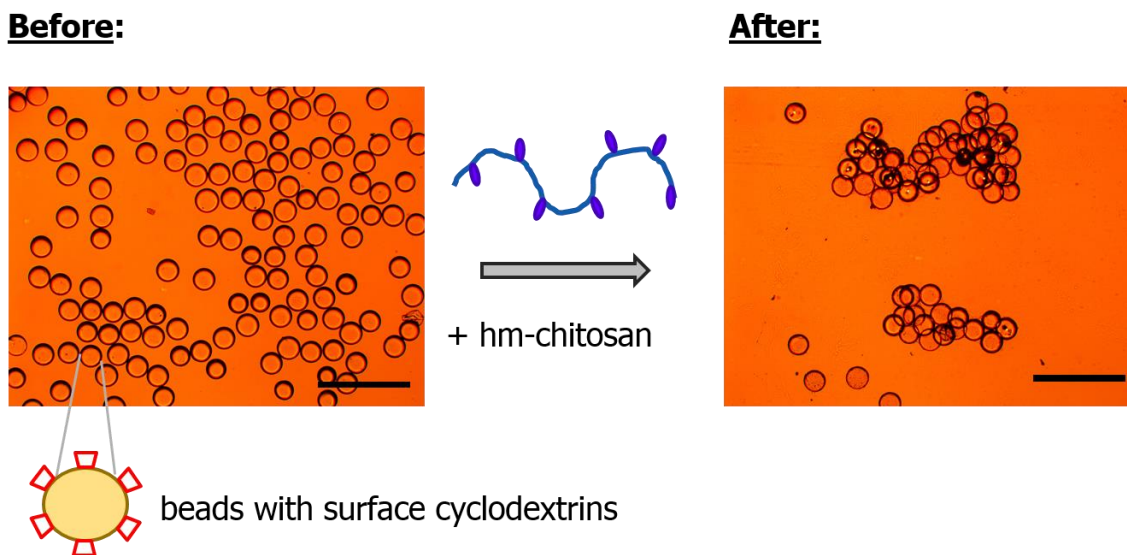


**Figure 4.3.** Optical microscopy images showing clustering of cyclodextrin coated microbeads ( $\approx 165 \mu\text{m}$ ) upon mixing with hm-chitosan. Microbeads, which are covered with cyclodextrins, are mixed on a slide glass with hm-chitosan solution and microbead clustering is observed within a minute after exposure. Scale bars: 1 mm.

We then proceeded to study the effect of adding hm-chitosan to the CD-functionalized beads. The experiments were done under the optical microscope to allow changes to be observed in real time. A dilute (0.1 wt%) solution of hm-chitosan was added to the beads at time  $t = 0$ . Note that the beads are initially discrete and unaggregated (Figure 4.3a). Within a minute of hm-chitosan addition, we found that large clusters of the microbeads were formed (Figure 4.3b). Importantly, hm-chitosan was an essential trigger for this clustering; no clustering of the microbeads was observed using the same concentration of native (unmodified) chitosan. Moreover, surface coating with CDs was also essential for the clustering; microbeads that did not have the CDs did not cluster upon adding hm-chitosan, regardless of the concentration. Taken together, these

observations suggest that interactions between the hydrophobes on hm-chitosan and the hydrophobic binding pockets of the CDs are important in this microbead clustering system.

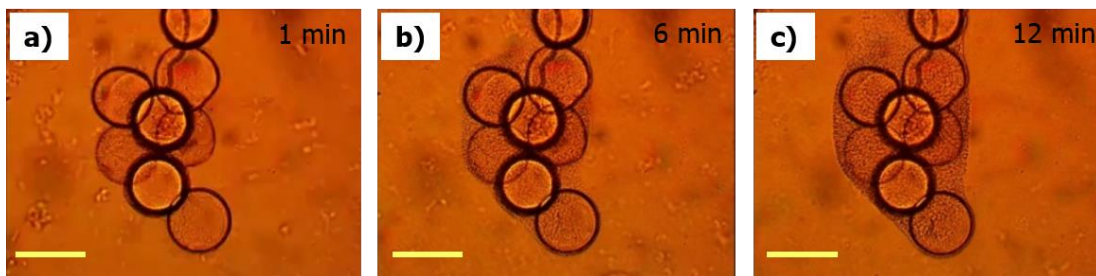


**Figure 4.4.** Optical microscopy images showing growth over time of a visible hm-chitosan precipitation around the microbead clusters after initial cluster formation. Scale bars: 200  $\mu\text{m}$ .

Further interesting changes were observed in the hm-chitosan + CD-microbead system as time progressed (Figure 4.4). As mentioned, the initial clustering of microbeads occurs rapidly (within  $t = 1$  min, see Figure 4.4a). Subsequently, we observed the growth of a precipitate around the microbead clusters over the course of  $t = 12$  min (Figure 4.4b and c). Note that the precipitate is like a porous mesh and it coats all the particles in the cluster. At the same time, the precipitate does not nucleate from the surrounding bulk solution. This precipitate is most likely the hm-chitosan chains falling out of solution, evidently due to strong interactions with the CDs on the bead surface. This is also supported by observations of individual CD-coated microbeads immersed in an hm-chitosan solution (Figure 4.5a). We further verified the identity of the precipitation by labeling hm-chitosan with a green fluorescent dye and combining it with the CD-coated beads. It can be noted from Figure 4.5c, that the precipitate around the cluster shows a green fluorescence, indicating that precipitate is indeed hm-chitosan.

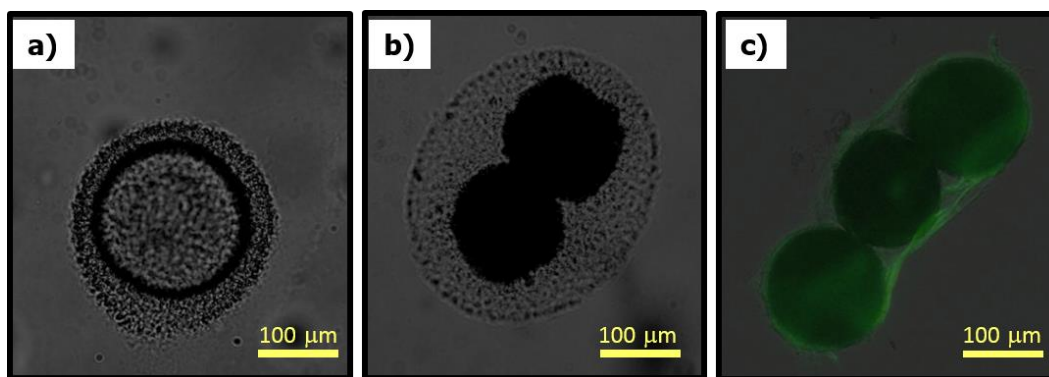


**Figure 4.5.** Optical microscopy images showing polymer precipitation around individual and small groups of microbeads. An individual cyclodextrin coated microbead is observed with precipitation around the bead surface upon hm-chitosan stimulation (a). Pair of cyclodextrin coated microbeads are held together in hm-chitosan precipitated web (b). Fluorescent labelled hm-chitosan is used to confirm that the precipitated web on the surface of the beads is hm-chitosan (c). For Image (c), brightfield and fluorescent microscopy image were taken and overlaid. Note: carbon black was encapsulated for visualization and to reduce autofluorescence (b, c).

This was further verified by mixing dissolved hm-chitosan (0.1 wt%) solution directly with sulfated  $\alpha$ -CDs (5 wt%) as shown in Figure 4.6a. The initially soluble hm-chitosan precipitates out of solution upon strong interactions with sulfated  $\alpha$ -CDs. By pre-coating the surface of the chitosan microbeads with sulfated CDs, we can ensure that the hm-chitosan precipitation nucleates from the bead surface to generate these unique types of microbead clusters as shown in Figure 4.5. Alternatively, if the chitosan beads were not pre-coated with sulfated  $\alpha$ -CDs, and instead simultaneously mixed with sulfated  $\alpha$ -CDs and hm-chitosan, precipitation was observed to nucleate within the solution and not directly around chitosan microbeads (Figure 4.6b). Importantly, the growth of the polymer web on the surface of the beads was only seen on beads that were previously coated with cyclodextrins. To show this point, we prepared two populations of beads, with and without cyclodextrin coating, and combined them with hm-chitosan (Figure 4.7a).



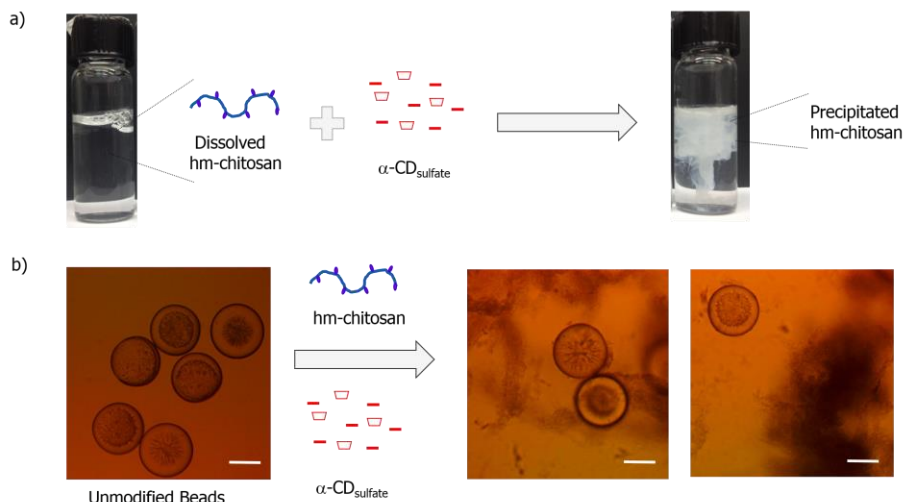


**Figure 4.6.** Visual and optical microscopy observations of hm-chitosan precipitation out of solution. Initially, hm-chitosan is dissolved in an aqueous solution; however, upon addition of sulfated  $\alpha$ -cyclodextrins, the hm-chitosan precipitates out of solution (a). When unmodified chitosan beads (not pre-exposed to sulfated cyclodextrins), were mixed simultaneously with dissolved hm-chitosan and sulfated  $\alpha$ -cyclodextrins solutions, the precipitation was observed to nucleate within the solution and not directly around the chitosan microbeads (b). Scale bars: 100  $\mu$ m.

One set of beads are the same transparent ones from Figure 4.3 with a diameter of 165  $\mu$ m and having CDs on their surfaces. The other set of beads contain carbon black and their diameter is 150  $\mu$ m; these beads are opaque and black due to the carbon black, and they are also inert, i.e., there are no CDs on their surfaces. As seen in Figure 4.7, only the transparent CD-coated microbeads have a growth of a polymer precipitate around them (Figure 4.7b), while the inert black beads do not show a visible precipitate on their surface (Figure 4.7c). Interestingly, the inert beads either remained as individual entities (i.e., did not cluster) or they were trapped in the polymer web around the CD-coated beads (Figure 4.7d). This shows that the precipitated polymer web can trap surrounding inert objects.

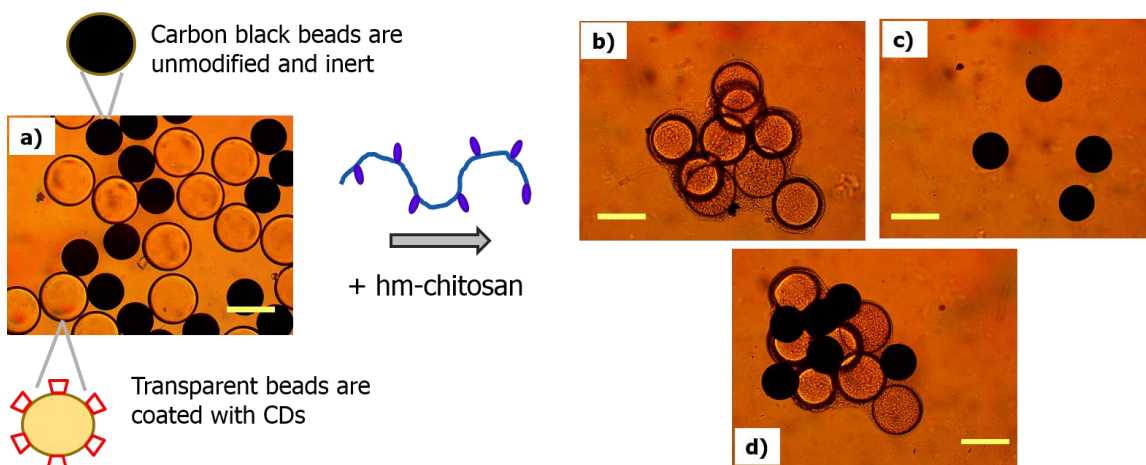


**Figure 4.7.** Two sets of beads are mixed together and exposed to hm-chitosan. One of set of beads (transparent beads) are covered in cyclodextrins and the second set of beads (encapsulated with carbon black) do not have cyclodextrins on the surface (a). Upon exposure to hm-chitosan, the transparent beads generate a surrounding precipitated polymer web (b), while the inert carbon black beads do not generate their own polymer matrix; they either remain as independent beads (c), or they are trapped within the polymer web of the transparent beads (d). Scale bars: 200  $\mu\text{m}$ .

Our observations suggest an analogy between the above structures and the structures formed during blood clotting. As mentioned earlier, one of the first physical processes in the blood clotting cascade involves fibrinogen interaction with the surface receptors on platelets, which leads to formation of visible “platelet plugs” that act as a temporary barrier on the wound, until strengthened by the formation of the fibrin mesh. The initial clustering of CD-coated microbeads, driven by hydrophobe-CD interactions, is thus similar to the formation of a platelet plug. The growth of the hm-chitosan polymer web from the surfaces of the beads in this cluster is reminiscent of fibrin precipitating out of solution around the initial platelets plug to form the blood clot. Just as surrounding red blood cells, which are not active in the clotting cascade, are trapped in the fibrin polymer web, here also the inert beads are trapped in the polymer web that forms around the initial cluster of CD-coated microbeads. Such clustering in a mixed bead/polymer system could

be useful in making artificial blood clots for embolization. This process commonly uses biopolymer beads of similar sizes to occlude blood vessels, either for the purpose of treating internal hemorrhage or to starve tumors of blood.<sup>88</sup>

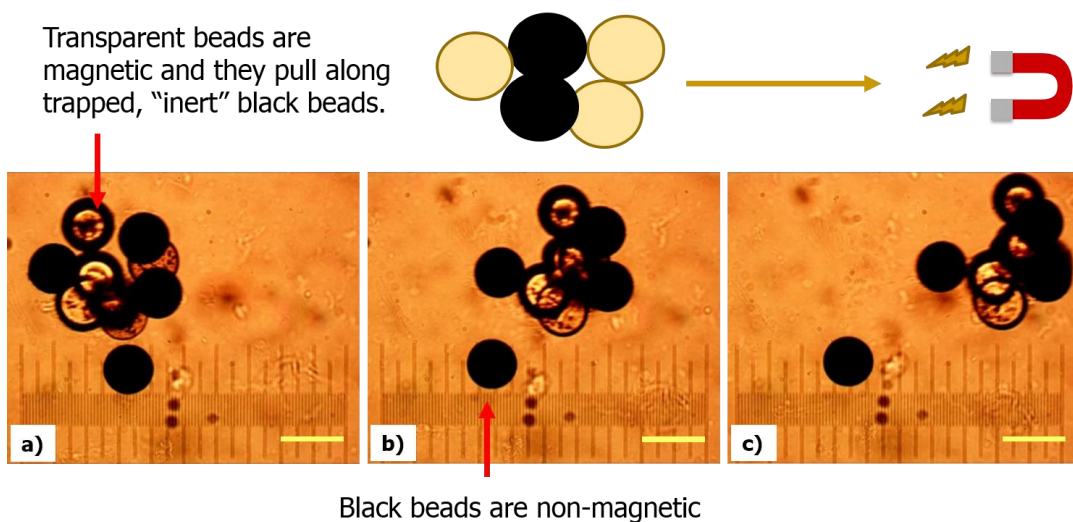


**Figure 4.8.** Images showing the entire bead-polymer matrix being moved with a magnet. The carbon black beads are completely inert (i.e. nonmagnetic and not covered in cyclodextrins) and they are trapped in the polymer matrix of the transparent beads (magnetic beads that are covered in cyclodextrins). The magnetic beads move the entire matrix, including the inert carbon black beads, from left to right. Scale bars: 200  $\mu\text{m}$ .

The trapping of inert objects within the polymer-bead cluster/mesh also suggests a means to deliver groups of micron-sized objects to a targeted location. To demonstrate this concept, we encapsulated magnetic nanoparticles in the transparent cyclodextrin CD-coated beads from Figure 4.7. The inert black beads are non-magnetic and represent hypothetical cargo that needs to be moved towards a desired location. As before, the black beads are trapped in the polymer web generated around the CD-coated transparent beads (Figure 4.8a). We can then use a magnet to move the whole entire aggregate,

together with the inert black beads that are trapped in it (Figure 4.8b, and c). Note that the uncaptured single black microbead below the cluster does not move and is unaffected by the magnet.

#### **4.4. CONCLUSIONS**

We have developed a class of microbeads that undergo clustering (aggregation) in the presence of specific polymers. The morphology of the clusters resembles those that occur during blood clotting. Our system consists of chitosan microbeads coated with CDs, which are then exposed to hm-chitosan, a polymer with hydrophobic pendant groups. Interactions between the hydrophobes on the polymer and the CDs on the microbeads are important to the clustering of the microbeads. Initial clusters mimic the temporary “platelet plugs” that form during clotting. Subsequently, the hm-chitosan precipitates out of solution and forms a matrix around the particle clusters. This is reminiscent of the conversion of soluble fibrinogen to an insoluble fibrin mesh around the platelet plugs in the case of a blood clot. The precipitated hm-chitosan matrix or web is able to entrap “bystanders”, i.e., inert microbeads within it; this web is strong enough to transport the captured bystander beads to desired locations. Such microbead clustering could be useful in embolization, which is used to occlude blood vessels within the circulation.

## Chapter 5

# DEVELOPMENT OF “KILLER” MICROPARTICLES

---

### 5.1. INTRODUCTION

The controlled release of cargo from polymer microbeads and microcapsules is of considerable interest, particularly in applications related to drug delivery.<sup>93,94</sup> As carriers of a potentially valuable payload, these microparticles need to be carefully designed; they must both be robust enough to protect the payload from external threats and simultaneously be susceptible to breaking, when required, to release the payload at the appropriate time and location. Thus, many research groups have explored various routes towards triggered degradation of polymer microparticles, in response to stimuli such as biomolecules (e.g. enzymes), temperature, osmotic pressure, light, and pH.<sup>95,96</sup>

Interestingly, nature has developed more sophisticated methods for targeted degradation of biological cells, which serves as a useful inspiration for triggered microparticle degradation. For example, consider biological cells in the body that are infected with pathogens like viruses. The immune system can both identify and eliminate these infected cells.<sup>97</sup> Specifically, a subset of white blood cells, known as killer T cells, have the machinery for targeted degradation of infected cells. For example, T cells can generate and secrete cytotoxic proteins such as perforin and granzymes,<sup>98</sup> (packaged within exosomes). The immune cells move towards the infected cells and locally release the cytotoxic proteins, which induce degradation of the infected cells. Note that, because

the process occurs only near the infected cells, properly functioning neighboring cells are not affected.<sup>99</sup> The same killer T cell can then move on and use the same mechanism to eliminate infected cells in other regions of the body.

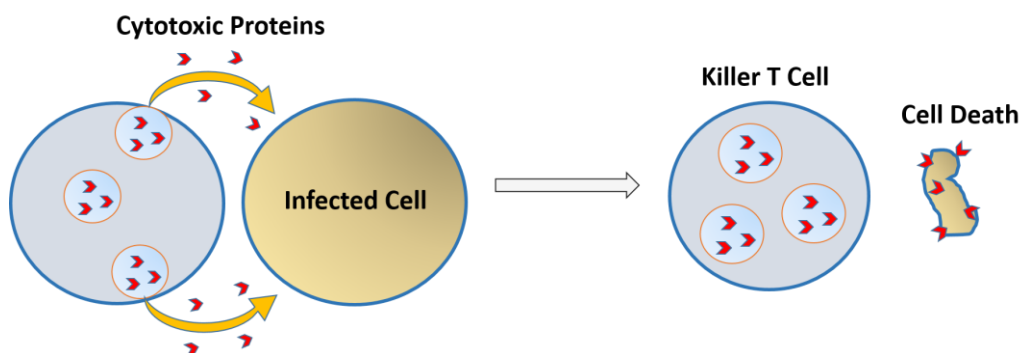


**Figure 5.1.** Schematic illustrating destruction of an infected cell in the body by a killer T cell. This is a simplified illustration of how a killer T cell attacks infected cells. Once the killer T cell is near the infected cell, it binds and delivers a “lethal burst” of cytotoxic proteins at the infected cell, resulting in apoptosis (programmed cell death) of the infected cell.<sup>99</sup>

In this Chapter, we describe the development of particles that are inspired by the functions of immune cells. Specifically, our particles have the ability to selectively target certain kinds of surrounding particles for destruction. To accomplish this, we immobilize the enzyme glucose oxidase (GOx) in chitosan capsules, thus creating “killer” capsules. In the presence of glucose from the external environment, our killer capsules continuously generate gluconate ions, which are a known chelator of metal ions like copper ( $\text{Cu}^{2+}$ ). Thus, the killer capsule can target particles that are crosslinked by metal ions. Here, our targets are beads of alginate crosslinked by  $\text{Cu}^{2+}$ . When the killer capsules and target beads are brought close to each other, the gluconate chelator released from the killer capsules removes the  $\text{Cu}^{2+}$  from the alginate bead, thereby causing its destruction.

This is analogous to how killer T cells secrete the cytotoxic proteins in the vicinity of infected cells. Overall, this chapter presents the first study, to best of our knowledge, to explore the concept of using one polymer particle as the vehicle to destroy another particle. The concept could have potential applications in localized release of drugs or other solutes.

Moreover, the killer T cell-inspired capsule concepts could have future impact in the larger artificial cell field. Other groups have developed simple protocells from similar nonbiotic components that mimic basic functions of the biological cell. For instance, the Bentley group has developed biopolymer capsules with the ability to communicate and participate in biological signaling through small molecules.<sup>12</sup> In addition, others have made cell membrane-mimetic barriers on capsules through coating of polymer capsules with phospholipids.<sup>100</sup> Also, functions associated with specific types of cells have been mimicked through protocells: the DeSimone group designed polymer microparticles that are shaped like red blood cells and have the ability to transport hemoglobin.<sup>101</sup> As the emerging protocell field matures, new cell-like functionalities for microparticles/capsules, such as targeted degradation, could be useful for development of more sophisticated protocells with even greater cell-like functionalities.

## 5.2 EXPERIMENTAL SECTION

**Materials and Chemicals.** Chitosan (medium molecular weight; degree of deacetylation  $\approx 80\%$ ), sodium alginate (low viscosity, 1 wt%  $\approx 5\text{--}40$  cP; molecular weight 110–150 kDa) sodium tripolyphosphate (TPP), glutaraldehyde, calcium chloride dihydrate,

glucose oxidase (GOx) from *Aspergillus niger* (100000 units/g), D-glucose, sodium gluconate, pluronic F-127, copper (II) sulfate, strontium chloride hexa-hydrate, and HEPES were obtained from Sigma-Aldrich. Green-fluorescent latex nanospheres (100 nm) were obtained from Polysciences Inc. (Cat# 17150).

**Synthesis of Target Beads.** Target beads were produced by cross-linking alginate droplets with copper ions. Using a syringe pump (1 mL/min), the alginate solution (2 wt% in DI water) was extruded through a 22 gauge needle to generate droplets that were collected in an aqueous solution of 1 wt% copper sulfate (with 0.3 wt% Pluronic F127 added as a surfactant) and allowed to crosslink for 30 min. The copper-alginate beads were then washed in DI water (5 times) and stored at 4°C in DI water. For entrapment of the fluorescent nanoparticles, the alginate solution was combined with the fluorescent latex nanospheres (0.2 wt%), prior to bead formation.

**Synthesis of Killer Capsules.** The “killer” chitosan capsules were generated by immobilizing GOx within a chitosan-TPP matrix. GOx enzyme (200 units/mL) was dispersed in chitosan solution (2 wt% in DI water) and using a syringe pump (1 mL/min), was extruded through a 22 gauge needle to generate droplets that were collected in a TPP solution (10 wt% in acidified water; pH = 5) and allowed to crosslink for 30 min. The chitosan-TPP beads were then incubated in a glutaraldehyde solution (1 wt% in DI water) for 1 h to immobilize the GOx enzyme, as recommended in other studies.<sup>102,103</sup> Next, the killer chitosan beads were washed in DI water (5 times) and stored at 4°C in DI water.



For micron-sized killer chitosan capsules, a pulsed gas-flow microcapillary device designed by Oh et. al was adapted for use.<sup>104</sup> The chitosan solution (2 wt%) was pumped (1.5  $\mu\text{L}/\text{min}$ ) through a silica capillary (diameter  $\approx 100 \mu\text{m}$ ) and pulses of gas (3 Hz; 9 psi) were controlled by a digital gas flow controller. Chitosan droplets with dispersed GOx (200 units/mL) were then collected in an aqueous TPP solution for 30 min (10 wt%), then incubated in glutaraldehyde (1 wt%) for 1 h, washed in DI water (5 times), and stored at 4°C in DI water.

**Bead Degradation Experiments.** For the experiments in Figure 5.3 (degradation through direct addition of GOx enzyme), the target copper-alginate bead was placed in 1 mL of HEPES buffer (0.02 M; pH = 7.4), which contained dissolved glucose (1 wt%). The negative control was the same HEPES buffer solution that did not contain any glucose. The GOx enzyme was added at  $t = 0$  (working concentration of enzyme in overall solution was 1 unit/mL). Brightfield microscopy images (2.5X objective) were taken every 5 min. Similarly, for the subsequent experiments, instead of directly adding the GOx enzyme to initiate target bead degradation, the chitosan capsule (which contains the immobilized GOx) was added to the same buffered glucose solution at  $t = 0$  of the respective experiment. For micron-sized degradation experiments, the populations of killer microcapsules, target microbeads, and inert microbeads were mixed at roughly equal ratios in the same buffered-glucose solution (1 wt% glucose; 0.02 M HEPES; pH = 7.4) and again, brightfield microscopy images were taken every 5 min.

**Optical and Fluorescence Microscopy.** A Zeiss Axiovert 135 TV inverted light microscope equipped with ToupView Imaging software was used for brightfield microscopy. Beads were imaged with either a 2.5 X or 10 X objective. To observe release of the fluorescent latex nanospheres, fluorescent images were taken using a band pass excitation filter (530-585 nm) and a long pass emission filter of 615 nm.

**Fluorescence Measurements.** Release profiles for the fluorescent nanoparticles were collected using five target Cu-alginate beads (which contained the nanoparticles) mixed with five killer chitosan capsules in a buffered-glucose solution (1 wt% glucose; 0.02 M HEPES; pH = 7.4; 2 mL total solution). Fluorescence intensity measurements were taken hourly using a Synergy HTX Multi-Mode Microplate Reader (BioTek) on aliquots (200  $\mu$ L) that were removed from the surrounding solution. Following measurement of fluorescence intensity, the aliquots were placed back in the sample solution. Additionally, to allow for uniform fluorescent intensity readings, the sample was shaken on a rotary mixer (50 rpm) throughout the experiment.

### 5.3. RESULTS AND DISCUSSION

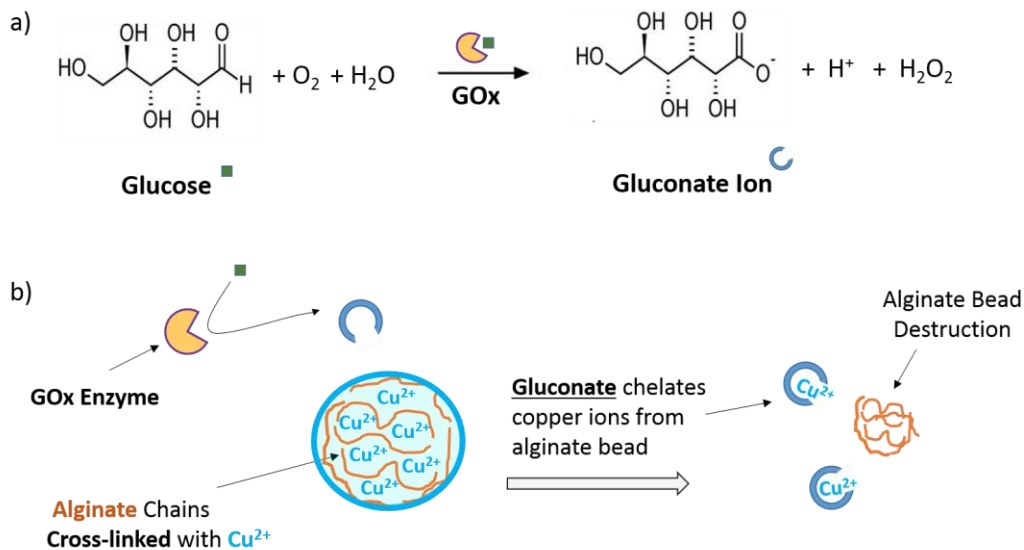


**Figure 5.2.** Schematic of proposed bead degradation method. The enzyme glucose oxidase (GOx) can catalyze the production of gluconate from ambient glucose (a). As a chemical chelator, the gluconate ions have strong interactions with the copper ion cross-links of an alginate bead, and thereby remove the Cu<sup>2+</sup> cross-links from the target alginate bead, resulting in destruction of the alginate bead (b).

We formed alginate beads by introducing sodium alginate into a solution of the multivalent metal cation, Cu<sup>2+</sup>.<sup>105</sup> These beads are susceptible to degradation through exposure to Cu<sup>2+</sup> chelators such as gluconate, as described in Chapter 2.<sup>106</sup> Here, we will use enzymes to generate the gluconate. The enzyme chosen is glucose oxidase (GOx), which converts D-glucose to gluconate in the presence of water and oxygen, as shown by the scheme in Figure 5.2a.<sup>106</sup> (The intermediate D-glucono- $\delta$ -lactone (GDL) is first formed from glucose, and GDL slowly undergoes hydrolysis in water to become gluconate; this step is omitted from the scheme for simplicity.)<sup>107</sup> The key point in our system is that the generation of gluconate ions in the vicinity of a Cu-alginate bead can

lead to the chelation of the  $\text{Cu}^{2+}$  ions and thereby to the destruction of the Cu-alginate bead (Figure 5.2b).

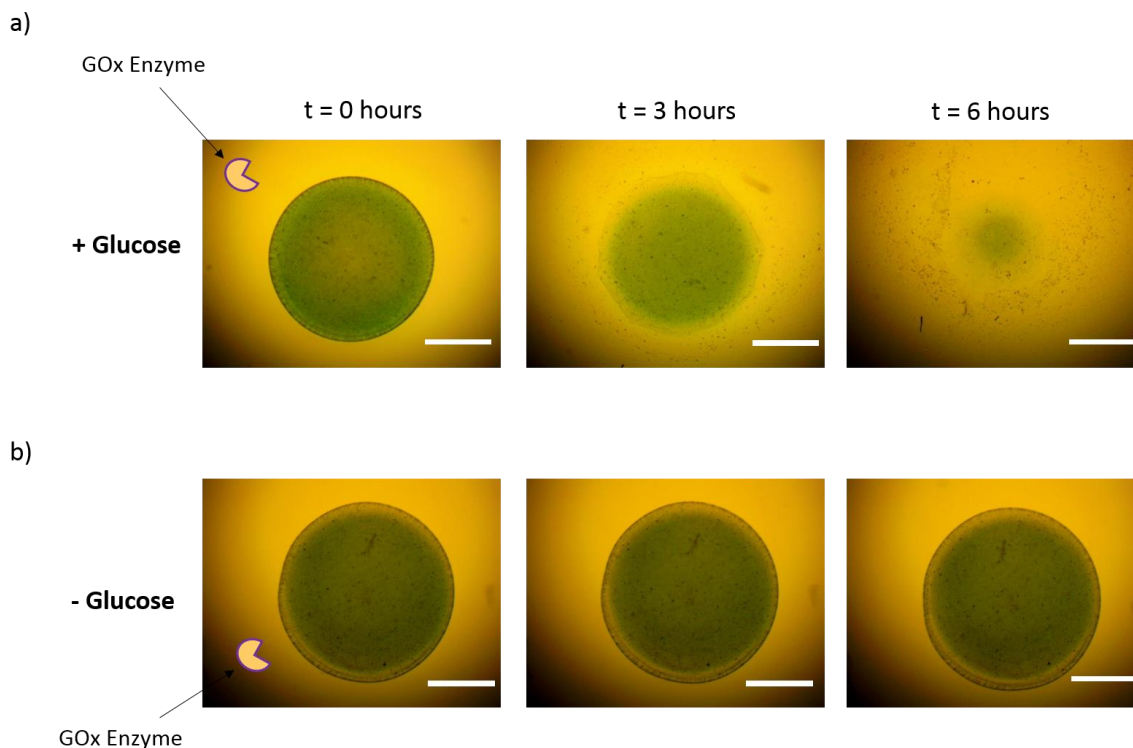


**Figure 5.3.** Optical microscopy images over time of an alginate microbead (cross-linked with copper ions) in the presence of GOx enzyme. In the presence of glucose, at  $t = 0$ , the glucose oxidase enzyme is added to the sample and the Cu-alginate bead degrades over the course of 6 hours (a). When the same experiment is conducted without glucose, the Cu-alginate bead remains intact, as the enzyme has no source to generate gluconate chelator ions (b). Scale bars: 1 mm.

The above concept was initially tested by exposing Cu-alginate beads to free GOx. Figure 5.3 shows optical microscopy images of this process. In the presence of glucose (1 wt%) and free GOx (1 unit/mL), the alginate bead disintegrates over the course of 6 h. Conversely, with free GOx, but no glucose added, the bead remains intact because the chelator cannot be generated without glucose. Note that the above experiments were

conducted in HEPES buffer (a common buffer that does not interact with metal ions).<sup>108</sup> The buffer is needed to maintain pH, as the chelation efficiency of gluconate drops at lower pH. Also, we should point out the reason behind the choice of  $\text{Cu}^{2+}$  as the cation to crosslink the alginate in our studies. The reason for this is that gluconate is an effective chelator for  $\text{Cu}^{2+}$ , with the stability constant for gluconate- $\text{Cu}^{2+}$  chelation being 18.3. In comparison, the chelation efficiency is much lower for gluconate with  $\text{Ca}^{2+}$  and  $\text{Sr}^{2+}$  (two cations that are commonly used to crosslink alginate), with the stability constants for the latter being only about 1 (see Table 2.1 in Chapter 2). As a result, the GOx/glucose reaction is effective at degrading Cu-alginate beads, but not Ca-alginate or Sr-alginate ones.

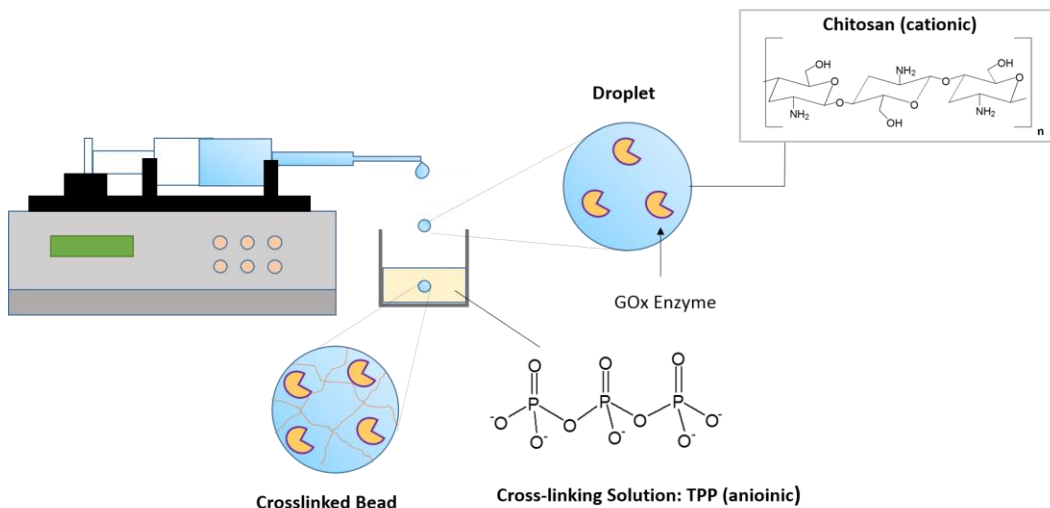


**Figure 5.4.** Preparation of killer chitosan capsules. The enzyme (GOx) is dispersed in a cationic polymer solution (chitosan) and a syringe pump generates droplets, which are collected in a cross-linking solution containing the anion, tripolyphosphate (TPP). The chitosan droplets are cross-linked into a solid hydrogel capsule by the TPP molecules, which results in immobilized enzymes within the chitosan capsule.

Having demonstrated that the GOx enzymatic reaction can destroy Cu-alginate beads, we then explored the encapsulation of GOx within “killer” capsules. The latter

were made by an alternative chemistry, i.e., using the cationic polymer, chitosan, the multivalent anion, TPP, and the chemical crosslinker glutaraldehyde.<sup>103,109,110</sup> First, GOx enzyme (200 units/mL) was added to a chitosan solution and droplets of this solution were collected in a solution of TPP. Electrostatic interactions between the cationic chitosan and the anionic TPP result in the conversion of the droplets into soft capsules/gels.<sup>111</sup> To further strengthen the chitosan-TPP particles, they were exposed to glutaraldehyde.<sup>102,103</sup> This gives us stable “killer” capsules with the GOx in their lumen.

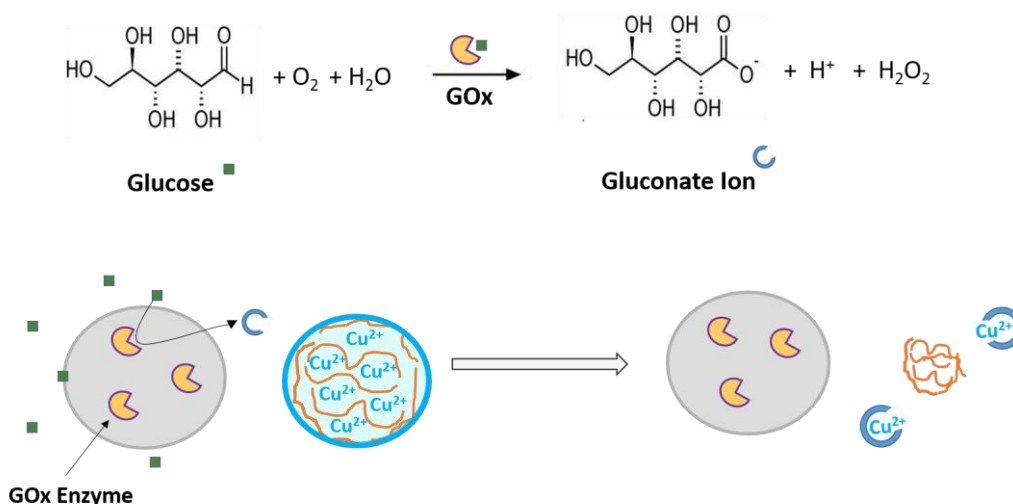


**Figure 5.5.** Schematic of killer chitosan capsule with encapsulated glucose oxidase (GOx) that targets neighboring Cu-alginate beads. Ambient glucose diffuses into the killer capsule, wherein, immobilized GOx enzyme converts glucose to gluconate ions, which diffuses out and targets neighboring Cu-alginate beads, resulting in destruction of the neighboring alginate bead.

Overall, the action of the killer capsules (bearing GOx) on their target Cu-alginate beads is conceptualized in Figure 5.5. Dissolved glucose from the surroundings diffuse into the killer capsule, where the glucose is catalyzed by the GOx enzyme and converted to gluconate. The gluconate molecules then diffuse out of the capsule and towards the

neighboring target Cu-alginate bead. As the gluconate molecules diffuse into the bead, they chelate the  $\text{Cu}^{2+}$  ions, which form the crosslinks in the bead. Thereby, the target bead is degraded into soluble alginate chains. To test this concept, we conducted the experiment shown in Figure 5.6. Here, the killer capsule has an orange color while the target Cu-alginate bead is blue-green (both structures have diameters around 2.5 mm). The two are placed in a buffered solution containing 1 wt% glucose. As expected, the alginate bead is observed to degrade over a period of 18 h, which is due to loss of its  $\text{Cu}^{2+}$  crosslinks.

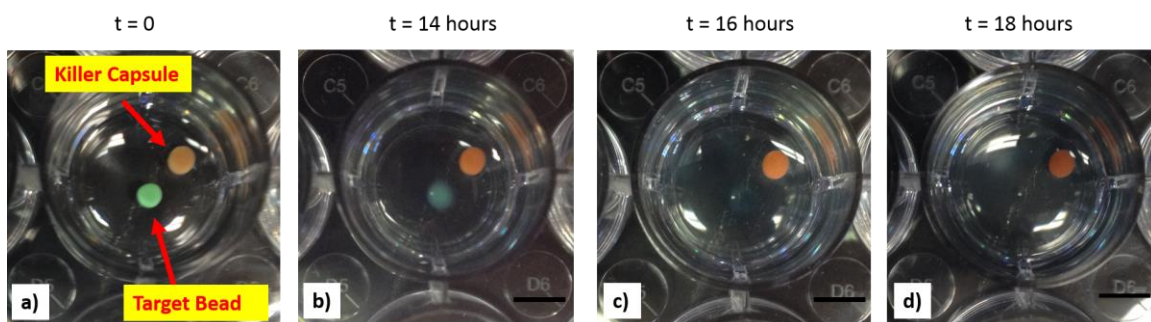


**Figure 5.6.** Visual observations depicting the degradation of a target Cu-alginate bead in the presence of a GOx loaded killer chitosan capsule. At  $t = 0$ , the killer capsule and target bead are placed together in a buffered glucose solution; Over the course of 18 hours, the target bead is completely destroyed. Scale bars: 5 mm.

Targeted bead degradation in the above manner could be useful for localized release of trapped cargo from the beads. We sought to demonstrate this by encapsulating fluorescent nanoparticles ( $\approx 100$  nm) within the target Cu-alginate bead matrix. In Figure 5.7, a killer chitosan capsule was placed near a target bead containing the nanoparticles, both were placed in a buffered 1 wt% glucose solution, and the system was visualized by fluorescence microscopy. Initially, the nanoparticles are contained within the bead and so

the fluorescence is confined to the bead volume. However, as the  $\text{Cu}^{2+}$  crosslinks are removed from the Cu-alginate bead, the nanoparticles get released into the surrounding solution. We thus see the emergence of background fluorescence in the solution once the bead is sufficiently degraded.

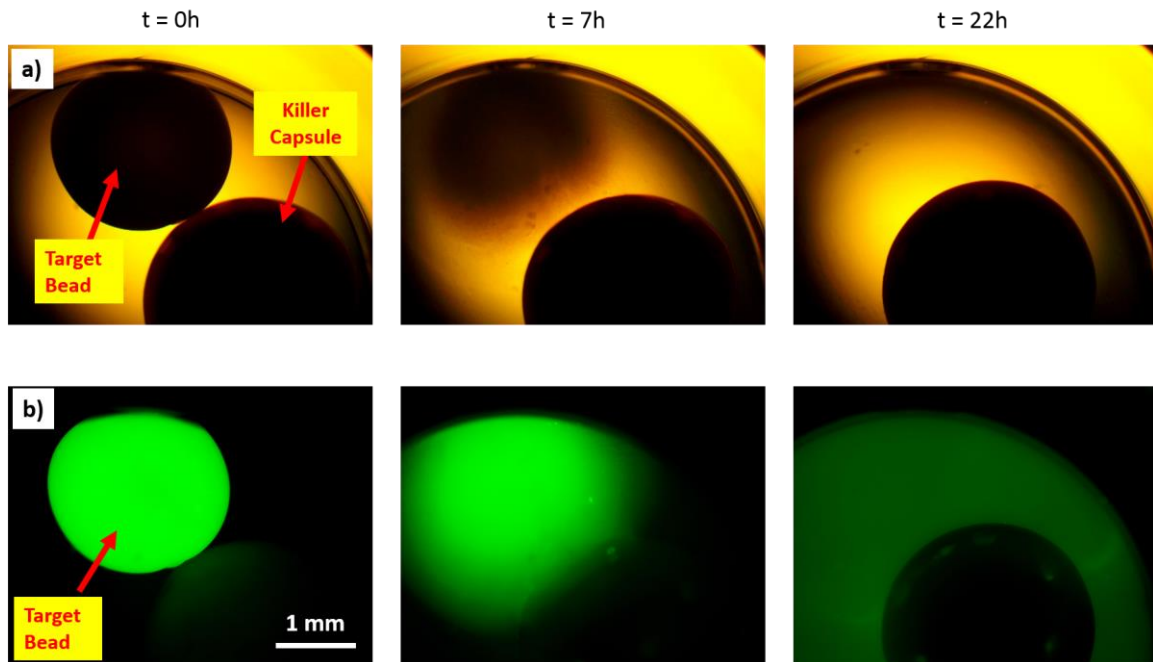


**Figure 5.7.** Fluorescent microscopy images demonstrating release of fluorescent nanoparticles from a degrading Cu-alginate bead. At  $t = 0$  the killer chitosan capsule was placed next to the target Cu-alginate bead. The top row of optical microscopy images depicts destruction of the target bead by the killer capsule and the corresponding fluorescent images in the bottom row depict the release of fluorescent particles as the target bead is degraded.



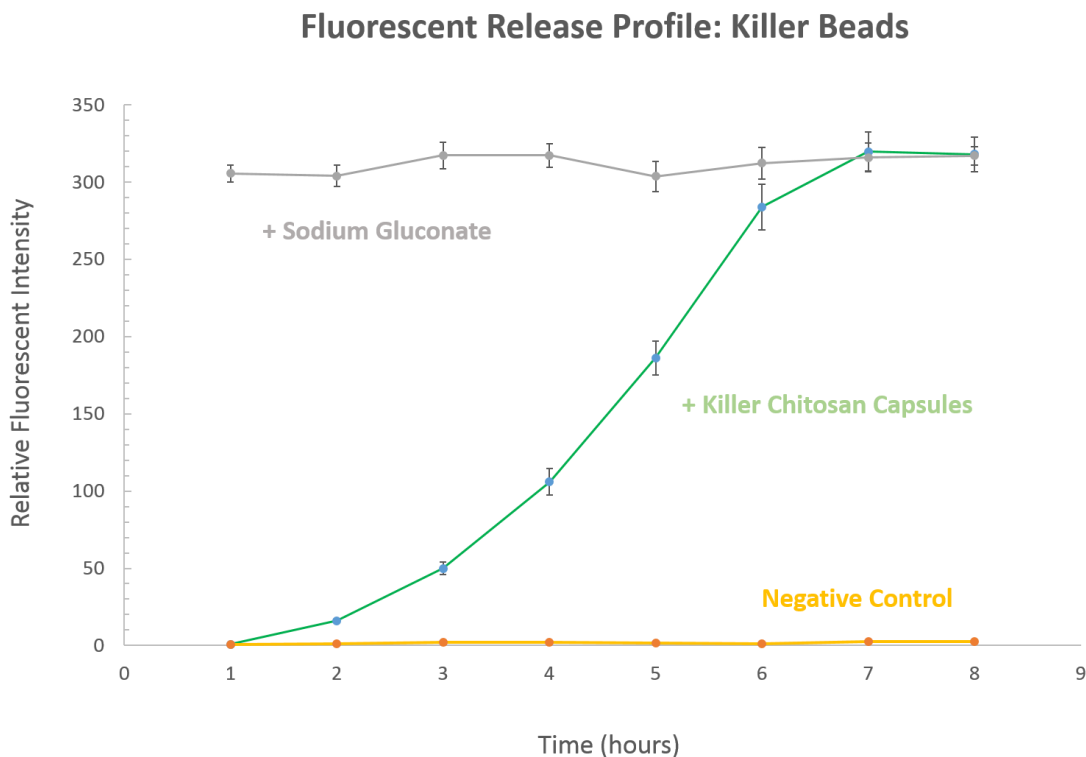


**Figure 5.8.** Quantifying release of fluorescent nanoparticles from a target alginate-copper bead. Using a plate reader, relative fluorescent intensities were measured hourly from aliquots of the surrounding solution. Target Cu-alginate beads exposed directly to pure chelator (sodium gluconate) quickly dissolved (within 1 hr) and released the fluorescent particles into the surrounding solution. Samples containing the killer chitosan capsules slowly degraded and the fluorescent intensity of the surrounding solution steadily increased. Negligible relative fluorescent intensity values were detected for the negative control (fluorescent target beads alone in buffer solution) indicating that the fluorescent nanoparticles cannot leak out of intact Cu-alginate beads. Error bars for each point represent one standard deviation among 5 runs.

To quantify release of fluorescent nanoparticles from Cu-alginate beads, the experimental design from Figure 5.7 was repeated under gentle stirring. Aliquots of the surrounding solution were analyzed over time to measure the background fluorescence. The results are represented in Figure 5.8. The negative control here is Cu-alginate beads with fluorescent nanoparticles in glucose-buffer solution—here there is no degradation and hence no fluorescence in the external solution over time. As a positive control, Cu-

alginate beads with fluorescent nanoparticles were exposed to pure chelator (sodium gluconate)—in this case, the beads degraded completely within 1 h, releasing their fluorescent payload into the solution. The intermediate case is when killer chitosan capsules are added to the target beads. In this case, the target beads are destroyed over a period of several hours. Over this time, the fluorescent nanoparticles will be increasingly released into solution, and as a result, we find a monotonic increase in fluorescence intensity until it plateaus at a value close to that of the positive control.

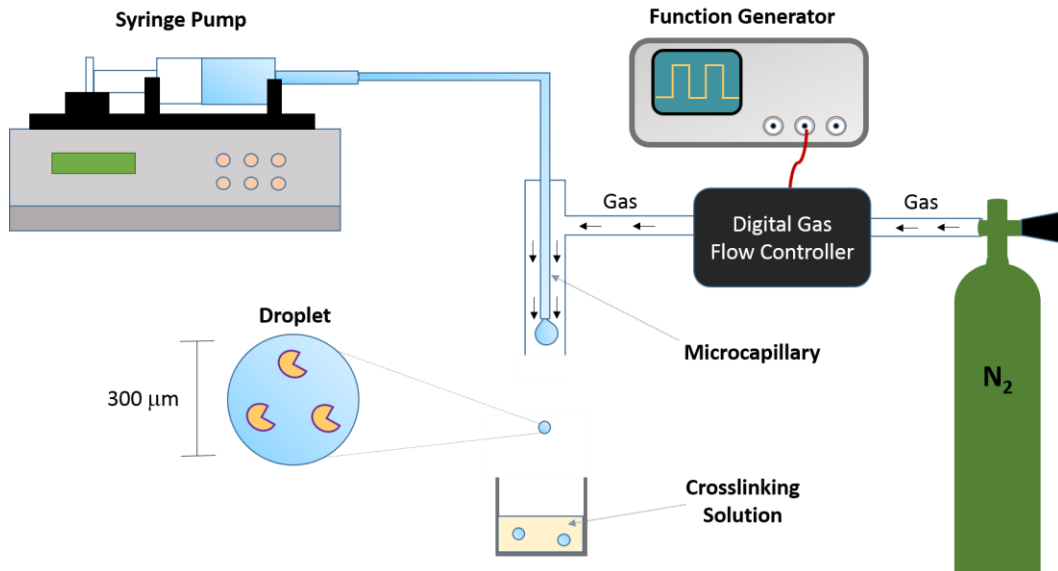


**Figure 5.9.** Preparation of killer chitosan microcapsules using a pulsed gas flow device. Smaller microdroplets, which results in smaller microcapsules, were generated by flowing the chitosan solution through a microcapillary (diameter  $\approx 100 \mu\text{m}$ ) and coaxial pulses of gas (regulated by a digital gas flow controller) sheared the chitosan solution into micron-sized droplets that were collected in a TPP cross-linking solution, resulting in cross-linked microcapsules. GOx enzyme was dispersed in the chitosan solution to generate killer chitosan capsules, similar to Figure 5.4.

The above experiments with killer and target particles were conducted using large mm-sized particles. We now proceed to test the same concept with smaller (micron-scale

particles). To create smaller counterparts of our particles, a method developed recently in our lab to form microdroplets<sup>104</sup> was adapted (Figure 5.9). Briefly, a digital gas flow controller connected to a function generator was used to regulate pulses of nitrogen gas, which sheared aqueous chitosan droplets (containing dispersed GOx enzyme) from a glass micro-capillary (diameter  $\approx 100 \mu\text{m}$ ). Similar to Figure 5.4, the chitosan droplets were introduced into aqueous TPP and then combined with glutaraldehyde to give killer microcapsules with encapsulated GOx enzyme. The same method was used to form aqueous droplets of sodium alginate, which were then added to a  $\text{Cu}^{2+}$  solution to form target Cu-alginate microbeads.

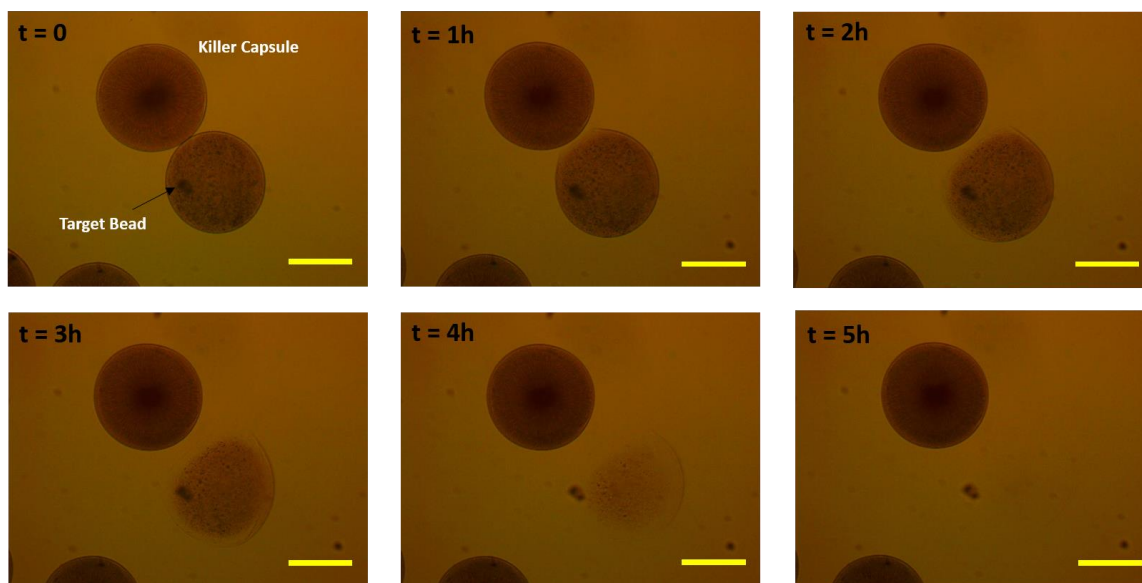


**Figure 5.10.** Optical microscopy images depicting degradation of a target Cu-alginate microbead by a neighboring killer chitosan microcapsule over the course of 5 hours. Scale bars:  $200 \mu\text{m}$ .

We tested the killer microcapsules against the target microbeads (both have diameters  $\approx 300 \mu\text{m}$ ) in a buffered glucose solution. The results are shown in Figure 5.10.

As before, the target Cu-alginate bead gets destroyed over the course of 5 h by its neighboring killer chitosan microcapsule. We found that the degradation is more rapid when the target microbead is very close to a killer microcapsule. In comparison, target microbeads that are relatively far from a killer microcapsule degrade more slowly. This shows the local nature of the destruction and is due to the fact that it relies on diffusion of the gluconate chelator from the killer to the target.

For a final proof-of-concept demonstration, we wanted to show specificity in destruction of target microbeads by the killer capsules. In the immune system, killer T cells destroy virus infected cells whereas they leave healthy bystander cells alone. To show this, we synthesized three different populations of microparticles, and their mixture in roughly equal numbers is shown in Figure 5.11a. One population is of killer chitosan microcapsules (diameter  $\approx 300 \mu\text{m}$ ), another population is the Cu-alginate target beads (diameter  $\approx 300 \mu\text{m}$ ), and the third population is composed of inert chitosan beads from Chapter 4 with encapsulated carbon black (diameter  $\approx 150 \mu\text{m}$ ). As time progresses, only the target Cu-alginate beads susceptible to the chelator are destroyed, as shown in Figure 5.11b and 5.11c. At the end of the experiment (Figure 5.11c), only two sets of particles (killer capsules and inert bystander beads) remain.

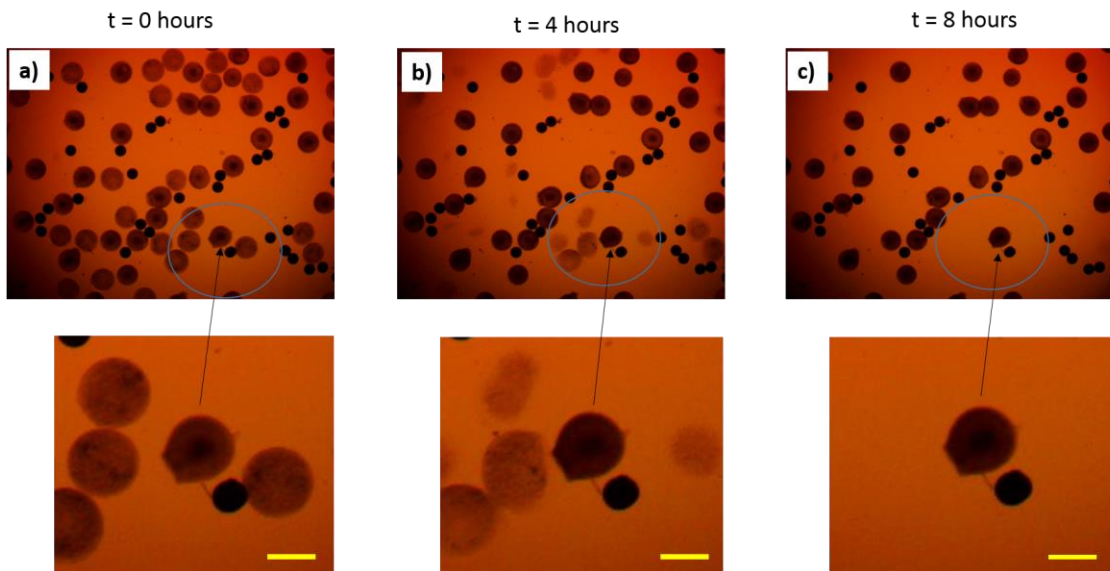


**Figure 5.11.** Optical microscopy images depicting selective degradation amongst 3 population sets of microparticles. One set of particles is comprised of killer chitosan capsules, another population contained the target Cu-alginate beads, and the third population was composed of black inert chitosan beads used in previous chapters. Due to selective targeting by the killer capsule, only two sets of particles (inert black beads and killer chitosan capsules) remained at the end of the experiment. Scale bars: 200  $\mu\text{m}$ .

## 5.4. CONCLUSIONS

We have shown development of killer T cell inspired chitosan capsules. This was done by immobilizing the glucose oxidase enzyme within the chitosan capsule. Glucose molecules in the surrounding solution are converted into gluconate ions by the GOx enzyme within the killer capsule. The gluconate molecules remove the copper ions ( $\text{Cu}^{2+}$ ) that cross-link a neighboring alginate bead, resulting in target bead destruction. To support this, we first demonstrated that direct addition of the GOx enzyme, in the presence of glucose (the substrate), can cause degradation of a Cu-alginate bead. Additionally, it was confirmed that the presence of both glucose and GOx were necessary to degrade the target Cu-alginate bead. Next, we encapsulated the GOx enzyme within a

killer chitosan capsule and observed killer capsule initiated destruction of Cu-alginate beads on two different size scales. Finally, the potential of this bead degradation system for release of cargo was demonstrated through encapsulation of fluorescent nanoparticles within the target bead. Upon degradation of the target Cu-alginate bead, the release of the fluorescent nanoparticles was visualized using fluorescent microscopy and quantified using a plate reader.

## Chapter 6

# CONCLUSION AND RECOMMENDATIONS

---

### 6.1. PROJECT SUMMARY AND PRINCIPAL CONTRIBUTIONS

In this dissertation we have shown three new concepts for engineering microparticles with bio-inspired functionalities. Each chapter focused on designing microparticles to have customized interactions with their surroundings as inspired by biological cells. Microparticle analogues were designed to demonstrate (1) selective adherence to surfaces (essential for pathogen identification by immune cells); (2) stimulus based clustering (necessary in blood clot formation by platelet cells) and (3) selective destruction of neighboring microparticles (inspired by killer T cells).

In Chapter 3, we functionalized chitosan microbeads with streptavidin that allowed for recognition and selective adherence to specific types of biological cells. Additionally, using simple commercially available microtubing, we developed bulk generation methods for the functionalized chitosan microbeads to allow for an inexpensive platform to conduct in-house customized cell capture studies. Moreover, through encapsulation of carbon black within the chitosan microbeads, we addressed a major barrier (intrinsic autofluorescence) towards implementation of chitosan microbeads in quantitative cell capture and detection studies.

In Chapter 4, we created a unique stimulus-based microbead clustering system that mimics the physical assembly of cells as seen in biological blood clot formation. The

chitosan microbeads from Chapter 3 are functionalized with cyclodextrins to embed cell membrane-like hydrophobic pockets, which resulted in rapid microbead clustering (similar to “platelet plugs”) upon recognition of an associating polymer (hm-chitosan). After initial clustering, the hm-chitosan polymer precipitates around the cluster and traps surrounding bystander microbeads in the polymer web. This hm-chitosan bead-polymer matrix (analogous to a fibrin-cell blood clot) was strong enough to transport captured bystander beads to desired locations. Such bio-inspired, stimulus-induced microbead clusters could be useful in embolization and bulk transport of micron-sized objects.

In Chapter 5, we describe development of killer chitosan microcapsules that can locally and selectively destroy neighboring alginate beads that were cross-linked with  $\text{Cu}^{2+}$ . Chitosan microcapsules are functionalized by encapsulating GOx enzyme, which allows for secretion of gluconate ions that remove  $\text{Cu}^{2+}$  cross-links from the target alginate bead. This results in chitosan microcapsules that can selectively destroy neighboring Cu-alginate beads. To the best of our knowledge, this was the first study to explore the concept of using one polymer particle as the vehicle to destroy another particle. Additionally, this was the first reported use of an enzyme to generate chelators for destruction of a metal cross-linked alginate bead. The findings in this Chapter could be useful in studies related to controlled release of payloads from microparticles.



## **6.2. RECOMMENDATIONS FOR FUTURE WORK**

### **6.2.1. Future Work with Microparticles Presented in this Dissertation**

It would be useful to combine functionalities demonstrated in the previous chapters to make even smarter and more cell-like microparticles. In Chapter 3, we described the functionalization of chitosan beads to selectively adhere to target surfaces through biotin-streptavidin interactions, while in Chapter 5, we described development of killer chitosan capsules that can selectively destroy neighboring alginate beads. To further add functionality and more closely mimic killer T cells, an exciting future study would be to combine the streptavidin-biotin binding system with the killer chitosan capsules from Chapter 5. Ideally, these new killer chitosan microcapsules, in addition to encapsulation of GOx enzyme, would have streptavidin molecules on their surface, while the payload carrying alginate bead would be modified with biotin molecules; this would allow selective adhesion of the killer chitosan capsules to only the target alginate beads, prior to target bead degradation. For this potential future study, alginate could be chemically modified with biotin, prior to cross-linking copper ions, as shown by others.<sup>112</sup>

In addition it would be very interesting to combine the microbead assembly system demonstrated in Chapter 4 with the bead degradation functionalities presented in Chapter 5. In Chapter 4, we demonstrated assembly of a bead-polymer matrix that can trap and transport surrounding bystander microbeads to desired locations. Interesting future studies could involve trapping and delivery of payload carrying target alginate

beads from Chapter 5, where nearby killer chitosan capsules could initiate release of the cargo through chelator based degradation.

Finally, each cell-inspired microparticle system presented in this dissertation employed microparticles ranging from 100-300 microns in size. That size scale was convenient, due to easily accessible commercial microtubing for microparticle synthesis, and useful for initial proof-of-concepts studies as shown in this dissertation; however, biological cells are an order of magnitude smaller in size  $\approx$  10-20 microns. Interesting future studies would be to apply the cell-inspired microbead systems presented in previous chapters with technologies that allow for synthesis of the microparticles at even smaller scales, closer to actual sizes of cells. One such technology is through use of pulled glass microcapillaries as presented by the Weitz group.<sup>113,114</sup> Overall, future studies to demonstrate concepts from this dissertation using smaller microparticles could be very interesting.

### **6.2.2. Red Blood Cell Shaped Microparticles**

In addition to the microparticle analogues presented in this dissertation, new types of microparticles could be designed to mimic other types of specialized biological cells. For instance, microparticles mimicking the biconcave shape of red blood cells have been explored in other studies.<sup>101,115,116</sup> Generally, on the micron scale, controlling the shape of the polymer particles is a challenge due to the effects of surface tension, which favor spherical morphologies.<sup>117</sup> Thus, an additional “manufacturing” step to control shape is required in a microfluidic droplet generator. The Weitz group was the first to show how

anisotropic microparticles could be generated through controlled solidification of a polymer droplet in a microfluidic device.<sup>117</sup> Their microfluidic system can yield red blood cell shaped microparticles from various synthetic polymers such as polysulfone, polymethyl methacrylate, and polyvinylidene fluoride. Alternatively, the DeSimone group generates biocompatible red blood cell shaped microparticles from biopolymers and have found that tuning their shape and elasticity can affect their biological retention time, when intravenously injected into mice.<sup>118</sup> However, the DeSimone group uses prefabricated molds (Print®) for generation of biocompatible biopolymer based particles. Additional studies adapting the red blood cell shaped particles in a microfluidic generation system for biopolymers could be useful.

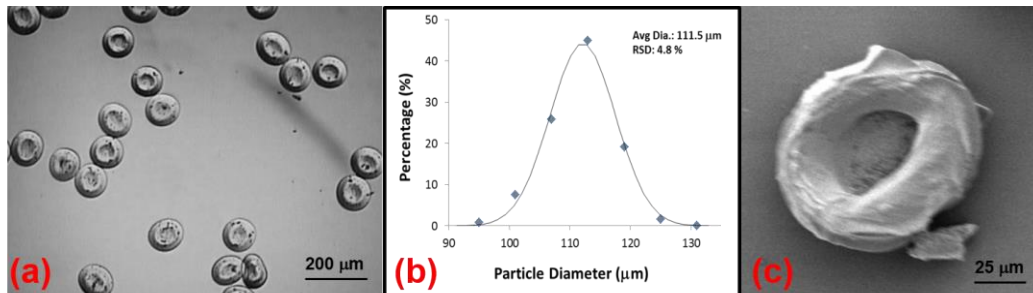


**Figure 6.1.** Images of red blood cell shaped alginate microparticles from: (a) optical microscopy; and (c) SEM. In (b) the size distribution of microparticles in (a) is plotted. The average diameter is 111.5 μm with a relative standard deviation of 4.8% (n = 100). The solid line in (b) is a Gaussian fit to the data.

We conducted preliminary experiments where red blood cell shaped alginate particles were created through a simple microfluidic process. First, aqueous droplets of alginate were generated in a microfluidic device through shearing by a continuous oil phase comprised of 1-decanol. Next, the alginate droplets (flowing in a continuous 1-decanol

stream) were then collected in an ethanol solution, resulting in precipitation of the alginate droplet into red blood cell shaped alginate particles as shown in Figure 6.1. Future studies further exploring the mechanism for shape transformation in this alginate microparticles system would be very interesting.

## APPENDIX:

### DETAILED PROCEDURES MICROBEAD SYNTHESIS

---

Two phase flow (continuous oil phase and dispersed aqueous phase) was used to generate chitosan droplets in a tubing device manufactured from commercial fittings and tubing. The chitosan droplets were converted into solid chitosan microbeads upon collection into an oil solution containing the cross-linker glutaraldehyde (GA). A washing procedure was developed to provide stable transfer of the chitosan beads into aqueous solutions. A detailed procedure is provided below.

#### 1) Construction of the Tubing Device

1.1) Cut out small length ( $\approx 6.5$  cm) of silica tubing ( $\approx 150$   $\mu\text{m}$  inner diameter / 220  $\mu\text{m}$  outer diameter ) and attach Luer Lock fittings to the Luer Tee.

1.2) Insert silica tubing through the Luer Tee and have roughly an even amount of silica tubing exposed on each side ( $\approx 1.0$  cm) of the Luer Tee.

1.3) From one end, insert the PTFE ( $\approx 300$   $\mu\text{m}$ ) tubing over the exposed silica tubing (without changing the position of the silica tubing in the Luer Tee), until the PTFE tubing is halfway through the Luer Tee.

1.4) Use 5 minute epoxy to seal both ends of the Luer Tee, on the orifice of the Luer Lock fittings

1.5) Connect the Tygon tubing over the other two Luer Lock orifices on the Luer Tee.

The tubing device is designed for the aqueous phase to flow through the silica capillary, where it will meet a faster flowing oil stream at the end of the silica capillary (which is inside the PTFE tubing, but outside the Luer Tee). The droplets are generated at this location and the size of the droplets correlates to the inner diameter of the PTFE tubing. The oil phase will enter through the perpendicular orifice on the Luer Tee and completely fill the Luer Tee body without interacting with the aqueous phase (which is inside the silica capillary), until it exists towards the PTFE tubing where it will meet the aqueous phase at the end of the silica capillary.

## 2) Generation of Chitosan Beads using the Tubing Device

2.1) Prepare an aqueous 2 wt% chitosan (pH 5.5) solution and load the solution into a 5 mL plastic syringe.

2.2) Prepare a second solution with 2 wt% SPAN 80 in Hexadecane and load into a 20 mL plastic syringe.

2.3) Tap both syringes to remove all bubbles. As the chitosan solution is more viscous, significantly longer tapping may be required to remove the bubbles.

2.4) Connect the chitosan solution syringe to a female Luer Lock fitting and then connect that fitting to the tygon tubing, which is connected to the tubing device. Prepare the same connections between the oil solution syringe and the tubing device. Lock in the two syringes on two separate syringe pumps.

2.5) Pump the hexadecane containing syringe at 30  $\mu\text{L}/\text{min}$  and the syringe containing chitosan at 2  $\mu\text{L}/\text{min}$  (we are running the solutions at higher flow rates initially to quickly reach the maximum pressure buildup within the device for equilibrium droplet generation) until all the air bubbles have been eliminated and the first chitosan droplets are generated. These first chitosan droplets can be collected in a vial containing hexadecane with 2 wt% Span 80.

2.6) Lower the syringe pump rates to 10  $\mu\text{L}/\text{min}$  (oil solution) and 0.33  $\mu\text{L}/\text{min}$  (aqueous chitosan solution). The settings at 10  $\mu\text{L}/\text{min}$  (oil solution) and 0.33  $\mu\text{L}/\text{min}$  (aqueous chitosan solution) will be the final steady state settings for generation and collection of droplets. Run the system at these rates for at least 45 minutes. Check that the droplets are being generated at a steady state (the droplets should be flowing at a constant rate throughout the 300 micron tube) before collecting the droplets in the cross-linking solution.

2.7) Put outlet of tubing device (PTFE tubing) into the cross-linking solution (2% by volume Glutaraldehyde, 2 wt% Span 80, in Hexadecane), with mild mixing conditions (200-500 RPM) using a magnetic stir bar such that the droplets are mixing throughout the collection container before settling.

Droplets can be collected for approximately 20 hours without the need to refill the syringes or worrying about overflowing the collection vial. Once the desired amount of droplets is generated, remove the tubing from the collection container as well as the stir bar. Store the droplets in the cross-linking solution for 5 days.



**Figure A1.** Microfluidic tubing device setup for the generation of chitosan microbeads. The 5 mL syringe (top) is loaded with the chitosan solution and the 20 mL syringe (bottom) is loaded with the oil solution. The collection vial, placed at the center of the stir plate, contains the cross-linking solution, which turns turbid when the glutaraldehyde is dispersed in the oil. The tip of the PTFE tubing is submerged in the GA solution, but should be held close to the surface of the liquid (i.e. it should not be in contact with the bottom or the walls of the vial).

### 3) Washing Procedure for the Chitosan Beads

Before using the chitosan beads in aqueous buffers, it is suggested to conduct a series of solvent exchange steps to transfer the dispersed beads from the oil-based GA solution to an aqueous buffer. The first step is to remove the residual GA and water surrounding the beads via nitrogen gas evaporation.

3.1) Transfer all the beads within the collection solution to various small glass vials ( $\approx 5$  mL).

3.2) Wait for the beads to settle to the bottom of the container ( $\approx 1$ -2 minutes) as shown in Figure A2.

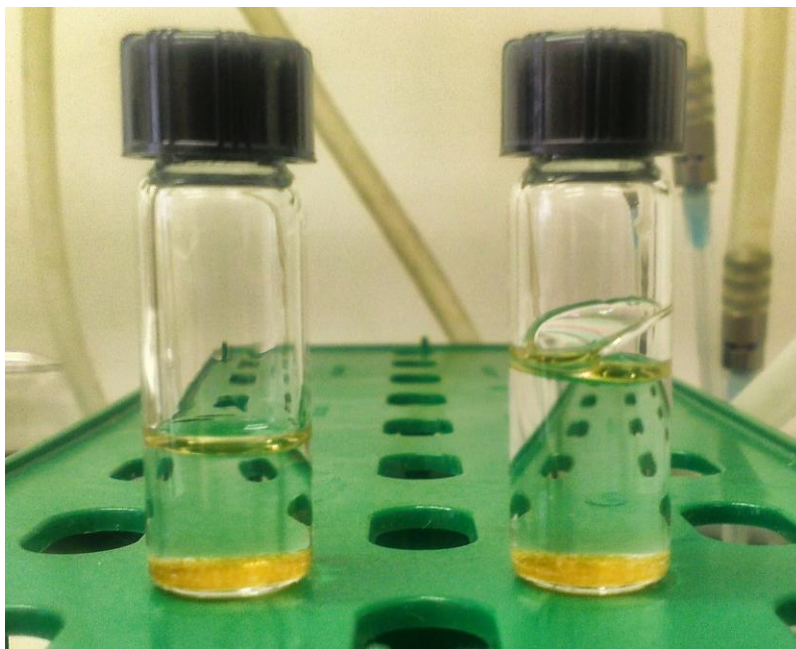


**Figure A2.** Chitosan microbeads in the cross-linking solution (2 wt% Span 80, 2 % by volume glutaraldehyde in hexadecane) after a five-day storage period. The beads are allowed to settle to the bottom before removing most of the cross-linking solution.

3.3) Remove the collection solution (all but 1 mL as shown in Figure A3a) and replace it with pure 1-decanol. Fill half of the vial with 1-decanol; otherwise, the vial will overflow once  $N_2$  is added.

3.4) Air the 1-decanol and beads mixture with nitrogen gas for 3 hours to evaporate the GA and water in the solution. To deliver the nitrogen gas (1-2 psi), insert the degassing needle into a plastic transfer pipette before placing it in the vial (Figure A3). This method will help create a broader and stronger convection current and will allow the beads to float freely in the solution. Remember to tape the vial to a stable surface to avoid spilling the contents of the vial.



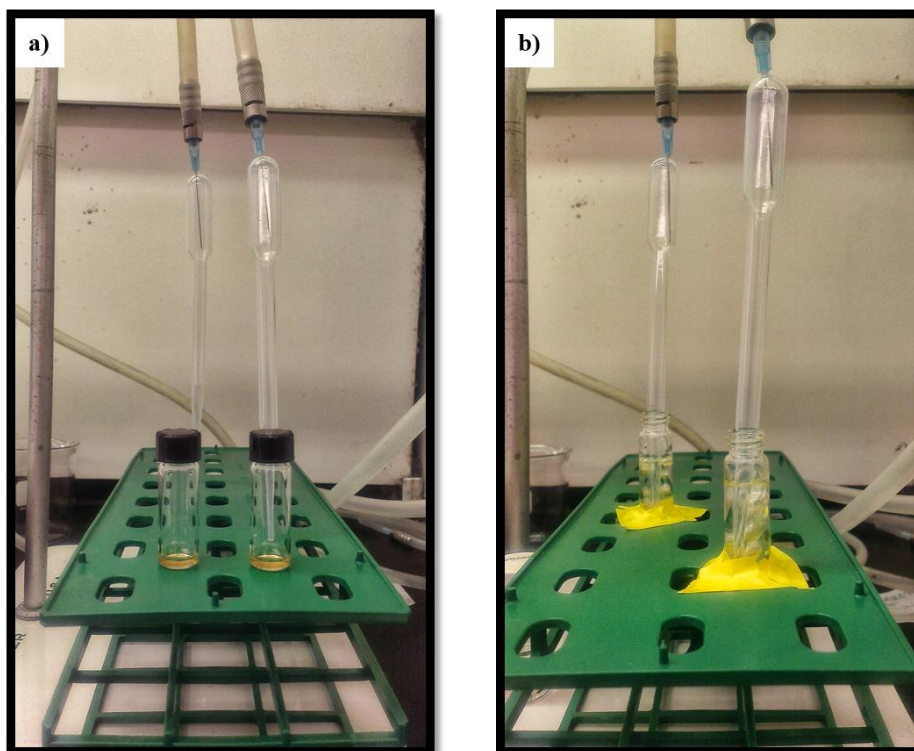


**Figure A3.** Picture a) shows the vial of beads after removing the cross-linking solution and before adding the pure 1-decanol. After approximately half of the vial containing the beads is filled with 1-decanol, the transfer pipette is placed in the vial (b). Then, the vial is taped to the supporting platform and the nitrogen gas valve is opened (1-2 psi). Adding nitrogen gas to the solution will create convection and air bubbles (b). The configuration of the needles (covered with plastic transfer pipettes) that deliver the nitrogen gas is illustrated in both pictures.

3.5) After the degasification process, transfer the beads to larger vial ( $\approx 30$  mL) and then remove the existing 1-decanol solution. Replace this solution by filling the vial with fresh 1-decanol. This solvent exchange process will be considered a single wash. Any further references to washing of the chitosan beads in the protocol will refer to allowing beads to settle and replacement of the existing solution with the stated new solution.

3.6) Repeat the 1-decanol wash one more time and then sequentially wash the beads with ethanol (3 times) and water (3 times).

After performing this washing procedure, the beads can be stored in aqueous solutions, where they will remain stable and dispersed as individual beads over time. For maximum stability in aqueous solution ( $\approx 2$  years), functionalize the beads with streptavidin as described in Chapter 3.

## REFERENCES

- [1] Youtie, J.; Shapira, P.; Porter, A. L. "Nanotechnology publications and citations by leading countries and blocs." *Journal of Nanoparticle Research* **2008**, *10*, 981-986.
- [2] Kamholz, A. E. "Proliferation of microfluidics in literature and intellectual property." *Lab on a Chip* **2004**, *4*, 16N-20N.
- [3] Bedau, M. A.; Parke, E. C.; Tangen, U.; Hantsche-Tangen, B. "Social and ethical checkpoints for bottom-up synthetic biology, or protocells." *Systems and Synthetic Biology* **2009**, *3*, 65-75.
- [4] Adamala, K.; Szostak, J. W. "Competition between model protocells driven by an encapsulated catalyst (vol 5, pg 495, 2013)." *Nature Chemistry* **2013**, *5*, 634-634.
- [5] Zenisek, S. F. M.; Hayden, E. J.; Lehman, N. "Genetic exchange leading to self-assembling RNA species upon encapsulation in artificial protocells." *Artificial Life* **2007**, *13*, 279-289.
- [6] Kamat, N. P.; Henry, S. J.; Lee, D.; Hammer, D. A. "Single-Vesicle Patterning of Uniform, Giant Polymersomes into Microarrays." *Small* **2013**, *9*, 2272-2276.
- [7] Gibson, D. G.; Glass, J. I.; Lartigue, C.; Noskov, V. N.; Chuang, R. Y.; Algire, M. A.; Benders, G. A.; Montague, M. G.; Ma, L.; Moodie, M. M.; Merryman, C.; Vashee, S.; Krishnakumar, R.; Assad-Garcia, N.; Andrews-Pfannkoch, C.; Denisova, E. A.; Young, L.; Qi, Z. Q.; Segall-Shapiro, T. H.; Calvey, C. H.; Parmar, P. P.; Hutchison, C. A.; Smith, H. O.; Venter, J. C. "Creation of a Bacterial Cell Controlled by a Chemically Synthesized Genome." *Science* **2010**, *329*, 52-56.
- [8] Rasmussen, S.; Chen, L. H.; Nilsson, M.; Abe, S. "Bridging nonliving and living matter." *Artificial Life* **2003**, *9*, 269-316.
- [9] Hammer, D. A.; Kamat, N. P. "Towards an artificial cell." *Febs Letters* **2012**, *586*, 2882-2890.
- [10] Campos, E.; Branquinho, J.; Carreira, A. S.; Carvalho, A.; Coimbra, P.; Ferreira, P.; Gil, M. H. "Designing polymeric microparticles for biomedical and industrial applications." *European Polymer Journal* **2013**, *49*, 2005-2021.
- [11] De Geest, B. G.; Willart, M. A.; Lambrecht, B. N.; Pollard, C.; Vervaet, C.; Remon, J. P.; Grooten, J.; De Koker, S. "Surface-Engineered Polyelectrolyte Multilayer Capsules: Synthetic Vaccines Mimicking Microbial Structure and Function." *Angewandte Chemie-International Edition* **2012**, *51*, 3862-3866.

- [12] Gupta, A.; Terrell, J. L.; Fernandes, R.; Dowling, M. B.; Payne, G. F.; Raghavan, S. R.; Bentley, W. E. "Encapsulated fusion protein confers "sense and respond" activity to chitosan-alginate capsules to manipulate bacterial quorum sensing." *Biotechnology and Bioengineering* **2013**, *110*, 552-562.
- [13] Teh, S. Y.; Lin, R.; Hung, L. H.; Lee, A. P. "Droplet microfluidics." *Lab on a Chip* **2008**, *8*, 198-220.
- [14] Wang, J. T.; Wang, J.; Han, J. J. "Fabrication of Advanced Particles and Particle-Based Materials Assisted by Droplet-Based Microfluidics." *Small* **2011**, *7*, 1728-1754.
- [15] Kamat, N. P.; Katz, J. S.; Hammer, D. A. "Engineering Polymersome Protocells." *Journal of Physical Chemistry Letters* **2011**, *2*, 1612-1623.
- [16] Chu, L. Y.; Utada, A. S.; Shah, R. K.; Kim, J. W.; Weitz, D. A. "Controllable monodisperse multiple emulsions." *Angewandte Chemie-International Edition* **2007**, *46*, 8970-8974.
- [17] Moller, J.; Luhmann, T.; Chabria, M.; Hall, H.; Vogel, V. "Macrophages lift off surface-bound bacteria using a filopodium-lamellipodium hook-and-shovel mechanism." *Scientific Reports* **2013**, *3*.
- [18] Ariens, R. A. S.; Lai, T. S.; Weisel, J. W.; Greenberg, C. S.; Grant, P. J. "Role of factor XIII in fibrin clot formation and effects of genetic polymorphisms." *Blood* **2002**, *100*, 743-754.
- [19] Kumar, M. N. V. R. "A review of chitin and chitosan applications." *Reactive & Functional Polymers* **2000**, *46*, 1-27.
- [20] Rinaudo, M. "Chitin and chitosan: Properties and applications." *Progress in Polymer Science* **2006**, *31*, 603-632.
- [21] Jayakumar, R.; Menon, D.; Manzoor, K.; Nair, S. V.; Tamura, H. "Biomedical applications of chitin and chitosan based nanomaterials-A short review." *Carbohydrate Polymers* **2010**, *82*, 227-232.
- [22] Bernkop-Schnurch, A. "Chitosan and its derivatives: potential excipients for peroral peptide delivery systems." *International Journal of Pharmaceutics* **2000**, *194*, 1-13.
- [23] Mourya, V. K.; Inamdar, N. N. "Chitosan-modifications and applications: Opportunities galore." *Reactive & Functional Polymers* **2008**, *68*, 1013-1051.

- [24] Desbrieres, J.; Martinez, C.; Rinaudo, M. "Hydrophobic derivatives of chitosan: Characterization and rheological behaviour." *International Journal of Biological Macromolecules* **1996**, *19*, 21-28.
- [25] Javvaji, V. PhD dissertation, New Concepts for Gelation of Alginate and its Derivatives, University of Maryland, **2006**.
- [26] Lee, K. Y.; Mooney, D. J. "Alginate: Properties and biomedical applications." *Progress in Polymer Science* **2012**, *37*, 106-126.
- [27] Pawar, S. N.; Edgar, K. J. "Alginate derivatization: A review of chemistry, properties and applications." *Biomaterials* **2012**, *33*, 3279-3305.
- [28] Augst, A. D.; Kong, H. J.; Mooney, D. J. "Alginate hydrogels as biomaterials." *Macromolecular Bioscience* **2006**, *6*, 623-633.
- [29] Macquarrie, D. J.; Bacheva, A. "Efficient subtilisin immobilization in chitosan, and peptide synthesis using chitosan-subtilisin biocatalytic films." *Green Chemistry* **2008**, *10*, 692-695.
- [30] Jiang, K. Q.; Xue, C.; Arya, C. D.; Shao, C. R.; George, E. O.; DeVoe, D. L.; Raghavan, S. R. "A New Approach to In-Situ "Micromanufacturing": Microfluidic Fabrication of Magnetic and Fluorescent Chains Using Chitosan Microparticles as Building Blocks." *Small* **2011**, *7*, 2470-2476.
- [31] Yang, C. H.; Lin, Y. S.; Huang, K. S.; Huang, Y. C.; Wang, E. C.; Jhong, J. Y.; Kuo, C. Y. "Microfluidic emulsification and sorting assisted preparation of monodisperse chitosan microparticles." *Lab on a Chip* **2009**, *9*, 145-150.
- [32] Galant, C.; Wintgens, W.; Amiel, C.; Auvray, L. "A reversible polyelectrolyte involving a beta-cyclodextrin polymer and a cationic surfactant." *Macromolecules* **2005**, *38*, 5243-5253.
- [33] Tonelli, A. E. "Nanostructuring and functionalizing polymers with cyclodextrins." *Polymer* **2008**, *49*, 1725-1736.
- [34] Dowling, M. B.; Kumar, R.; Keibler, M. A.; Hess, J. R.; Bochicchio, G. V.; Raghavan, S. R. "A self-assembling hydrophobically modified chitosan capable of reversible hemostatic action." *Biomaterials* **2011**, *32*, 3351-3357.
- [35] Lee, J.; Gustin, J.; Chen, T.; Payne, G.; Raghavan, S. "Vesicle-biopolymer gels: Networks of surfactant vesicles connected by associating biopolymers." *Langmuir* **2005**, *21*, 26-33.
- [36] Dowling, M.; Javvaji, V.; Payne, G.; Raghavan, S. "Vesicle capture on patterned surfaces coated with amphiphilic biopolymers." *Soft Matter* **2011**, *7*, 1219-1226.

- [37] Birdi, G.; Bridson, R. H.; Smith, A. M.; Bohari, S. P. M.; Grover, L. M. "Modification of alginate degradation properties using orthosilicic acid." *Journal of the Mechanical Behavior of Biomedical Materials* **2012**, *6*, 181-187.
- [38] Bresnahan, W. T.; Grant, C. L.; Weber, J. H. "Stability-Constants for Complexation of Copper(II) Ions with Water and Soil Fulvic Acids Measured by an Ion-Selective Electrode." *Analytical Chemistry* **1978**, *50*, 1675-1679.
- [39] Smith, R. A.; Martell, A. E. "NIST Standard reference database 46; U.S. Department of Commerce: Gaithersburg, MD." **1997**.
- [40] Murphy, D. B. *Fundamentals of Light Microscopy and Electronic Imaging* Wiley-Liss: New York, NY, 2001.
- [41] McIntyre, T. M.; Prescott, S. M.; Weyrich, A. S.; Zimmerman, G. A. "Cell-cell interactions: leukocyte-endothelial interactions." *Current Opinion in Hematology* **2003**, *10*, 150-158.
- [42] Bevan, M. J. "Helping the CD8(+) T-cell response." *Nature Reviews Immunology* **2004**, *4*, 595-602.
- [43] den Toonder, J. "Circulating tumor cells: the Grand Challenge." *Lab on a Chip* **2011**, *11*, 375-377.
- [44] Nagrath, S.; Sequist, L. V.; Maheswaran, S.; Bell, D. W.; Irimia, D.; Ulkus, L.; Smith, M. R.; Kwak, E. L.; Digumarthy, S.; Muzikansky, A.; Ryan, P.; Balis, U. J.; Tompkins, R. G.; Haber, D. A.; Toner, M. "Isolation of rare circulating tumour cells in cancer patients by microchip technology." *Nature* **2007**, *450*, 1235-9.
- [45] Li, P.; Stratton, Z. S.; Dao, M.; Ritz, J.; Huang, T. J. "Probing circulating tumor cells in microfluidics." *Lab on a Chip* **2013**, *13*, 602-609.
- [46] Lin, H. K.; Zheng, S. Y.; Williams, A. J.; Balic, M.; Groshen, S.; Scher, H. I.; Fleisher, M.; Stadler, W.; Datar, R. H.; Tai, Y. C.; Cote, R. J. "Portable Filter-Based Microdevice for Detection and Characterization of Circulating Tumor Cells." *Clinical Cancer Research* **2010**, *16*, 5011-5018.
- [47] Hong, B.; Zu, Y. L. "Detecting Circulating Tumor Cells: Current Challenges and New Trends." *Theranostics* **2013**, *3*, 377-394.
- [48] Shi, G. X.; Cui, W. J.; Benchimol, M.; Liu, Y. T.; Mattrey, R. F.; Mukthavaram, R.; Kesari, S.; Esener, S. C.; Simberg, D. "Isolation of Rare Tumor Cells from Blood Cells with Buoyant Immuno-Microbubbles." *Plos One* **2013**, *8*.

- [49] Rosenberg, R.; Gertler, R.; Friederichs, J.; Fuehrer, K.; Dahm, M.; Phelps, R.; Thorban, S.; Nekarda, H.; Siewert, J. R. "Comparison of two density gradient centrifugation systems for the enrichment of disseminated tumor cells in blood." *Cytometry* **2002**, *49*, 150-158.
- [50] Konigsberg, R.; Obermayr, E.; Bises, G.; Pfeiler, G.; Gneist, M.; Wrba, F.; de Santis, M.; Zeillinger, R.; Hudec, M.; Dittrich, C. "Detection of EpCAM positive and negative circulating tumor cells in metastatic breast cancer patients." *Acta Oncologica* **2011**, *50*, 700-710.
- [51] Hatch, A.; Hansmann, G.; Murthy, S. K. "Engineered Alginate Hydrogels for Effective Microfluidic Capture and Release of Endothelial Progenitor Cells from Whole Blood." *Langmuir* **2011**, *27*, 4257-4264.
- [52] Kralj, J. G.; Arya, C.; Tona, A.; Forbes, T. P.; Munson, M. S.; Sorbara, L.; Srivastava, S.; Forry, S. P. "A simple packed bed device for antibody labelled rare cell capture from whole blood." *Lab on a Chip* **2012**, *12*, 4972-4975.
- [53] Payne, G. F.; Raghavan, S. R. "Chitosan: a soft interconnect for hierarchical assembly of nano-scale components." *Soft Matter* **2007**, *3*, 521-527.
- [54] Koev, S. T.; Dykstra, P. H.; Luo, X.; Rubloff, G. W.; Bentley, W. E.; Payne, G. F.; Ghodssi, R. "Chitosan: an integrative biomaterial for lab-on-a-chip devices." *Lab on a Chip* **2010**, *10*, 3026-3042.
- [55] Nisisako, T.; Torii, T.; Higuchi, T. "Novel microreactors for functional polymer beads." *Chemical Engineering Journal* **2004**, *101*, 23-29.
- [56] De Geest, B. G.; Urbanski, J. P.; Thorsen, T.; Demeester, J.; De Smedt, S. C. "Synthesis of monodisperse biodegradable microgels in microfluidic devices." *Langmuir* **2005**, *21*, 10275-10279.
- [57] Seiffert, S.; Weitz, D. A. "Controlled fabrication of polymer microgels by polymer-analogous gelation in droplet microfluidics." *Soft Matter* **2010**, *6*, 3184-3190.
- [58] Duncanson, W. J.; Lin, T.; Abate, A. R.; Seiffert, S.; Shah, R. K.; Weitz, D. A. "Microfluidic synthesis of advanced microparticles for encapsulation and controlled release." *Lab on a Chip* **2012**, *12*, 2135-2145.
- [59] Lorber, N.; Sarrazin, F.; Guillot, P.; Panizza, P.; Colin, A.; Pavageau, B.; Hany, C.; Maestro, P.; Marre, S.; Delclos, T.; Aymonier, C.; Subra, P.; Prat, L.; Gourdon, C.; Mignard, E. "Some recent advances in the design and the use of miniaturized droplet-based continuous process: Applications in chemistry and high-pressure microflows." *Lab on a Chip* **2011**, *11*, 779-787.

- [60] Baroud, C. N.; Gallaire, F.; Dangla, R. "Dynamics of microfluidic droplets." *Lab on a Chip* **2010**, *10*, 2032-2045.
- [61] Seemann, R.; Brinkmann, M.; Pfohl, T.; Herminghaus, S. "Droplet based microfluidics." *Reports on Progress in Physics* **2012**, *75*.
- [62] Ballard, D. H. "Generalizing the Hough Transform to Detect Arbitrary Shapes." *Pattern Recognition* **1981**, *13*, 111-122.
- [63] Meyer, C. D.; Joiner, C. S.; Stoddart, J. F. "Template-directed synthesis employing reversible imine bond formation." *Chemical Society Reviews* **2007**, *36*, 1705-1723.
- [64] Rasband, W. S. "ImageJ, US National Institutes of Health." <http://imagej.nih.gov/ij> **1997-2012**.
- [65] Quevedo, E.; Steinbacher, J.; McQuade, D. T. "Interfacial polymerization within a simplified microfluidic device: Capturing capsules." *Journal of the American Chemical Society* **2005**, *127*, 10498-10499.
- [66] Nurumbetov, G.; Ballard, N.; Bon, S. A. F. "A simple microfluidic device for fabrication of double emulsion droplets and polymer microcapsules." *Polymer Chemistry* **2012**, *3*, 1043-1047.
- [67] Wei, W.; Wang, L. Y.; Yuan, L.; Yang, X. D.; Su, Z. G.; Ma, G. H. "Bioprocess of uniform-sized crosslinked chitosan microspheres in rats following oral administration." *European Journal of Pharmaceutics and Biopharmaceutics* **2008**, *69*, 878-886.
- [68] Wei, W.; Wang, L. Y.; Yuan, L.; Wei, Q.; Yang, X. D.; Su, Z. G.; Ma, G. H. "Preparation and application of novel microspheres possessing autofluorescent properties." *Advanced Functional Materials* **2007**, *17*, 3153-3158.
- [69] Oliveira, V. C.; Carrara, R. C. V.; Simoes, D. L. C.; Saggioro, F. P.; Carlotti, C. G.; Covas, D. T.; Neder, L. "Sudan Black B treatment reduces autofluorescence and improves resolution of in situ hybridization specific fluorescent signals of brain sections." *Histology and Histopathology* **2010**, *25*, 1017-1024.
- [70] Allen, N. S.; Pena, J. M.; Edge, M.; Liauw, C. M. "Behaviour of carbon black pigments as excited state quenchers in LDPE." *Polymer Degradation and Stability* **2000**, *67*, 563-566.
- [71] Shi, X. W.; Liu, Y.; Lewandowski, A. T.; Wu, L. Q.; Wu, H. C.; Ghodssi, R.; Rubloff, G. W.; Bentley, W. E.; Payne, G. F. "Chitosan biotinylation and electrodeposition for selective protein assembly." *Macromolecular Bioscience* **2008**, *8*, 451-457.

- [72] Gallacher, L.; Murdoch, B.; Wu, D. M.; Karanu, F. N.; Keeney, M.; Bhatia, M. "Isolation and characterization of human CD34(-)Lin(-) and CD34(+)Lin(-) hematopoietic stem cells using cell surface markers AC133 and CD7." *Blood* **2000**, *95*, 2813-2820.
- [73] Ramachandran, S.; Nandhakumar, S.; Dhanaraju, M. D. "Formulation and Characterization of Glutaraldehyde Cross-Linked Chitosan Biodegradable Microspheres Loaded with Famotidine." *Tropical Journal of Pharmaceutical Research* **2011**, *10*, 309-316.
- [74] Ngomsik, A. F.; Bee, A.; Draye, M.; Cote, G.; Cabuil, V. "Magnetic nano- and microparticles for metal removal and environmental applications: a review." *Comptes Rendus Chimie* **2005**, *8*, 963-970.
- [75] Kim, J. S.; Ligler, F. S. "Utilization of microparticles in next-generation assays for microflow cytometers." *Analytical and Bioanalytical Chemistry* **2010**, *398*, 2373-2382.
- [76] Wang, B.; Shum, H.; Weitz, D. "Fabrication of Monodisperse Toroidal Particles by Polymer Solidification in Microfluidics." *Chemphyschem* **2009**, *10*, 641-645.
- [77] Jiang, K.; Thomas, P.; Forry, S.; DeVoe, D.; Raghavan, S. "Microfluidic synthesis of monodisperse PDMS microbeads as discrete oxygen sensors." *Soft Matter* **2012**, *8*, 923-926.
- [78] Velev, O. D.; Gupta, S. "Materials Fabricated by Micro- and Nanoparticle Assembly - The Challenging Path from Science to Engineering." *Advanced Materials* **2009**, *21*, 1897-1905.
- [79] Furst, E. M.; Suzuki, C.; Fermigier, M.; Gast, A. P. "Permanently linked monodisperse paramagnetic chains." *Langmuir* **1998**, *14*, 7334-7336.
- [80] Haldar, A.; Pal, S. B.; Roy, B.; Gupta, S. D.; Banerjee, A. "Self-assembly of microparticles in stable ring structures in an optical trap." *Physical Review A* **2012**, *85*, 9.
- [81] Wu, H. K.; Thalladi, V. R.; Whitesides, S.; Whitesides, G. M. "Using hierarchical self-assembly to form three-dimensional lattices of spheres." *Journal of the American Chemical Society* **2002**, *124*, 14495-14502.
- [82] Molina-Bolivar, J. A.; Galisteo-Gonzalez, F. "Latex immunoagglutination assays." *Journal of Macromolecular Science-Polymer Reviews* **2005**, 59-98.



- [83] Nguyen, L.; Yang, W.; Wang, Q.; Hirst, L. "Molecular dynamics simulation of F-actin reveals the role of cross-linkers in semi-flexible filament assembly." *Soft Matter* **2009**, *5*, 2033-2036.
- [84] Modery-Pawlowski, C.; Tian, L.; Ravikumar, M.; Wong, T.; Sen Gupta, A. "In vitro and in vivo hemostatic capabilities of a functionally integrated platelet-mimetic liposomal nanoconstruct." *Biomaterials* **2013**, *34*, 3031-3041.
- [85] Ariens, R.; Lai, T.; Weisel, J.; Greenberg, C.; Grant, P. "Role of factor XIII in fibrin clot formation and effects of genetic polymorphisms." *Blood* **2002**, *100*, 743-754.
- [86] Meng, Q.; Li, Z.; Li, G.; Zhang, X.; An, Y.; Zhu, X. "Aggregation of biotinylated polymeric microspheres induced by interaction with avidin." *Pure and Applied Chemistry* **2007**, *79*, 1575-1582.
- [87] Riggin, C.; Beltz, G.; Hung, C.; Thorn, R.; Marciani, D. "Detection of antibodies to human-immunodeficiency-virus by latex agglutination with recombinant antigen." *Journal of Clinical Microbiology* **1987**, *25*, 1772-1773.
- [88] Weng, L.; Rostamzadeh, P.; Nooryshokry, N.; Le, H.; Golzarian, J. "In vitro and in vivo evaluation of biodegradable embolic microspheres with tunable anticancer drug release." *Acta Biomaterialia* **2013**, *9*, 6823-6833.
- [89] Forster, R.; Thurmer, F.; Wallrapp, C.; Lloyd, A.; Macfarlane, W.; Phillips, G.; Boutrand, J.; Lewis, A. "Characterisation of physico-mechanical properties and degradation potential of calcium alginate beads for use in embolisation." *Journal of Materials Science-Materials in Medicine* **2010**, *21*, 2243-2251.
- [90] Arya, C.; Kralj, J. G.; Jiang, K. Q.; Munson, M. S.; Forbes, T. P.; DeVoe, D. L.; Raghavan, S. R.; Forry, S. P. "Capturing rare cells from blood using a packed bed of custom-synthesized chitosan microparticles." *Journal of Materials Chemistry B* **2013**, *1*, 4313-4319.
- [91] Wu, L.; Yi, H.; Li, S.; Rubloff, G.; Bentley, W.; Ghodssi, R.; Payne, G. "Spatially selective deposition of a reactive polysaccharide layer onto a patterned template." *Langmuir* **2003**, *19*, 519-524.
- [92] Chiu, S. H.; Chung, T. W.; Giridhar, R.; Wu, W. T. "Immobilization of beta-cyclodextrin in chitosan beads for separation of cholesterol from egg yolk." *Food Research International* **2004**, *37*, 217-223.
- [93] De Geest, B. G.; De Koker, S.; Sukhorukov, G. B.; Kreft, O.; Parak, W. J.; Skirtach, A. G.; Demeester, J.; De Smedt, S. C.; Hennink, W. E. "Polyelectrolyte microcapsules for biomedical applications." *Soft Matter* **2009**, *5*, 282-291.

- [94] Borodina, T.; Markvicheva, E.; Kunizhev, S.; Moehwald, H.; Sukhorukov, G. B.; Kreft, O. "Controlled release of DNA from self-degrading microcapsules." *Macromolecular Rapid Communications* **2007**, *28*, 1894-1899.
- [95] Esser-Kahn, A. P.; Odom, S. A.; Sottos, N. R.; White, S. R.; Moore, J. S. "Triggered Release from Polymer Capsules." *Macromolecules* **2011**, *44*, 5539-5553.
- [96] De Geest, B. G.; Stubbe, B. G.; Jonas, A. M.; Van Thienen, T.; Hinrichs, W. L. J.; Demeester, J.; De Smedt, S. C. "Self-exploding lipid-coated microgels." *Biomacromolecules* **2006**, *7*, 373-379.
- [97] Vicente-Manzanares, M.; Sanchez-Madrid, F. "Role of the cytoskeleton during leukocyte responses." *Nature Reviews Immunology* **2004**, *4*, 110-122.
- [98] Tschopp, J.; Nabholz, M. "Perforin-Mediated Target-Cell Lysis by Cytolytic Lymphocyte-T." *Annual Review of Immunology* **1990**, *8*, 279-302.
- [99] Vollenweider, I.; Groscurth, P. "Ultrastructure of Cell-Mediated Cytotoxicity." *Electron Microscopy Reviews* **1991**, *4*, 249-267.
- [100] Liu, H.; Faucher, K. M.; Sun, X. L.; Feng, J.; Johnson, T. L.; Orban, J. M.; Apkarian, R. P.; Dluhy, R. A.; Chaikof, E. L. "A membrane-mimetic barrier for cell encapsulation." *Langmuir* **2002**, *18*, 1332-1339.
- [101] Chen, K.; Merkel, T. J.; Pandya, A.; Napier, M. E.; Luft, J. C.; Daniel, W.; Sheiko, S.; DeSimone, J. M. "Low Modulus Biomimetic Microgel Particles with High Loading of Hemoglobin." *Biomacromolecules* **2012**, *13*, 2748-2759.
- [102] Qi, W.; Yan, X. H.; Juan, L.; Cui, Y.; Yang, Y.; Li, J. B. "Glucose-Sensitive Microcapsules from Glutaraldehyde Cross-Linked Hemoglobin and Glucose Oxidase." *Biomacromolecules* **2009**, *10*, 1212-1216.
- [103] Ghanem, A.; Ghaly, A. "Immobilization of glucose oxidase in chitosan gel beads." *Journal of Applied Polymer Science* **2004**, *91*, 861-866.
- [104] Oh, H.; Goyal, A.; Raghavan, S. "Multicompartment Capsules that Mimic the Architecture of Biological Cells." *ACS Colloids & Surface Science Symposium* **2014**.
- [105] Sun, J. C.; Tan, H. P. "Alginate-Based Biomaterials for Regenerative Medicine Applications." *Materials* **2013**, *6*, 1285-1309.
- [106] Ramachandran, S.; Fontanille, P.; Pandey, A.; Larroche, C. "Stability of glucose oxidase activity of *Aspergillus niger* spores produced by solid-state fermentation

- and their role as biocatalysts in bioconversion reaction." *Food Technology and Biotechnology* **2008**, *46*, 190-194.
- [107] Pocker, Y.; Green, E. "Hydrolysis of D-Glucono-Delta-Lactone .1. General Acid-Base Catalysis, Solvent Deuterium-Isotope Effects, and Transition-State Characterization." *Journal of the American Chemical Society* **1973**, *95*, 113-119.
- [108] Good, N. E.; Izawa, S. "Hydrogen Ion Buffers." *Methods in Enzymology* **1972**, *24B*, 53-68.
- [109] Zhu, H. G.; Srivastava, R.; Brown, J. Q.; McShane, M. J. "Combined physical and chemical immobilization of glucose oxidase in alginate microspheres improves stability of encapsulation and activity." *Bioconjugate Chemistry* **2005**, *16*, 1451-1458.
- [110] Brown, J. Q.; Srivastava, R.; McShane, M. J. "Encapsulation of glucose oxidase and an oxygen-quenched fluorophore in polyelectrolyte-coated calcium alginate microspheres as optical glucose sensor systems." *Biosensors & Bioelectronics* **2005**, *21*, 212-216.
- [111] Barakat, N. S.; Almurshedi, A. S. "Preparation and Characterization of Chitosan Microparticles for Oral Sustained Delivery of Gliclazide: In Vitro/In Vivo Evaluation." *Drug Development Research* **2011**, *72*, 235-246.
- [112] Polyak, B.; Geresh, S.; Marks, R. S. "Synthesis and characterization of a biotin-alginate conjugate and its application in a biosensor construction." *Biomacromolecules* **2004**, *5*, 389-396.
- [113] Kim, S. H.; Park, J. G.; Choi, T. M.; Manoharan, V. N.; Weitz, D. A. "Osmotic-pressure-controlled concentration of colloidal particles in thin-shelled capsules." *Nature Communications* **2014**, *5*.
- [114] Shah, R. K.; Shum, H. C.; Rowat, A. C.; Lee, D.; Agresti, J. J.; Utada, A. S.; Chu, L. Y.; Kim, J. W.; Fernandez-Nieves, A.; Martinez, C. J.; Weitz, D. A. "Designer emulsions using microfluidics." *Materials Today* **2008**, *11*, 18-27.
- [115] Haghgoie, R.; Toner, M.; Doyle, P. S. "Squishy Non-Spherical Hydrogel Microparticles." *Macromolecular Rapid Communications* **2010**, *31*, 128-134.
- [116] Fang, A. P.; Gaillard, C.; Douliez, J. P. "Template-Free Formation of Monodisperse Doughnut-Shaped Silica Microparticles by Droplet-Based Microfluidics." *Chemistry of Materials* **2011**, *23*, 4660-4662.
- [117] Wang, B. G.; Shum, H. C.; Weitz, D. A. "Fabrication of Monodisperse Toroidal Particles by Polymer Solidification in Microfluidics." *Chemphyschem* **2009**, *10*, 641-645.

- [118] Merkel, T. J.; Jones, S. W.; Herlihy, K. P.; Kersey, F. R.; Shields, A. R.; Napier, M.; Luft, J. C.; Wu, H. L.; Zamboni, W. C.; Wang, A. Z.; Bear, J. E.; DeSimone, J. M. "Using mechanobiological mimicry of red blood cells to extend circulation times of hydrogel microparticles." *Proceedings of the National Academy of Sciences of the United States of America* **2011**, *108*, 586-591.

## Manuscripts in Print

- [1] **Arya, C.**; Kralj J. G.; Jiang, K. Q.; Munson M. S.; Forbes T. P.; DeVoe D. L.; Raghavan S. R.; Forry S. P., "Capturing Rare Cells from Blood Using a Packed Bed of Custom Synthesized Chitosan Microparticles." *Journal of Materials Chemistry B*, 2013, 1, (34), 4313-4319.
  
- [2] Kralj, J. G.; **Arya, C.**; Tona, A.; Forbes, T. P.; Munson, M. S.; Sorbara, L.; Srivastava, S.; Forry, S. P., "A simple packed bed device for antibody labelled rare cell capture from whole blood." *Lab on a Chip* 2012, 12, (23), 4972-4975.
  
- [3] Jiang, K. Q.; Xue, C.; **Arya, C.**; Shao, C. R.; George, E. O.; DeVoe, D. L.; Raghavan, S. R., "A New Approach to In-Situ "Micromanufacturing": Microfluidic Fabrication of Magnetic and Fluorescent Chains Using Chitosan Microparticles as Building Blocks." *Small* 2011, 7, (17), 2470-2476.

## Conference Presentations

- [1] **Arya, C.**; Saez C.; Huang, H.; Raghavan S.R., (24 June 2014) "Clustering of Cyclodextrin Functionalized Microbeads Visualized in Real-Time." *88th ACS Colloids and Surface Science Summer Symposium, University of Pennsylvania, Philadelphia, Pennsylvania.*
  
- [2] **Arya, C.**; Kralj J.G.; Jiang, K.Q.; Munson M.S.; Forbes T.P.; DeVoe D.L.; Raghavan S.R.; Forry S.P. (10 April 2013) "A New Approach for Capturing Circulating Tumor Cells in a Microfluidic Device Using a Packed Array of Functionalized Chitosan Beads." *2013 MRS Spring Meeting and Exhibit, San Francisco, California.*
  
- [3] **Arya, C.**; Kralj J.G.; Forbes T.P.; Tona A.; DeVoe D.L.; Raghavan S.R.; Forry S.P. (June 11 2012). "A New Approach for Capturing Circulating Tumor Cells in a Microfluidic Device Using a Packed Array of Functionalized Chitosan Beads." *86th ACS Colloid and Surface Science Summer Symposium, Johns Hopkins University, Baltimore, Maryland.*